frontiers | Research Topics

Mechanisms and applications of chemical techniques for effective development of unconventional reservoirs

Edited by
Zhilin Cheng, Hui Gao, Liangbin Dou, Qingbang Meng and Jianlin Zhao

Published in
Frontiers in Earth Science

ISSN 1664-8714
ISBN 978-2-83251-615-7
DOI 10.3389/978-2-83251-615-7

About Frontiers

Frontiers is more than just an open access publisher of scholarly articles: it is a pioneering approach to the world of academia, radically improving the way scholarly research is managed. The grand vision of Frontiers is a world where all people have an equal opportunity to seek, share and generate knowledge. Frontiers provides immediate and permanent online open access to all its publications, but this alone is not enough to realize our grand goals.

Frontiers journal series

The Frontiers journal series is a multi-tier and interdisciplinary set of open-access, online journals, promising a paradigm shift from the current review, selection and dissemination processes in academic publishing. All Frontiers journals are driven by researchers for researchers; therefore, they constitute a service to the scholarly community. At the same time, the *Frontiers journal series* operates on a revolutionary invention, the tiered publishing system, initially addressing specific communities of scholars, and gradually climbing up to broader public understanding, thus serving the interests of the lay society, too.

Dedication to quality

Each Frontiers article is a landmark of the highest quality, thanks to genuinely collaborative interactions between authors and review editors, who include some of the world's best academicians. Research must be certified by peers before entering a stream of knowledge that may eventually reach the public - and shape society; therefore, Frontiers only applies the most rigorous and unbiased reviews. Frontiers revolutionizes research publishing by freely delivering the most outstanding research, evaluated with no bias from both the academic and social point of view. By applying the most advanced information technologies, Frontiers is catapulting scholarly publishing into a new generation.

What are Frontiers Research Topics?

Frontiers Research Topics are very popular trademarks of the *Frontiers journals series*: they are collections of at least ten articles, all centered on a particular subject. With their unique mix of varied contributions from Original Research to Review Articles, Frontiers Research Topics unify the most influential researchers, the latest key findings and historical advances in a hot research area.

Find out more on how to host your own Frontiers Research Topic or contribute to one as an author by contacting the Frontiers editorial office: frontiersin.org/about/contact

Mechanisms and applications of chemical techniques for effective development of unconventional reservoirs

Topic editors

Zhilin Cheng — Xi'an Shiyou University, China
Hui Gao — Xi'an Shiyou University, China
Liangbin Dou — Xi'an Shiyou University, China
Qingbang Meng — China University of Geosciences Wuhan, China
Jianlin Zhao — ETH Zürich, Switzerland

Citation

Cheng, Z., Gao, H., Dou, L., Meng, Q., Zhao, J., eds. (2023). *Mechanisms and applications of chemical techniques for effective development of unconventional reservoirs*. Lausanne: Frontiers Media SA. doi: 10.3389/978-2-83251-615-7

Table of contents

frontiers | Frontiers in Earth Science

TYPE Editorial
PUBLISHED 24 January 2023
DOI 10.3389/feart.2023.1142032

OPEN ACCESS

EDITED AND REVIEWED BY
Martyn Tranter,
Aarhus University, Denmark

*CORRESPONDENCE
Zhilin Cheng,
zhilin_cheng1992@163.com
Qingbang Meng,
mengqb@cug.edu.cn
Jianlin Zhao,
zhaojia@ethz.ch
Hui Gao,
ghtopsun1@163.com
Liangbin Dou,
doulb@xsyu.edu.cn

SPECIALTY SECTION
This article was submitted to Geochemistry, a section of the journal Frontiers in Earth Science

RECEIVED 11 January 2023
ACCEPTED 16 January 2023
PUBLISHED 24 January 2023

CITATION
Cheng Z, Meng Q, Zhao J, Gao H and Dou L (2023), Editorial: Mechanisms and applications of chemical techniques for effective development of unconventional reservoirs.
Front. Earth Sci. 11:1142032.
doi: 10.3389/feart.2023.1142032

Editorial: Mechanisms and applications of chemical techniques for effective development of unconventional reservoirs

Zhilin Cheng[1]*, Qingbang Meng[2]*, Jianlin Zhao[3]*, Hui Gao[1]* and Liangbin Dou[1]*

[1]School of Petroleum Engineering, Xi'an Shiyou University, Xi'an, Shaanxi, China, [2]Key Laboratory of Tectonics and Petroleum Resources, China University of Geosciences, Ministry of Education, Wuhan, China, [3]Chair of Building Physics, Department of Mechanical and Process Engineering, ETH Zürich, Zürich, Switzerland

KEYWORDS

chemical recovery method, chemical recovery mechanism, unconventional reservoir, microscale simulation, CCUS

Editorial on the Research Topic
Mechanisms and applications of chemical techniques for effective development of unconventional reservoirs

The proved reserves and production from unconventional reservoirs, such as tight sandstone, carbonate, and shale oil and gas, have increased yearly. How to effectively develop such tight reservoirs is still an urgent Research Topic for current and future decades. Researchers have accumulated a wealth of experience in exploiting conventional reservoirs. However, the geological conditions, petrophysical properties, and fluid mobility of unconventional resources are quite different from those of conventional ones. Usually, abundant micro-nanopores are well developed within unconventional reservoir rocks, resulting in a very high displacement pressure and hindering the application of most flooding approaches. In addition, fluids in tight formations are under the nanoconfinement environment but not the bulk condition. The fluid flow mechanisms and solid-fluid interactions remain elusive throughout the production stage, particularly when chemical recovery methods are involved. Therefore, this Research Topic is focused on the application of chemical-based techniques in promoting hydrocarbon extraction in unconventional reservoirs and revealing the mechanisms and intricate processes of chemical additives for improving recovery.

We have collected twelve papers on this Research Topic, mainly including the chemical-assisted hydraulic fracturing and the displacement of oil and gas in reservoir development. For instance, the paper "*Analysis of the influence of CO_2 pre-injection during hydraulic fracturing on enhanced oil recovery in shale reservoirs*" by Yang et al. discussed the effects of CO_2 pre-injection on reservoir rocks and fluids. They demonstrated that the CO_2-rock and CO_2-oil/water interaction could change the reservoir porosity, permeability, wettability, and fluid properties and impede clay swelling. These changes could lead to a reduction in initiation pressure, an increase in fracture complexity, and the enhancement in reservoir pressure, which is thus conducive to the hydraulic fracturing operation. Similarly, to mitigate the drawback of single HCl during matrix acidizing of tight carbonate formations, in their work "*Comparative analysis of matrix retarded acidizing methods for tight carbonate reservoirs: gelled acid, foamed*

acid and micro-emulsified acid," Wang et al. proposed three promising matrix acidizing formulas for carbonate reservoirs. Among them, the foam-based acids have several advantages over other acidizing methods. Specifically, the foam-based acids show good compatibility with formation water and could lower the filtrate rate of acid and cause less formation damage. Therefore, it is highly recommended in the matrix acidizing process. Additionally, in the study "*Comparative study on the analysis methods of fracture pressure interference in shale oil three-dimensional fracturing,*" Chen et al. concluded that the tracer monitoring, microseismic, and pressure monitoring technology were commonly used to identify the interlayer fracture pressure and evaluate the fracturing performance. The tracer monitoring method is the most accurate, but the latter two have a wider range of applications. Thus, the synthetic application of the three methods could be more appropriate.

Given the significance of environmental protection, CCUS (carbon capture, utilization, and storage) has become a hot spot and has attracted much more attention from academia and industry in recent years. Several papers collected in this Research Topic are associated with this Research Topic. The experimental paper "*Laboratory investigation of the influence of fractures on CO_2 flooding*" by Qing-Fu studied the effects of fracture length and aperture on CO_2 flooding pressure, displacement efficiency, and composition of produced fluids. They found that a longer and wider fracture could decrease the injected pressure; however, this impairs the oil displacement efficiency. Besides, the fracture properties have no significant influence on the composition of produced oil. In the paper "*Low Carbon Oil Exploitation: Carbon Dioxide Flooding Technology,*" Xia et al. reviewed the research status of CO_2 flooding worldwide, and summarized nine mechanisms of CO_2 flooding for oil and gas reservoirs. Finally, the authors raised their concerns in terms of the low oil recovery, economic problems, gas sources, etc. Furthermore, it is inevitable that gas channeling would occur when CO_2 is injected into the fractured tight oil reservoirs. Zhu et al. stated that this unfavorable circumstance could be eased by injecting the low-viscosity CO_2 responsive plugging materials, which can effectively block the high-permeable channels and reduce the upswept zone. The primary mechanisms of CO_2 responsive foam, CO_2 responsive surfactant, and CO_2 responsive gel, are elaborated in their paper "*The Application of CO_2-Responsive Materials (CRMs) on Enhanced Oil Recovery (EOR) for Fractured Tight Oil Reservoirs*". In another paper, "*Eco-development of oil and gas industry: CCUS-EOR technology,*" Yan et al. reviewed the current status and advance of CCUS technology from the perspective of ecological development, and they also gave their advice on the practical paths of reducing carbon in the world, the international development pattern and advanced technologies for the large-scale CO_2 storage and enhanced oil recovery. Additionally, oil recovery by spontaneous imbibition is also a vital enhanced oil recovery method for tight reservoirs. However, a prerequisite is that the reservoir rocks must be water-wet. Thus, in the paper "*Wettability alteration agents to promote spontaneous imbibition in tight reservoirs: Achievements and limitations,*" Zhong et al. proposed that the surfactants, nanoparticles, nano-emulsion, and inorganic salts can be used to shift the mixed-wet or oil-wet formations to the water-wet state to maximize the imbibition oil recovery. They also discussed the potential risks and future trends regarding the applications of these approaches in tight reservoirs.

Furthermore, several authors attempted to elaborate on the fluid flow behavior based on the pore scale modeling and mathematical model. For example, Jia et al. employed the phase-field model built in COMSOL to investigate the effect of fracture direction on displacement characteristics and residual oil distribution under the water flooding model. They also identified the evolution of residual oil types. The results were shown in the paper "*COMSOL-based investigation of the characteristics of microscopic water flooding and residual oil distribution in carbonate reservoirs.*" The paper "*Study on flow model of multi-stage fracturing horizontal well in stress-dependent dual medium reservoir*" by Jiaming et al. considered the stress sensitivity of carbonate reservoir and established a semi-analytical model to flow regimes of multistage fracturing horizontal well. Results showed that fluids flow in the horizontal well can be classified into six types, and ignoring the stress sensitivity would bring about a substantial error in production prediction. On the other hand, there are two additional papers concentrated on the fluid mobility in tight sandstone (*Research on fluid mobility in tight sandstone with a NMR fractal theory pore classification method* by Gao et al.) and the competitive adsorption of different gas on hydrate surface (*Comparison of CO_2, N_2, CO, H_2S, CH_4, and H_2O adsorptions onto sI methane hydrate surface* by Zhang et al.). These results would provide significant guidance for the selection of sweet-spot and the development of unconventional reservoirs.

In conclusion, commercial development of unconventional resources cannot be achieved without the usage of chemical-related techniques. The papers on this Research Topic provide an overview of a variety of chemical-assisted approaches used in tight reservoirs. However, the mechanisms and applicability of different chemical methods still remain vague since addressing this Research Topic is very challenging, which entangles multi-disciplinary knowledge. Therefore, it could be more targeted by organizing a Research Topic that only specifically focuses on one or two aspects of chemical recovery systems.

Author contributions

All authors listed have made a substantial, direct, and intellectual contribution to the work and approved it for publication.

Conflict of interest

The authors declare that the research was conducted in the absence of any commercial or financial relationships that could be construed as a potential conflict of interest.

Publisher's note

frontiers | Frontiers in Earth Science

TYPE Opinion
PUBLISHED 08 September 2022
DOI 10.3389/feart.2022.1010741

OPEN ACCESS

EDITED BY
Qingbang Meng,
China University of Geosciences
Wuhan, China

REVIEWED BY
Dezhi Qiu,
Guangzhou Marine Geological Survey,
China
Xiao Z. Hang,
Shandong University, China

*CORRESPONDENCE
Guanglong Sheng,
shenggl2019@yangtzeu.edu.cn

SPECIALTY SECTION
This article was submitted to Frontiers in Earth Science,
a section of the journal Geochemistry

RECEIVED 03 August 2022
ACCEPTED 12 August 2022
PUBLISHED 08 September 2022

CITATION
Zhong X, Sheng G, Chen X, Wang Y, Zhang S and Zhang L (2022), Wettability alteration agents to promote spontaneous imbibition in tight reservoirs: Achievements and limitations.
Front. Earth Sci. 10:1010741.
doi: 10.3389/feart.2022.1010741

Wettability alteration agents to promote spontaneous imbibition in tight reservoirs: Achievements and limitations

Xun Zhong[1,2], Guanglong Sheng[1,2]*, Xingyu Chen[1], Yifan Wang[1], Sai Zhang[1] and Li Zhang[1]

[1]College of Petroleum Engineering, Yangtze University, Wuhan, China, [2]Key Laboratory of Drilling and Production Engineering for Oil and Gas, Wuhan, China

KEYWORDS

wettability alteration, spontaneous imbibition, tight reservoirs, achievements, limitations, enhanced oil recovery

1 Introduction

Though renewable energy is developing rapidly, fossil energy remains to be the most important source of energy and global oil consumption would keep rising to meet the needs of social development by 2040 (Sagala et al., 2019). Confronted with the situation that "easy oil" is depleting and new oilfield exploration is plummeting, increasing attention has been paid to the high-efficient exploitation and development of unconventional oil resources. Tight oil mainly occurs in tight sandstone, carbonate, or other reservoirs with overlaid matrix permeability less than 0.2 mD or air permeability less than 2 mD (Standard SY/T 6943-2013). The preliminarily proved tight oil geological reserves in China are about 125×10^8 tons (Wang et al., 2016; Sun et al., 2019) and about 40% of the national recoverable reserves are tight oil. The effective development of tight oil is vital to improving China's energy structure and ensuring national energy security.

Natural microfractures are ubiquitous in tight oil reservoirs, but the pores/throats are narrow, connectivity is poor, and the formation energy is low, thus, the primary oil recovery of tight reservoirs is generally below 10% (Wang et al., 2015; Bidhendi et al., 2019). And the advancements in multi-stage horizontal well fracturing technologies have offered some new opportunities to partially relieve these problems (Wang et al., 2018; Yu et al., 2021). In matrix-fracture dual-permeability media, spontaneous imbibition through which a non-wetting phase is displaced by a wetting phase is regarded as the most probable matrix-fracture transfer mechanism that plays a key role in unlocking the tight oil potentials (Harimi et al., 2019). In general, original tight rocks are water-wet, but can be changed to oil-wet after a long time contacting with crude oil when asphaltenes deposit, calcite, and dolomite adsorb organic acids or resin acids and quartz and clay adsorb organic bases and aromatics (Liang T. et al., 2021). To ensure the occurrence of effective spontaneous imbibition in mix-wet or oil-wet tight reservoirs, the wettability of porous media should always be altered water-wet, and adding chemical agents is indispensable. Surfactants, nanomaterials, and inorganic salts are extensively used to enhance the imbibition rate and boost the oil recovery factor. However, challenges usually coexist with opportunities. In this paper, the potential risks associated with surfactants,

nanomaterials, and inorganic salts usage in tight formations are highlighted, and the possible directions for future studies were discussed to guide the effective design of EOR scenarios in tight oil reservoirs.

2 Surfactants

Surfactants with different structures can alter wettability through different means, including ion-pairing, hydrophobic interactions, solubilization, polarization of electrons, etc., (Hou et al., 2015; Patil et al., 2018) Numerous studies have been conducted, and the potentials of different types of surfactants to promote spontaneous imbibition in tight formations were verified. For example, cationic surfactant CTAB could extract additional 2.5% OOIP and 7.5% OOIP after brine imbibition from 0.11 mD (water-wet) and 0.018 mD (mix-wet) tight cores, respectively (Wang et al., 2019). Anionic surfactant petroleum sulfonate could yield an oil recovery of 35.9% from 1 mD tight cores, which was 21.7% higher than brine (Zhou et al., 2022). Nonionic surfactant APG could recover 27.02% OOIP from 0.26–0.31 mD tight sandstone cores, which was 21.02% higher than brine (Sun et al., 2021). However, there are still many problems to be solved before extending to field tests, such as.

1) Tight formations are abundant in narrow pores and throats, and the clay content can be higher than 15%. The large specific surface area will result in a significant surfactant retention density of 10–30 mg/g (Zhang et al., 2016; Zhong et al., 2019), which greatly limits surfactant penetration depth and efficiency. However, the contribution of surfactant adsorption to wettability alteration is also substantial, therefore, the economic and optimal adsorption density, as well as adsorption rate should be better clarified. Moreover, dynamic adsorption tests instead of static adsorption tests based on intact tight cores rather than rock powders should be conducted to mimic the real situations.
2) Surfactant penetration speed and depth are key parameters necessary for surfactant EOR modeling and are important to guide the scaling up of laboratory findings for field operation design (Liang T. et al., 2021; Wang et al., 2021). But there is scarce information on the direct measurements of surfactant dispersion coefficient in tight rocks, and the accuracy of numerical models can hardly be verified. Therefore, more laboratory evidence is necessary to increase the robustness and reliability of numerical simulations.
3) Normal surfactants usually undergo either phase change or separation in high temperature and high salinity (HTHS) conditions (Liu et al., 2021; Yao et al., 2021). Anionic-nonionic, zwitterionic and Gemini surfactants show high salt and thermal tolerance, but their functional mechanisms to induce wettability alteration remain elusive and further research is desperately needed.
4) The cost of surfactants especially novel surfactants is still relatively high. Though the advances in natural surfactants may help to relieve this problem, the industrialization production of natural surfactants still faces many challenges.
5) The current method to screen surfactants for tight formations mainly borrows from conventional reservoirs, without fully considering the specificity of tight formations and the discrepancies in reservoir physical properties. Thus, designing a systematic screening method especially for tight formations is urgent, in which surfactant micelle size, the optimal rock wettability, the adsorption density should be comprehensively considered.

3 Nanomaterials

3.1 Nanoparticles

Nanoparticles (NPs) induce wettability change mainly by forming microstructure formation or imposing structural disjoining pressure, and it is believed that NP adsorption on liquid-liquid/liquid-solid interfaces can increase the stability of water film adsorbed on rocks (Yuan et al., 2021). A summary of the recent progress of NPs applications in tight reservoirs was provided in Table 1 (Part I). Most research showed that nanofluids with or without surfactants were capable to enhance the oil recovery of spontaneous imbibition by over 10% through wettability alteration. However, there is also still more work that needs to be done, for instance.

1) The optimal NP concentration highly depends on NP type, rock properties, solution environment, etc. Zhou et al. (2022) reported that the highest efficiency of 38.1% could be obtained with 0.1 wt% SiDots in 1 mD tight cores and a further increase in SiDot concentration to 0.5 wt% would decrease the rate to 22.27% due to intense particle aggregation. They also indicated that the optimal SiO_2 NP (15 nm) concentration to be in 0.5 mD tight cores was also around 0.1 wt% (Zhou et al., 2019). However, Lu et al. (2017) held a different view. They highlighted that though viscosity and asphaltene content of the produced oil would decrease with increasing NP concentration, the silica concentration to be used should be around 10 mg/L in 0.68–0.95 mD tight cores to eliminate pore plugging. Authors tried to use pore plugging in most cases to explain the decrease in recovery when NP concentration increased without even knowing whether the nanofluid can seep into the tight cores or not. Therefore, a comprehensive study on NP transport and retention behaviors in tight porous media should be implemented and the permeability damage caused by NPs should better be quantified.
2) The optimal oil/water interfacial tension of nanofluids for tight formation remains bewilderment. Zhang et al.

TABLE 1 Nanomaterials for tight formation EOR.

Part I nanoparticle

Nanoparticle	Size, nm	C, mg/L	Additives	k, mD	Solution environment	IFT, mN/m	Contact angle, °	Recovery incremental, %	Ref
Carbon NP	10	500	—	0.6	3% NaCl, 60°C	16.4	98 (oil)	22.3 (Imbibition)	Li et al. (2017)
SiO_2 NP	19.4	10	—	0.68–0.95	0.75% NaCl, 50°C	—	90–128 (oil)	5.32–10.33 (Flooding)	Lu et al. (2017)
SiO_2 NP (Modified)	10–20	10,000	—	0.6	3% NaCl, 60°C	7.0	142 (oil)	25.0 (Imbibition)	Li et al. (2018)
SiO_2 (Modified)	15	1,000	—	0.5	3% NaCl, 60°C	12.2	120 (oil)	~24.5 (Imbibition)	Zhou et al. (2019)
SiO_2 (Modified)	—	5,000	—	0.009	12.65% brine 25°C	0.267–0.190	57 (water)	—	Yuan et al. (2021)
Silicon dots (Modified)	3–5	1,000	—	1.0	Low salinity, 60 °C	18.7	—	23.9 (Imbibition)	Zhou et al. (2022)
NP	10–20	3,000	—	0.013–0.077	DI, 20°C	1	—	—	Qiu et al. (2022)
Carbon NP	7	1,500	0.05% Tween-80	0.113–0.125	3% NaCl, 75°C	11.2	89 (oil)	13.0 (Imbibition)	Zhao et al. (2020)
SiO_2 NP	20.56	100	0.05% KD	0.2–0.3	1% NaCl, 90°C	4×10^{-4}	140 (oil)	17.64 (Flooding)	Xu et al. (2018)
SiO_2 NP	20	1,000	0.1% AOS	0.1	3% brine, 80°C	3.5×10^{-3}	131.8 (oil)	19.6 (Imbibition)	Zhao et al. (2022a)
SiO_2 NP	10	500	0.1% SLES	0.072–0.088	DI	~6.0	155 (oil)	28.71 (Imbibition)	(Zhang et al., 2022a; 2022b)
Silicon dots	5	1,200	0.1% Betaine	0.0091	15% brine, 80°C	0.085	124.1 (oil)	13.39 (Imbibition)	Zhou et al. (2020)

Part II Nanoemulsions

Shell	Kernel	C, mg/L	Size, nm	k, mD	Solution environment	IFT, mN/m	Contact angle, °	Recovery incremental, %	Ref
C_8–C_{12} alkane	Gemini surfactant	3,000	<25	0.1–0.3	0.77% brine, 90°C	1×10^{-2}	—	27.5 (Flooding)	Ding et al. (2021)
Alkanes or olefins	Non-ionic surfactant	1,000	14	0.005	2% KCl, 85°C	2.6	126.8 (oil)	30 (Imbibition)	Liang et al. (2021b)
C_{10}–C_{14} alkane	Diphenyl ether surfactant	1,000	15.7	0.1	3.08% brine, 70°C	10^{-2}	76.6 (water)	19.2 (Imbibition)	Zhang et al. (2021)
Cyclooctane	Non-ionic surfactant	500–3,000	10	0.0839–0.101	DI, 60°C	3.56	11.7 (water)	7.53–24.83 (Imbibition)	Zhao et al. (2022b)
N-hexane	Non-ionic, cationic surfactants	3,000	6–11	0.1	0–1% brine, 60°C	0.005	32.7 (water)	20.5 (Imbibition)	Qu et al. (2022)

(2022a) systematically appraised the synergistic effects between surfactants and silica NP and highlighted that the IFT and contact angle should be tailored to higher than 1 mn/m and 140°, respectively to maximize the recovery factor of nanofluid spontaneous imbibition. Similarly, both numerical simulations and experimental studies indicated that the optimal IFT to generate satisfying oil recovery in water-wet tight porous media by surfactant imbibition is between 10–20 mn/m (Wang et al., 2019). However, Zhao M. et al. (2022) proposed that by further decreasing IFT to 3.5×10^{-3} mn/m and water contact angle to 48°, AOS-based silica nanofluid could recover 28.5% OOIP from 0.1 mD tight cores, comparing to those of 8.9 and 14.33% OOIP by brine and surfactant, respectively. To clear the confusion, further microscopic mechanism study on how IFT will affect the spontaneous imbibition by increasing the capillary number and/or capillary force is necessary and urgent.

3) The stability of nanofluid is preliminary for its applications and surfactants are generally used to disperse the NP. However, the applications of nanofluids in HTHS conditions are still limited and nanofluids with higher thermal and salt resistance should be developed. To improve the stability of NPs, ligands with dendritic structure or copolymers can be used (Zuniga et al., 2016; Zhong et al., 2020), but particle size should be carefully screened, and smaller particles are better preferred.
4) Structural disjoining pressure is proposed as the underlying mechanism in most studies to explain the wettability alteration by nanofluids by simply drawing a schematic diagram without compelling substantial evidence. Further study on the microscopic pore-scale wettability alteration mechanisms is required, and dynamic imbibition and pilot field tests should be conducted to convince the efficiency of NPs.
5) The cost of NPs is relatively high and industrial methods to produce functional NPs should be developed. Also, NP toxicity and its adverse impacts should be clearly defined.

3.2 Nano-emulsions

Broadly speaking, nanodroplets such as nanoemulsions with sizes between 10–100 nm can also be identified as nanomaterials (Shen et al., 2012). Nanoemulsions are generally characterized by a "shell-kernel" structure, in which surfactant functions as an external "shell" and disassociation agents (i.e., alkanes, cycloalkanes, etc.,) form the kernel (Ding et al., 2021). Compared to NPs mentioned in Section 3.1, nanoemulsions are kinetically stable and may be deformable (Aljabri et al., 2021). By splitting the crude oil into "nanosized oil droplets", reducing IFT, alternating wettability, and increasing sweep efficiency, the average recovery incremental by nano emulsions over brine imbibition was higher than 20% (Table 1, Part II), indicating huge EOR potential. However, the large-scale applications of nano-emulsions still face many challenges, such as.

1) Preparing nano emulsions consumes tremendous amounts of chemicals including surfactants, co-surfactants, organic solvents, etc., and the substantial energy might be required to promote the emulsification process, which greatly increases the cost. Thus, high-efficiency chemicals with lower costs and more economic emulsification methods should be developed.
2) Nanoemulsions are thermodynamically unstable and phase separation is unavoidable, but the influence laws of temperature, salinity, formula composition, and other factors and their transport behaviors in the complex porous media are not well comprehended, and extensive lab-scale and pilot tests are necessary.

4 Inorganic salts

Low salinity water (LSW) EOR has received considerable attention in recent decades thanks to its environmental-friendly and economical nature. The wettability alteration mechanisms of LSW include multi-ionic exchange, electrical double-layer effect, fine release, etc., and its effectiveness to enhance oil recovery has been widely confirmed through both laboratory and field scale tests (Sheng, 2014; Lyu et al., 2022; Mokhtari et al., 2022). For instance, an incremental spontaneous imbibition oil recovery of 4.5% OOIP was reported by Wei et al. (2021) when a brine with 0.21% TDS was applied in 0.3 mD tight cores. Mokhtari et al. (2022) revealed that an incremental recovery of over 10% could be obtained in 1.56 mD chalk cores by diluted seawater at the second stage compared to seawater. Webb et al. (2003) noticed a 25–50% reduction in residual oil saturation near the well region in a field-scale LSW flooding test. Overall, the research on LSW spontaneous imbibition in tight formations is relatively less common than surfactants or nanomaterials. The potential reasons may include.

1) LSW is viewed as an immature EOR technique with complicated EOR mechanisms, and due to the complex oil/brine/rock interactions, there is still no consensus over the dominant mechanisms so far. Also, though synergisms between LSW and surfactant/NPs to facilitate the spontaneous imbibition rate have been reported, their interactions, as well as the synergistic mechanisms are subject to debate.
2) The efficiency of LSW highly depends on brine salinity and composition and is sensitive to connate water saturation/composition, initial rock wettability, clay content, oil composition, etc., therefore, the benefits can hardly be ensured (Sheng, 2014; Katende and Sagala, 2019). Meanwhile, higher sulfate concentration is conducive to increased oil recovery but can also cause souring and scaling problems. The effects of fine release induced by LSW remain controversial, either a reduction or an increase in oil recovery is possible and the boundaries are yet to be identified. Also, the adverse impacts of clay expansion in LSW are not fully considered.
3) In most cases, seawater can hardly be used directly for LSW EOR and the compositions of LSW should be tailored by dissolving inorganic salts in freshwater or distilled water. The desalination of seawater usually requires high input, and the efficiency is generally low.

Author contributions

XZ: conceptualization, supervision, funding acquisition, and writing—original draft, review and editing. GS:

conceptualization, supervision, funding acquisition, and writing—review and editing, XC: funding acquisition and investigation. YW, SZ, and LZ: investigation and editing.

Funding

This work was supported by the Natural Science Foundation of China (NSFC) (Grant No.52104019), the Open Fund of Hubei Key Laboratory of Drilling and Production Engineering for Oil and Gas (Yangtze University) (Grant No. YQZC202203) and the Innovation and Entrepreneurship Training program for College Students of Yangtze University (Grant No. Yz2021238).

Conflict of interest

The authors declare that the research was conducted in the absence of any commercial or financial relationships that could be construed as a potential conflict of interest.

Publisher's note

References

Aljabri, N. M., Nan, S., and Adrian, C. (2021). Nanoemulsion: An emerging technology for oilfield applications between limitations and potentials. *J. Pet. Sci. Eng.* 208, 109306. doi:10.1016/j.petrol.2021.109306

Bidhendi, M. M., Kazempour, M., Ibanga, U., Arruda, Justin, Lantz, Mike, Mazon, Cooper, et al. (2019). "A set of successful chemical EOR trials in permian basin: Promising field and laboratory results," in *Presented at the SPE/AAPG/SEG unconventional resources technology conference* (Denver, CO: Society of Petroleum Engineers). doi:10.15530/urtec-2019-881

Ding, B., Guan, B., Liu, W., Chen, B., Sun, J., Li, M., et al. (2021). Mechanism of improving water flooding using the nanofluid permeation flooding system for tight reservoirs in Jilin oilfield. *Energy fuels.* 35 (21), 17389–17395. doi:10.1021/acs.energyfuels.1c02043

Harimi, B., Masihi, M., Mirzaei-Paiaman, A., and Hamidpour, E. (2019). Experimental study of dynamic imbibition during water flooding of naturally fractured reservoirs. *J. Pet. Sci. Eng.* 174, 1–13. doi:10.1016/j.petrol.2018.11.008

Hou, B., Wang, Y., and Yong, H. (2015). Mechanistic study of wettability alteration of oil-wet sandstone surface using different surfactants. *Appl. Surf. Sci.* 330, 56–64. doi:10.1016/j.apsusc.2014.12.185

Katende, A., and Sagala, F. (2019). A critical review of low salinity water flooding: Mechanism, laboratory and field application. *J. Mol. Liq.* 278, 627–649. doi:10.1016/j.molliq.2019.01.037

Li, Y., Dai, C., Zhou, H., Wang, X., Lv, W., Wu, Y., et al. (2017). A novel nanofluid based on fluorescent carbon nanoparticles for enhanced oil recovery. *Ind. Eng. Chem. Res.* 56 (44), 12464–12470. doi:10.1021/acs.iecr.7b03617

Li, Y., Dai, C., Zhou, H., Wang, X., Lv, W., and Zhao, M. (2018). Investigation of spontaneous imbibition by using a surfactant-free active silica water-based nanofluid for enhanced oil recovery. *Energy fuels.* 32 (1), 287–293. doi:10.1021/acs.energyfuels.7b03132

Liang, T., Zhao, X., Yuan, S., Zhu, J., Liang, X., Li, X., et al. (2021a). Surfactant-EOR in tight oil reservoirs: Current status and a systematic surfactant screening method with field experiments. *J. Pet. Sci. Eng.* 196, 108097. doi:10.1016/j.petrol.2020.108097

Liang, X., Zhou, F., Liang, T., Wang, R., Su, H., and Yuan, S. (2021b). Mechanism of using liquid nanofluid to enhance oil recovery in tight oil reservoirs. *J. Mol. Liq.* 324, 114682. doi:10.1016/j.molliq.2020.114682

Liu, Z., Zhao, G., Brewer, M., Lv, Q., and Sudholter, E. J. (2021). Comprehensive review on surfactant adsorption on mineral surfaces in chemical enhanced oil recovery. *Adv. Colloid Interface Sci.* 294, 102467. doi:10.1016/j.cis.2021.102467

Lu, T., Li, Z., Zhou, Y., and Zhang, C. (2017). Enhanced oil recovery of low-permeability cores by SiO_2 nanofluid. *Energy fuels.* 31 (5), 5612–5621. doi:10.1021/acs.energyfuels.7b00144

Lyu, C., Zhong, L., Ning, Z., Chen, M., and Cole, D. R. (2022). Review on underlying mechanisms of low salinity waterflooding: Comparisons between sandstone and carbonate. *Energy fuels.* 36 (5), 2407–2423. doi:10.1021/acs.energyfuels.1c04248

Mokhtari, R., Anabaraonye, B. U., Afrough, A., Mohammadkhani, S., and Feilberg, K. L. (2022). Experimental investigation of low salinity water-flooding in tight chalk oil reservoirs. *J. Pet. Sci. Eng.* 208, 109282. doi:10.1016/j.petrol.2021.109282

Patil, P. D., Rohilla, N., Katiyar, A., Falcone, Susan, Nelson, Christopher, Rozowski, Peter, et al. (2018). "Surfactant based EOR for tight oil reservoirs through wettability alteration: Novel surfactant formulations and their efficacy to induce spontaneous imbibition," in *Presented at the SPE EOR conference at oil and Gas west asia* (Muscat, Oman: Society of Petroleum Engineers). doi:10.2118/190397-MS

Qiu, R., Gu, C., Xue, P., Xu, D., and Gu, M. (2022). Imbibition characteristics of sandstone cores with different permeabilities in nanofluids. *Petroleum Explor. Dev.* 49 (2), 374–381. doi:10.1016/s1876-3804(22)60031-4

Qu, M., Liang, T., Xiao, L., Hou, J., Qi, P., Zhao, Y., et al. (2022). Mechanism study of spontaneous imbibition with lower-phase nano-emulsion in tight reservoirs. *J. Pet. Sci. Eng.* 211, 110220. doi:10.1016/j.petrol.2022.110220

Sagala, F., Montoya, T., Hethnawi, A., Vitale, G., and Nassar, N. N. (2019). Nanopyroxene-based nanofluids for enhanced oil recovery in sandstone cores at reservoir temperature. *Energy fuels.* 33, 877–890. doi:10.1021/acs.energyfuels.8b03749

Shen, Z., Zhao, Z., and Kang, W. (2012). *Colloid and surface chemistry*. 4th Edition, 39. Beijing: Chemical Industry Press. 978-7-122-12982-6.

Sheng, J. J. (2014). Critical review of low-salinity waterflooding. *J. Pet. Sci. Eng.* 120, 216–224. doi:10.1016/j.petrol.2014.05.026

Sun, L., Zou, C., Jia, A., Wei, Y., Zhu, R., Wu, S., et al. (2019). Development characteristics and orientation of tight oil and gas in China. *Petroleum Explor. Dev.* 46 (06), 1073–1087. doi:10.1016/S1876-3804(19)60264-8

Sun, Y. P., Xin, Y., Lyu, F. T., and Dai, C. L. (2021). Experimental study on the mechanism of adsorption-improved imbibition in oil-wet tight sandstone by a nonionic surfactant for enhanced oil recovery. *Pet. Sci.* 18 (4), 1115–1126. doi:10.1016/j.petsci.2021.07.005

Wang, F., Cheng, H., and Song, K. (2021). A mathematical model of surfactant spontaneous imbibition in a tight oil matrix with diffusion and adsorption. *Langmuir* 37 (29), 8789–8800. doi:10.1021/acs.langmuir.1c01139

Wang, H., Ma, F., Tong, X., Liu, Z., Zhang, X., Wu, Z., et al. (2016). Assessment of global unconventional oil and gas resources. *Petroleum Explor. Dev.* 43, 925–940. doi:10.1016/S1876-3804(16)30111-2

Wang, J., Liu, H., Qian, G., Yongcan, P., and Yang, G. (2019). Investigations on spontaneous imbibition and the influencing factors in tight oil reservoirs. *Fuel* 236, 755–768. doi:10.1016/j.fuel.2018.09.053

Wang, W., Shahvali, M., and Su, Y. (2015). A semi-analytical fractal model for production from tight oil reservoirs with hydraulically fractured horizontal wells. *Fuel* 158, 612–618. doi:10.1016/j.fuel.2015.06.008

Wang, X., Peng, X., Zhang, S., Du, Z., and Zeng, F. (2018). Characteristics of oil distributions in forced and spontaneous imbibition of tight oil reservoir. *Fuel* 224 (15), 280–288. doi:10.1016/j.fuel.2018.03.104

Webb, K. J., Black, C. J. J., and Al-Ajeel, H. (2003). "Low salinity oil recovery—log-inject-log," in *Presented at the SPE/DOE symposium on*

improved oil recovery (Tulsa, Oklahoma: Society of Petroleum Engineers). doi:10.2118/89379-MS

Wei, B., Wang, L., Song, T., Zhong, M., and Varfolomeev, M. A. (2021). Enhanced oil recovery by low-salinity water spontaneous imbibition (LSW-SI) in a typical tight sandstone formation of mahu sag from core scale to field scale. *Petroleum* 7 (3), 272–281. doi:10.1016/j.petlm.2020.09.005

Xu, D., Bai, B., Meng, Z., Zhou, Q., Li, Z., Lu, Y., et al. (2018). "A novel ultra-low interfacial tension nanofluid for enhanced oil recovery in super-low permeability reservoirs," in *Presented at the SPE asia pacific oil and Gas conference and exhibition* (Brisbane, QLD: Society of Petroleum Engineers). doi:10.2118/192113-MS

Yao, Y., Wei, M., and Kang, W. (2021). A review of wettability alteration using surfactants in carbonate reservoirs. *Adv. Colloid Interface Sci.* 294, 102477. doi:10.1016/j.cis.2021.102477

Yu, H., Fu, W., Zhang, Y., Lu, X., Cheng, S., Xie, Q., et al. (2021). Experimental study on EOR performance of CO_2-based flooding methods on tight oil. *Fuel* 290 (15), 119988. doi:10.1016/j.fuel.2020.119988

Yuan, L., Zhang, Y., and Dehghanpour, H. (2021). A theoretical explanation for wettability alteration by adding nanoparticles in oil-water-tight rock systems. *Energy fuels.* 35 (9), 7787–7798. doi:10.1021/acs.energyfuels.1c00001

Zhang, C., Jin, X., Tao, J., Xiong, B., Pan, Z., Meng, S., et al. (2021). Comparison of nanomaterials for enhanced oil recovery in tight sandstone reservoir. *Front. Earth Sci.* 9, 746071. doi:10.3389/feart.2021.746071

Zhang, J., Wang, D., and Olatunji, K. (2016). "Surfactant adsorption investigation in ultralower permeable rocks," in *Presented at the SPE low perm symposium* (Kuala Lumpur, Malaysia: Society of Petroleum Engineers). doi:10.2118/180214-MS

Zhang, T., Li, Z., Gao, M., Xu, Z., Adenutsi, C. D., and You, Q. (2022a). New insights into the synergism between silica nanoparticles and surfactants on interfacial properties: Implications for spontaneous imbibition in tight oil reservoirs. *J. Pet. Sci. Eng.* 215, 110647. doi:10.1016/j.petrol.2022.110647

Zhang, T., Zhi, P., Adenutsi, C. D., Wei, Y. Z., Ma, Z. F., and You, Q. (2022b). Quantitative investigation of nanofluid imbibition in tight oil reservoirs based on NMR technique. *Pet. Sci.* In Press. doi:10.1016/j.petsci.2022.04.013

Zhao, M., Cheng, Y., Wu, Y., Dai, C., Gao, M., Yan, R., et al. (2022a). Enhanced oil recovery mechanism by surfactant-silica nanoparticles imbibition in ultra-low permeability reservoirs. *J. Mol. Liq.* 348, 118010. doi:10.1016/j.molliq.2021.118010

Zhao, M., Song, X., Lv, W., Wu, Y., and Dai, C. (2020). The preparation and spontaneous imbibition of carbon-based nanofluid for enhanced oil recovery in tight reservoirs. *J. Mol. Liq.* 313, 113564. doi:10.1016/j.molliq.2020.113564

Zhao, Y., Hou, J., Qu, M., Xiao, L., and Liu, Y. (2022b). Performance evaluation and oil displacement mechanism analysis of nano-microemulsion using in tight oil reservoir *Oilfield Chem.* 39 (02), 338–342. doi:10.3760/cma.j.112147-20220225-00152

Zhong, X., Li, C., Li, Y., Pu, H., Zhou, Y., and Zhao, J. X. (2020). Enhanced oil recovery in high salinity and elevated temperature conditions with a zwitterionic surfactant and silica nanoparticles acting in synergy. *Energy fuels.* 34 (3), 2893–2902. doi:10.1021/acs.energyfuels.9b04067

Zhong, X., Pu, H., Zhou, Y., and Zhao, J. X. (2019). Comparative study on the static adsorption behavior of zwitterionic surfactants on minerals in Middle Bakken formation. *Energy fuels.* 33, 1007–1015. doi:10.1021/acs.energyfuels.8b04013

Zhou, B., You, Q., Li, Y., Chu, Z., Zhang, L., Wang, P., et al. (2022). Preparation and performance evaluation of an active nanofluid for enhanced oil recovery in ultra-low permeability reservoirs. *J. Mol. Liq.* 347, 118331. doi:10.1016/j.molliq.2021.118331

Zhou, H., Zhang, Q., Dai, C., Li, Y., Lv, W., Wu, Y., et al. (2019). Experimental investigation of spontaneous imbibition process of nanofluid in ultralow permeable reservoir with nuclear magnetic resonance. *Chem. Eng. Sci.* 201, 212–221. doi:10.1016/j.ces.2019.02.036

Zhou, Y., Wu, X., Zhong, X., Zhang, S., Pu, H., and Zhao, J. X. (2020). Development of silicon quantum dots based nano-fluid for enhanced oil recovery in tight Bakken cores. *Fuel* 277, 118203. doi:10.1016/j.fuel.2020.118203

Zuniga, G. A., Goods, J. B., Cox, J. R., and Swager, T. M. (2016). Long-term high-temperature stability of functionalized graphene oxide nanoplatelets in Arab-D and API brine. *ACS Appl. Mat. Interfaces* 8 (3), 1780–1785. doi:10.1021/acsami.5b09656

frontiers | Frontiers in Earth Science

TYPE Original Research
PUBLISHED 14 September 2022
DOI 10.3389/feart.2022.983442

OPEN ACCESS

EDITED BY
Jianlin Zhao,
ETH Zürich, Switzerland

REVIEWED BY
Zhao Zhang,
Shandong University, China
Tao Huang,
Zhejiang Ocean University, China

*CORRESPONDENCE
Zhang Qing-Fu,
zhangqingfu605@163.com

SPECIALTY SECTION
This article was submitted to Geochemistry, a section of the journal Frontiers in Earth Science

RECEIVED 01 July 2022
ACCEPTED 01 August 2022
PUBLISHED 14 September 2022

CITATION
Qing-Fu Z (2022), Laboratory investigation of the influence of fractures on CO_2 flooding. *Front. Earth Sci.* 10:983442. doi: 10.3389/feart.2022.983442

Laboratory investigation of the influence of fractures on CO_2 flooding

Zhang Qing-Fu[1,2]*

[1]Exploration and Development Research Institute, Shengli Oilfield Company, SINOPEC, Dongying, Shandong, China, [2]Key Laboratory on Exploration and Development for Unconventional Oil and Gas, Dongying, Shandong, China

CO_2 injection is a promising method for low-permeability reservoirs. CO_2 is much easier to inject underground compared with water. The solubility of CO_2 in oil decreases the oil density and viscosity, leading to an enhancement of the oil recovery. CO_2 flooding could achieve the dual purpose of developing oil effectively and reducing greenhouse gas. Therefore, this technique has both economic and social benefits and is an essential technology for achieving green development. Natural fractures are widely developed in low-permeability reservoirs, and artificial fractures are often used to improve oil development. These fractures have a significant influence on flow patterns during CO_2 flooding. In addition, fractures are also one of the key factors of CO_2 channeling. Therefore, the influence of fractures on CO_2 flooding pressure distribution, fluid composition, and displacement efficiency needs to be studied. In this work, a CO_2 flooding experiment was implemented to test the pressure distribution and outlet composition changes during CO_2 flooding under different fracture lengths and apertures. The experiment shows that a long and wide fracture could effectively reduce the injection-production pressure difference. However, fractures also had a negative effect on oil development. Fracture length and aperture had a significant effect on the gas phase composition at the outlet, but had little effect on the oil phase composition.

KEYWORDS

CO_2 flooding, low permeability reservoir, fractures, CO_2 flooding experiment, greenhouse gas

1 Introduction

The development of low-permeability reservoirs and tight-oil reservoirs is often unsatisfactory due to problems such as small pore radius and low permeability. The poor flow conditions lead to difficulties in water injection development. Laboratory experiments and field applications have shown that the injection of CO_2 into low-permeability reservoirs has a significant ability to enhance oil. In CO_2 injection, oil mixed with CO_2 has much increased mobility and reduces the interfacial tension. Therefore, CO_2 flooding could greatly improve oil recovery. CO_2 injection has been recognized as the second-largest enhanced oil recovery (EOR) process in the world.

CO_2 has attracted the attention of experts around the world because of its excellent oil displacement capacity. There is a long research history on CO_2 flooding in theory research, and it has been frequently used in applications in the field. Since the 1950s, a large amount of theoretical research and field application research has been carried out (Guo et al., 2002; Jiang et al., 2010; He et al., 2011). In the 1970s, the application of CO_2 flooding made great progress (Cao et al., 2020). China started research on CO_2 flooding theory and application in the 1960s. This technology has not been widely promoted in China because of the lack of CO_2.

Global warming is a major issue for the world, as increased amounts of CO_2 and other greenhouse gases in the atmosphere have resulted in increases in sea levels and changes in the climate. Many countries have proposed policies to reduce carbon emissions. In CO_2 flooding, the injected CO_2 is trapped underground, and it is an important way to reduce carbon emissions. Therefore, CO_2 flooding has the dual purpose of oil recovery and CO_2 reduction, and has broad application prospects.

Laboratory experiments of CO_2 flooding are applied to support the implementation of CO_2 flooding in the field (Xie, 1991; Cheng et al., 2008; Ma et al., 2020). Many experts have made great contributions in this field. The influence of CO_2 on the viscosity and volume of oil was studied by Hao et al. (2005) through laboratory experiments, and the mechanism of CO_2 EOR was researched. Miller and Jones studied the effect of CO_2 on the physical properties of heavy oil (Miller and Jones, 1981; Sankur and Emanuel, 1983). Gao et al. (2020) analyzed the influence of development parameters on the CO_2 EOR through experiments (Gao et al., 2020). Wang et al. (2016) discussed periodic CO_2 injection through experiments in low-permeability porous media, and the influence of injection slug and velocity is revealed in their work (Wang et al., 2016). The differences between miscible flooding and immiscible flooding were compared by Zhao et al. (2018), and field experiments were conducted to support the research. The above works mainly focus on the mechanism of CO_2 EOR, and the effect of fractures was not studied.

Oil development of low permeability and tight reservoirs is often affected by fractures. On the one hand, by fracturing the injection well, the injection rate of CO_2 is improved and the reservoir energy can be recovered in a short time. On the other hand, the oil production well is usually fractured to improve the production rate in low-permeability reservoirs. As a high-conductivity channel, fractures are closely related to important parameters such as the swept volume and gas channeling during reservoir development. It is necessary to carry out experimental research on the effect of fractures on CO_2 flooding. In order to explore the effect of fractures on CO_2 flooding, Huang used cores with annulus to represent fractures (Huang et al., 2008). An experimental study of CO_2 huff and puff was conducted, showing that fractures had a great influence on the CO_2 huff and puff. In order to optimize the injection methods of CO_2 flooding after water flooding, CO_2 compound flooding experiments with single fracture and complex fracture in a five-spot well pattern were implemented, respectively (Shi et al., 2021). The physical model of fracture radial flow was used in their work. To develop fractured tight reservoirs effectively, Wang (2017) designed a CO_2 flooding experiment to analyze pressure transfer in fractured porous media (Wang, 2017). In this experiment, the fractures were formed with different apertures. By comparing the CO_2 flooding results with the control experiment, it was shown that the gas channeling caused by fracture was the key factor in the production of oil in the matrix. Existing experiments show that fractures have a significant impact on the development of CO_2 flooding in low-permeability and tight reservoirs. However, further research is required on pressure distribution, fluid composition, and fluid displacement.

In this study, artificial cores were made according to the formation parameters in Shengli Oilfield. Fracture length and aperture are the primary factors affecting CO_2 flooding. Therefore these fractures were made with different lengths and apertures. During CO_2 flooding, the pressure along the core and the components at the outlet was recorded. Then the influence of fractures on CO_2 flooding was investigated.

2 Experimental method

The experimental equipment contained UQT-120-70 high temperature and high pressure long-core test system, Bruker 450 GC, and Agilent 7890A GC as the main components. The pressure was measured with SENEX DG2113-C-70/B. The pressure measurement signal was automatically recorded by the computer data acquisition system and was set to be recorded every 2 min. The cores used in this experiment were artificially produced according to the formation parameters of Shengli Oilfield. After cleaning and drying, the basic parameters of the cores are shown in Table 1. The fractures were made by wire cutting, and quartz sand was used as a filler to support the fractures as shown in Figure 1.

Since it is difficult to obtain a single core longer than 0.5m, the commonly used method is splicing conventional cores in a certain arrangement. Filter paper was applied to connect short cores to eliminate the terminal effect. The arrangement of each core was as follows.

1) The harmonic mean permeability $\bar{k}$ of the n cores was calculated using Eq. 1. A comparison was made between $\bar{k}$ and the permeability of the n cores, to find the core whose permeability was closest to $\bar{k}$. Then this core was put in the first place at the outlet of the experimental device:

$$\frac{L}{\bar{k}} = \frac{L_1}{K_1} + \frac{L_2}{K_2} + \cdots + \frac{L_n}{K_n} = \Sigma_{i=1}^{n} \frac{L_i}{K_i} \tag{1}$$

TABLE 1 Parameters of cores.

Number	Diameter (cm)	Length (cm)	Porosity (%)	Permeability (mD)
01	2.48	25.17	20.3	37.07
02	2.51	29.32	20.1	39.22
03	2.47	25.13	19.9	39.75
04	2.48	30.11	19.8	40.11
05	2.50	24.97	20.2	39.83
06	2.51	30.2	20.1	40.15

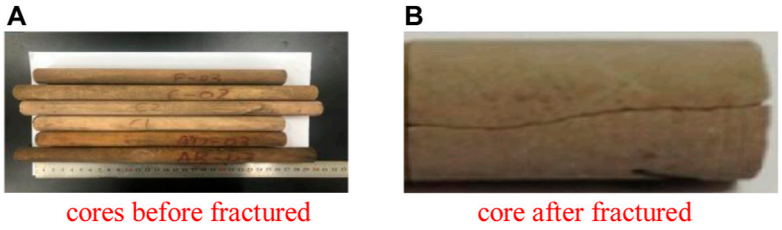

FIGURE 1
Part of cores used in this experiment. **(A)** Cores before fracture and **(B)** cores after being fracture.

where L is total length of the core, cm, $\bar{k}$ is the harmonized mean permeability of the core, $10^{-3}\mu m^2$, L_i is the length of the ith core, and K_i is the permeability of the ith core, $10^{-3}\mu m^2$.

2) The harmonic mean permeability of the remaining n-1 cores $\bar{k}$was calculated. The core whose permeability was closest to $\bar{k}$ was arranged in the second place.
3) The long cores were obtained using the above method.

Four kinds of cores were considered in this experiment: the control group (without fracture in cores), a core with fracture length 10 cm and aperture 0.05mm, a core with fracture length 20 cm and aperture 0.05 mm, and a core with fracture length 20 cm and aperture 0.1 mm. By carrying out CO_2 flooding experiments on different types of cores, the influences of fracture length and aperture on the pressure distribution, composition, and displacement effect during CO_2 flooding were studied. The fluid used in this experiment was obtained by compounding the oil and gas samples from the surface separator of a well in the block.

The experimental steps mainly included the following: ① Firstly, the core was cleaned with petroleum ether and dried with nitrogen, then dead oil was injected with a pump to fully saturate the core, and keep the pressure and temperature at formation conditions for some time. After the core was fully saturated, the amount of dead oil was recorded. ② The pressure and temperature at the outlet were set to 20 MPa and 50°C, respectively. Then the prepared live oil was used to displace the dead oil in the core until the gas-oil ratio at the inlet and outlet was the same to ensure that the core was completely saturated with live oil. ③ Industrial-purity CO_2 (99.9%) was injected at a constant rate to displace the oil in the core until no more oil was driven out at the outlet. The data record changed over time, including oil production, gas production, pressure at the measuring points, etc. The produced gas and oil samples were collected for chromatographic analysis. ④ After each experiment was finished, the cores were cleaned, dried with nitrogen, evacuated with a vacuum pump, and steps ① to ③ were repeated for the next set of experiments.

3 Results analysis

3.1 Analysis of the influence of fracture length on CO_2 flooding

3.1.1 Pressure distribution in cores with different fracture lengths

3.1.1.1 Control experiment

Firstly, the CO_2 flooding experiment in cores without fractures was carried out as a control experiment. The measuring points were set every 10 cm from the injection point. The outlet pressure remained unchanged, and the CO_2 was injected at a constant rate of 0.2 ml/min. The value of the

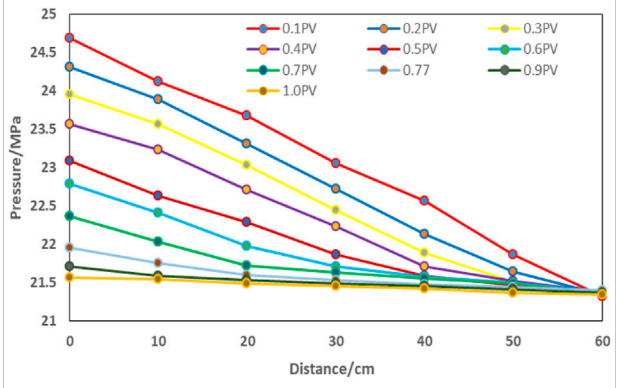

FIGURE 2
Pressure distribution at different times of the control experiment.

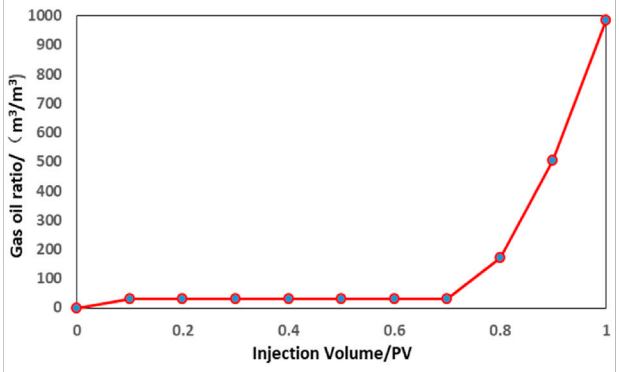

FIGURE 3
Gas-oil ratio at different times.

pressure at each measuring point was recorded, as shown in Figure 2.

The pressure at each measuring point gradually decreased with displacement time before CO_2 broke through the core. It indicated that in the initial stage of gas injection, high pressure was required to generate a pressure difference between the inlet and outlet. Stable flooding was formed after the experiment had been carried out for a period of time. At this stage, the required injection pressure at the inlet was decreased. The flow resistance was decreased by reducing the unswept area. Therefore the required pressure became smaller with CO_2 flooding. The gas-oil ratio in Figure 3 shows that the CO_2 broke through the core at 0.77 PV. Before CO_2 was detected at the outlet, it can be seen from Figure 2 that the pressure difference was significantly smaller than the initial pressure difference. It shows that, after the gas broke through, the constant-rate flooding could be achieved with a low pressure difference.

3.1.1.2 Fracture lengths of 10 and 20 cm

Two kinds of cores were considered in this case. One contained a 10-cm fracture and the other a 20-cm fracture. The aperture of both fractures was 0.05 mm. The measuring points were set every 10 cm from the injection point. The outlet pressure remained unchanged, and the CO_2 was injected at a constant rate of 0.2 ml/min. The values of the pressure at each measuring point were recorded, as shown in Figure 4. The curves of gas oil ratio for these two cases are shown in Figure 5.

Compared with the control experiment, the required injection pressure of the cores with fracture was smaller. Similarly, before CO_2 was detected at the outlet, the pressure at each measuring point decreased with the displacement time. The high permeability of the fractures led to low energy loss when fluid flowed through the fracture. Therefore the pressure in the fracture area did not decrease much with distance. But after passing through the fractured area, the descent rate of pressure was faster.

It indicates that fractures can reduce the required injection pressure because of their high permeability. As the experiment continued, the high-viscosity oil area gradually decreased and the flow resistance became smaller simultaneously. Figure 5 shows that the CO_2 broke through the core at 0.64 PV and 0.58 PV, respectively. Before CO_2 was detected at the outlet, it can be seen from Figure 4 that the pressure distribution had been reduced to 1.2 MPa. When the fracture length was 20 cm, the required injection pressure was lower than when the fracture length was 10 cm. It indicates that the fractures could effectively reduce the pressure difference between the injection and the production point.

3.1.2 Components at outlet of the cores with different fracture lengths

The outlet was used as the collection point to record the cumulative production of the cores at different times. The gas-oil ratio at different times was obtained according to the instantaneous production. The component composition under standard conditions was obtained by chromatography. Four time points were selected to analyze the component, including the time before CO_2 broke through the core, the time when CO_2 broke through the core, the time after CO_2 broke through the core, and the later stage of CO_2 flooding. The molar composition of each component in the gas phase and the oil phase was obtained according to the chromatographic analysis, as shown in the following Figures 6, 7.

1) Length of fracture 10 cm
2) Lengths of fracture 20 cm

The molar composition of gas and oil are shown in Figures 6, 7. It is obvious that CH_4 accounts for the largest proportion in the gas phase before CO_2 was detected. Part of the CO_2 was separated from the oil, less than 10%. After the CO_2 was detected, the proportion of CH_4 continued to decrease, and the proportion of CO_2 continued to increase, until the gas component at the outlet was mainly CO_2.

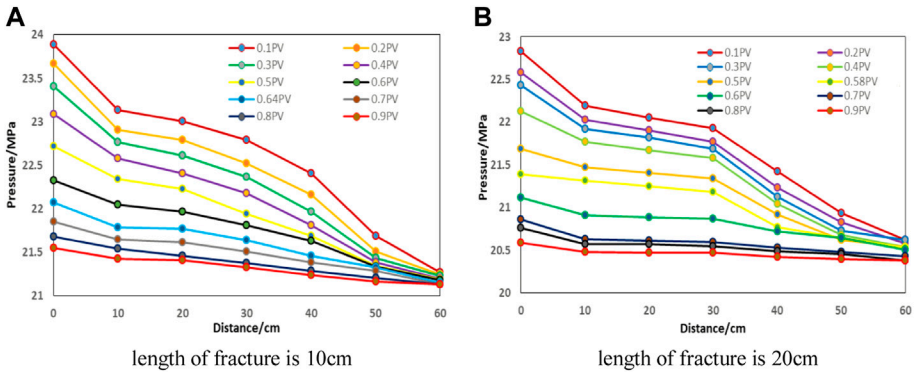

FIGURE 4
Pressure distribution in cores with different fracture lengths. **(A)** Length of fracture 10 cm and **(B)** length of fracture 20 cm.

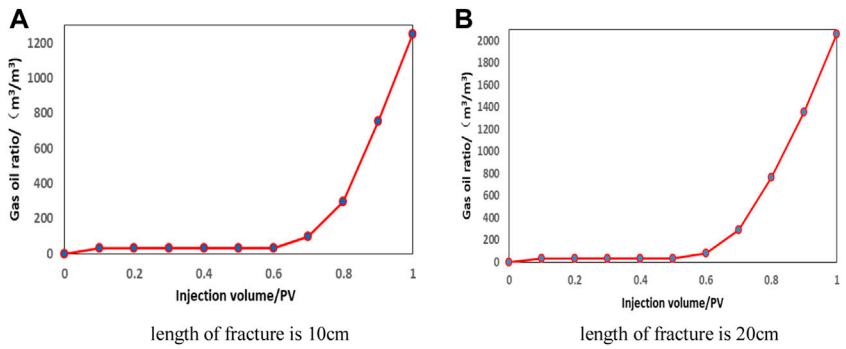

FIGURE 5
Gas oil ratio at outlet with different fracture lengths. **(A)** Length of fracture 10 cm and **(B)** length of fracture 20 cm.

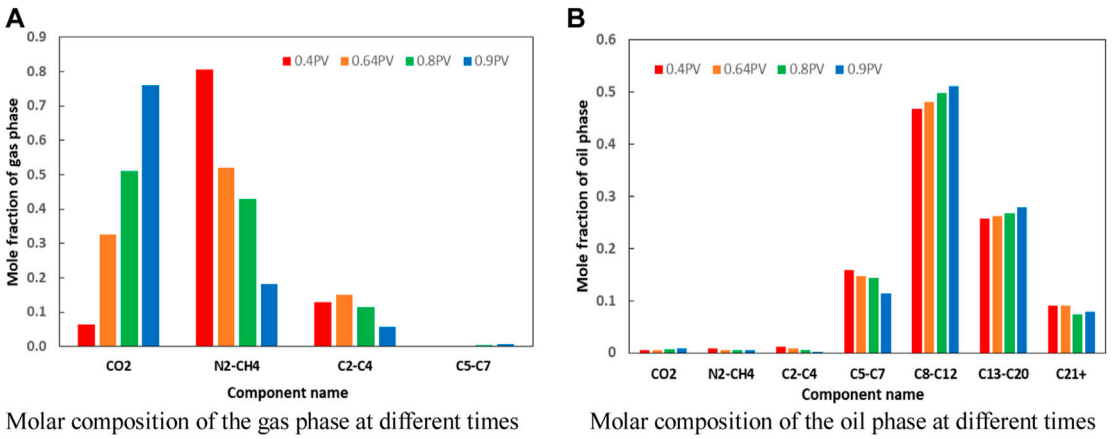

FIGURE 6
Molar composition at different times. **(A)** Molar composition of the gas phase at different times and **(B)** molar composition of the oil phase at different times.

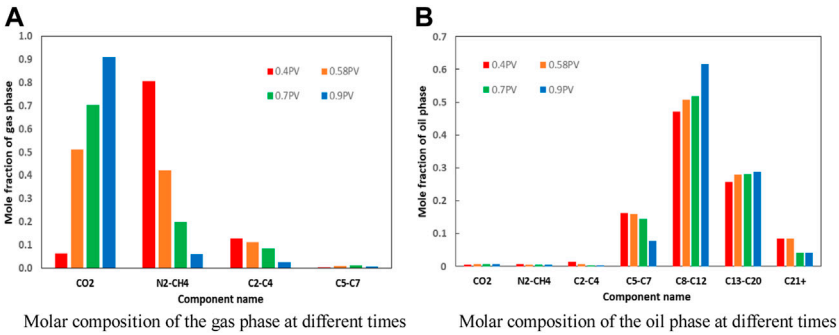

FIGURE 7
Molar composition at different times. **(A)** Molar composition of the gas phase at different times and **(B)** molar composition of the oil phase at different times.

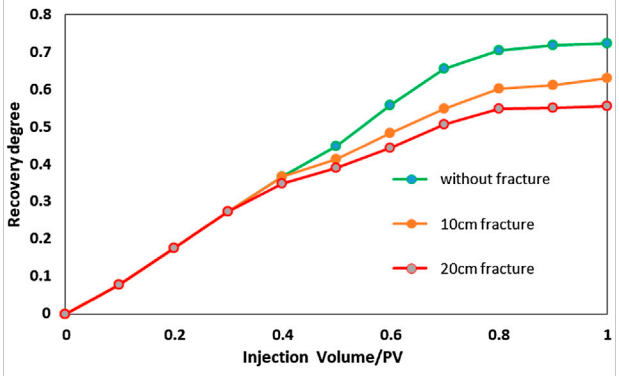

FIGURE 8
Comparison of the recovery degree of different fracture lengths.

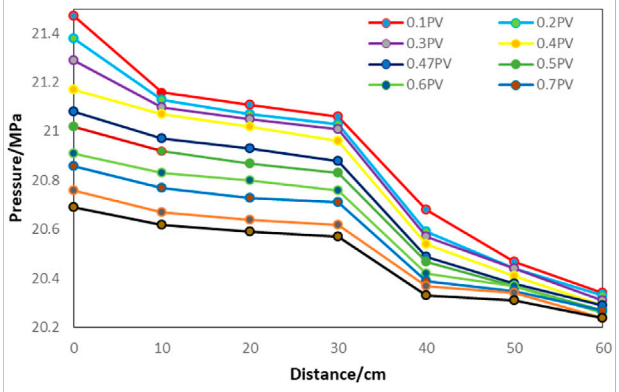

FIGURE 9
Pressure distribution at different times.

It can be seen from the oil phase composition that at the outlet, the proportion of light hydrocarbon components C_5-C_7 decreased after gas was detected. Meanwhile, the proportion of intermediate components C_8-C_{12} and heavy components C_{13}-C_{20} increased. This shows that CO_2 could extract light components from oil. After the light components were extracted, the viscosity of the oil in the swept area was increased, and it was difficult to bring out the heavy components. Therefore, the proportion of heavy components at the outlet continued to decrease.

The proportion of CO_2 in the gas was different, as seen by comparing the gas components in Figures 6, 7. The produced gas contained more CO_2 in the core with the 20-cm fracture. It demonstrates that the fracture could exacerbate the gas channeling of CO_2. On the other hand, the fracture had little effect on the component of the produced oil. The main difference was in the core with the 20-cm fracture; the final proportion of intermediate components C_8-C_{12} was increased (the molar fraction of C_8-C_{12} in the 10-cm fracture was increased to 0.51, and the mole fraction of C_8-C_{12} in 20 cm fracture was increased to 0.62). It indicates that the fracture could lead to the reduction of the extraction and displacement of CO_2.

The results in Figure 8 show that the final oil recovery was closely connected to the fracture length. A longer fracture had a greater influence on the gas channeling during the CO_2 flooding process. Therefore, the oil recovery decreased as the fracture length increased.

3.2 Analysis of the influence of fracture aperture on CO_2 flooding

The fracture with an aperture of 0.1 mm was made and compared with the above fracture with an aperture of 0.05 mm.

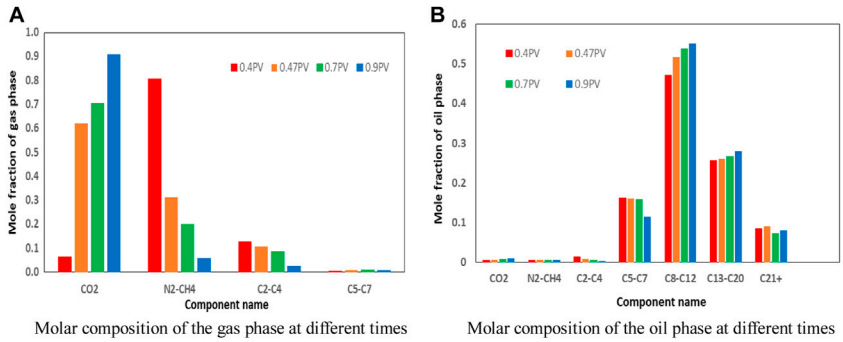

FIGURE 10
Molar composition at different times. **(A)** Molar composition of the gas phase at different times and **(B)** molar composition of the oil phase at different times.

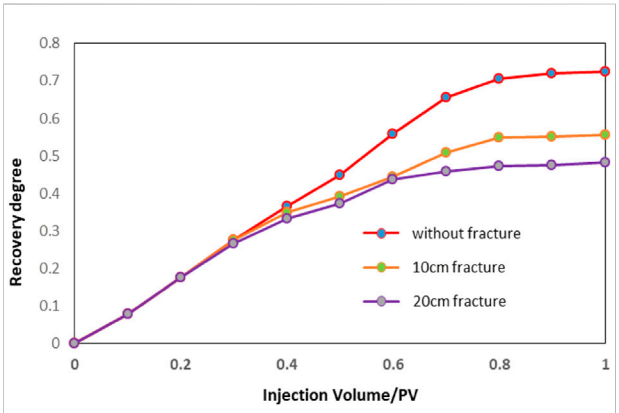

FIGURE 11
Comparison of the recovery degree of different fracture apertures.

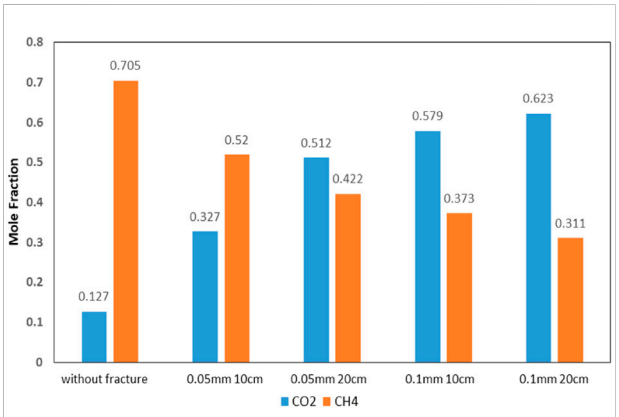

FIGURE 13
Main components of the gas phase at the moment when gas was detected.

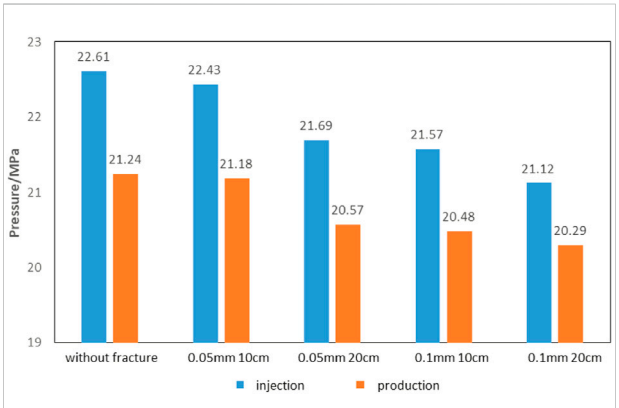

FIGURE 12
Pressure in different experiments.

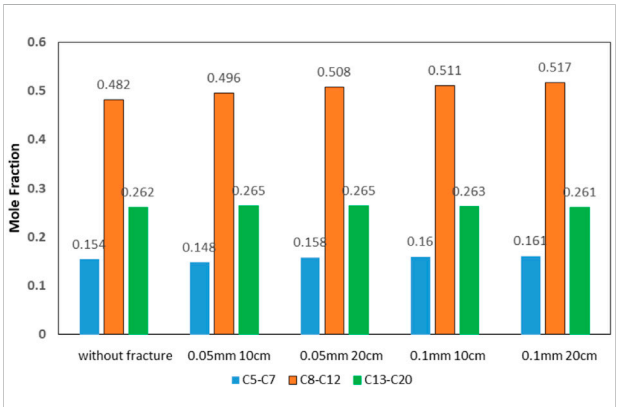

FIGURE 14
Main components of the oil phase at the moment when CO_2 was detected.

The lengths of both fractures were 20 cm. The measuring points were set every 10 cm from the injection point. The outlet pressure remained unchanged, and the CO_2 was injected at a constant rate of 0.2 ml/min. The pressure distribution is shown in the following Figure 9.

Compared with the 0.05 mm fracture aperture in the previous section, the required pressure was smaller. Similar to the conclusion of fracture length, the larger the fracture aperture, the smoother the pressure change. The fracture aperture led to greater effective permeability to reduce the injection-production pressure difference.

The proportion of CO_2 in gas was different in the cores with different apertures as shown in Figure 10. The produced gas contained more CO_2 in the core with the 0.1 mm fracture. More than 60% of CO_2 was detected at the outlet when the fracture aperture was 0.1 mm. The fracture had little effect on the component of the produced oil.

The results in Figure 11 show that although the larger fracture aperture may have reduced the pressure difference between the injection and the production point, the gas was able to flow along the high-permeability fracture; this was not conducive to a balanced displacement.

3.3 Analysis of the influence of fracture on CO_2 flooding

The pressure before CO_2 was detected at the injection and production point is shown in Figure 12.

The results show that before CO_2 was detected, a larger pressure difference was required in the control experiment. The pressure difference between the injection and production point was about 1.4 MPa. The pressure difference would drop if there was a fracture, and the longer the fracture, the smaller the injection-production pressure difference. The fracture aperture had a similar influence on the pressure. Comparing the control experiment and experiment with the fracture of 0.1 mm and aperture 20 cm length, the injection-production pressure difference was reduced by 40%.

The outlet molar fraction was taken at the moment of gas being detected under the five conditions for comparison, and the results are shown in Figure 13.

The results show that at the moment of gas being detected, the mole fraction of CO_2 was the lowest in the control experiment, which was only 12.7%. With an increase in fracture length and aperture, the proportion of CO_2 increased to 62.3% when the CO_2 broke through the core. Long and wide fractures shortened the CO_2 breakthrough time at the outlet, and the injected CO_2 had no chance to contact the oil and improve the condition. Therefore the rapid increase of CO_2 affected the displacement efficiency.

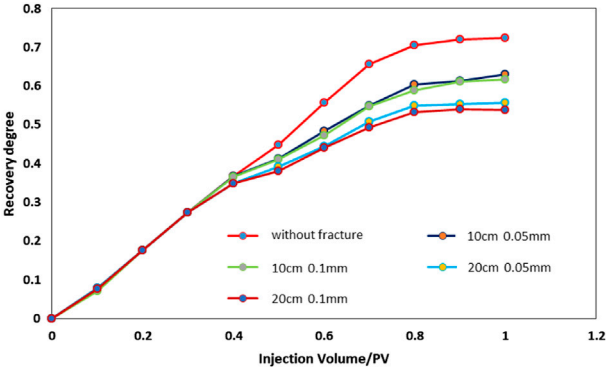

FIGURE 15
Comparison of the recovery degree of the different cases.

The light components C_5-C_7, intermediate components C_8-C_{12}, and heavy components C_{13}-C_{20} were taken under five conditions for comparison, and the results are shown in Figure 14.

The results show that the increase of fracture aperture and length had little influence on the oil phase composition at the moment of CO_2 breaking the core.

Figure 15 shows that the control experiment had the highest oil recovery. The increase in fracture length and aperture aggravated the gas channeling which led to a decrease in oil recovery. Besides this, compared with the fracture width, the fracture length had a greater impact on the CO_2 flooding.

4 Conclusion

A CO_2 flooding experiment in a long core was designed. The artificial cores and live oil were prepared according to the reservoir parameters in Shengli Oilfield. The inlet was injected with CO_2 at a constant speed of 0.2 ml/min. The pressure distribution along the core and components of the gas phase and oil phase at the outlet was tested. The results demonstrate the following:

1) The CO_2 flooding experiments on the matrix cores show that the pressure of each measuring point decreased rapidly with time in the early stage. After CO_2 broke through the core, the injection-production pressure difference decreased with the decrease of flow resistance. It indicates that constant speed displacement could be achieved without high injection pressure after the gas broke through. The proportion of CH_4 in the gas phase at the outlet exceeded 70% when CO_2 broke through the core. Then the proportion of methane continued to decrease, and the proportion of CO_2 continued to increase until the gas component at the outlet was mainly CO_2. The proportion of light and intermediate components increased after CO_2 broke through the core.

2) It shows that the long and wide fracture could effectively reduce the injection-production pressure difference. With the increase in fracture length and aperture, the recovery degree decreased from 72.41% to 48.15%. In general, the fracture length and aperture had obvious effects on the pressure distribution and the displacement efficiency.
3) Fracture length and aperture had a significant effect on the gas phase composition at the outlet. Wide and long fractures shortened the CO_2 breakthrough time, and the rapid increase of CO_2 at the outlet affected the displacement efficiency. Generally speaking, the increase of fracture aperture and length had little effect on the oil phase composition.

Data availability statement

The data analyzed in this study is subject to the following licenses/restrictions: The data are used for scientific analysis. Requests to access these datasets should be directed to emcgroup@163.com.

Author contributions

The author confirms being the sole contributor of this work and has approved it for publication.

Conflict of interest

ZQ-F was employed by Shengli Oilfield Company, SINOPEC.

Publisher's note

All claims expressed in this article are solely those of the authors and do not necessarily represent those of their affiliated organizations, or those of the publisher, the editors, and the reviewers. Any product that may be evaluated in this article, or claim that may be made by its manufacturer, is not guaranteed or endorsed by the publisher.

References

Cao, C., Liu, H., and Hou, Z. (2020). A Review of CO_2 Storage in View of Safety and Cost-Effectiveness[J]. *Energies* 13 (3), 600. doi:10.3390/en13030600

Cheng, J., Lei, Y., and Zhu, W. (2008). Pilot test on CO2 flooding in extra-low permeability Fuyu oil layer in DaQing placanticline. *Nat. Gas. Geosci.* 19 (3), 402–409.

Gao, M., Ni, J., Wang, X., Ma, B., and Wang, H. (2020). Experimental study on effects of CO2 flooding in ultra-low permeability reservoir under different parameters. *J. Xi'an Shiyou Univ. Nat. Sci. Ed.* 35 (3), 60–65. doi:10.3969/j.issn.1673-064X.2020.03.008

Guo, P., Li, S., and Du, Z. (2002). Evaluation of enhanced oil recovery by gas injection in low permeability reservoirs. *J. Southwest Petroleum Inst.* 24 (5), 46–50. doi:10.3863/j.issn.1000-2634.2002.05.015

Hao, Y., Bo, Q., and Chen, M. (2005). Laboratory investigation of CO_2 flooding. *Petroleum Explor. Dev.* 32 (2), 110–112. doi:10.3321/j.issn:1000-0747.2005.02.027

He, Y., Gao, H., and Zhou, X. (2011). Study on method for improving displacement ef-fect of CO2 in extra-low permeability reservoir. *Fault-block oil gas field* 18 (4), 512–515.

Huang, Q., Zhang, J., and Wang, K. (2008). Laboratory experimental study on CO2 huff and puff flooding in fractured core system. *Foreign oilfield Eng.* 24 (4), 9–12. doi:10.3969/j.issn.2095-1493.2008.04.003

Jiang, H., Shen, P., and Lu, Y. (2010). Research on the status of CO2 enhanced oil and gas resource recovery in the world. *Special Oil Gas Reservoirs* 17 (2), 5–10. doi:10.3969/j.issn.1006-6535.2010.02.002

Ma, Q., Hou, S., Lv, B., and Song, S. (2020). Expansion experiment study of CO2 injection in XG oilfield. *J. Green Sci. Technol.* 16, 222–224.

Miller, J. S., and Jones, R. A. (1981). "A laboratory study of determine physical characteristics of heavy oil after CO_2 saturation," in *SPE/DOE Enhanced Oil Recovery Symposium* (OnePetro). doi:10.2118/9789-MS

Sankur, V., and Emanuel, A. S. (1983). "A laboratory study of heavy oil recovery with CO_2 injection," in SPE California Regional Meeting (OnePetro). doi:10.2118/11692-MS

Shi, L., Wang, W., Wang, C., and Chen, L. (2021). Study on injection mode of CO_2 flooding based on physical model of fracture radial flow. *Special oil gas reservoirs* 28 (3), 112–117. doi:10.3969/j.issn.1006-6535.2021.03.017

Wang, P. (2017). Experimental study and application of carbon dioxide constant volume miscible-flooding in fractured-tight reservoir. *J. Chengde petroleum Coll.* 174 (1), 10–14. doi:10.3969/j.issn.1008-9446.2017.01.003

Wang, W., Chen, L., Tang, R., Wang, H., and Yang, H. (2016). Experimental study of cycle CO2 injection for low permeability reservoir. *Fault-block oil gas field* 23 (2), 206–209. doi:10.6056/dkyqt201602016

Xie, S. (1991). Laboratory study of CO2 flooding in Daqing oilfield. *Petroleum Geol. Oilfield Dev. Daqing* 10 (4), 51–58.

Zhao, Y., Zhao, X., Li, J., Yao, Z., and Zhao, Y. (2018). Indoor experiment and field application of CO2 flooding in ultra-low permeability oil reservoir. *Petroleum Geol. Oilfield Dev. Daqing* 37 (1), 128–133. doi:10.19597/J.ISSN.1000-3754.201706040

frontiers | Frontiers in Earth Science

TYPE Opinion
PUBLISHED 16 September 2022
DOI 10.3389/feart.2022.1007916

OPEN ACCESS

EDITED BY
Qingbang Meng,
China University of Geosciences
Wuhan, China

REVIEWED BY
Lei Li,
Shandong Institute of Petroleum and
Chemical Technology Dongying, China
Xiukun Wang,
China University of Petroleum, China

*CORRESPONDENCE
Xun Zhong,
zhongxun@yangtzeu.edu.cn

SPECIALTY SECTION
This article was submitted to
Geochemistry,
a section of the journal
Frontiers in Earth Science

RECEIVED 31 July 2022
ACCEPTED 22 August 2022
PUBLISHED 16 September 2022

CITATION
Chen Y, Zhong X, Huang L and Sheng G (2022), Comparative study on the analysis methods of fracture pressure interference in shale oil three-dimensional fracturing.
Front. Earth Sci. 10:1007916.
doi: 10.3389/feart.2022.1007916

Comparative study on the analysis methods of fracture pressure interference in shale oil three-dimensional fracturing

Yanan Chen[1,2], Xun Zhong[1,2]*, Luoyi Huang[1,2] and Guanglong Sheng[1,2]

[1]Hubei Key Laboratory of Drilling and Production Engineering for Oil and Gas, Yangtze University, Wuhan, China, [2]School of Petroleum Engineering, Yangtze University, Wuhan, China

KEYWORDS

shale oil, fracture morphology, interlayer connectivity, pressure interference identification, reservoir pressure

Introduction

With the improvement of oil exploration and development technology, the proportion of tight reservoirs in new reserves is getting higher and higher. As an important part of tight reservoirs, thin interbedded tight reservoirs account for more and more. According to investigation and evaluation, about 30% of the oil and gas in the world are stored in thin interbeds of sand and mudstone. Therefore, the rational development of such reservoirs is an important means to actively adjust the energy structure of our country and realize energy replacement. Thin interbedded low-permeability reservoirs of countries generally demonstrate the following geological characteristics: deeply buried with sandstone layer and mudstone layer appearing alternately, sand bodies scattered and developed, multiple vertical layers with small single-layer thickness, poor reservoir physical properties with low reserves abundance, small pores, narrow throats, and low permeability (Surdam et al., 1982; Surdam and Crossey, 1985; Seewald, 2003; Sonnenberg et al., 2009). The development of thin interbedded low-permeability reservoirs is facing many challenges, such as low oil production rate, low recovery, low single-well production capacity, and great difficulty in production stabilization (Du et al., 2014; Feng et al., 2020; Sheng et al., 2020). Meanwhile, the fracture morphology is hard to control, and the stage number in a horizontal staged fracturing can be very limited. The results are far from satisfying (Zhang et al., 2014; Li et al., 2016; Tan et al., 2017; Sheng et al., 2019; Zhou et al., 2020). Without a sufficient understanding of interlayer fracture pressure interference in a fracturing operation, the effective development of thin interbedded low-permeability reservoirs would be restricted (Liu et al., 2018; Lu et al., 2020; Meng et al., 2020). Therefore, it is of crucial importance to accurately analyze and identify the interlayer fracture pressure interference and quantitatively describe the actual fracturing effect and fracture morphology of thin interbedded shale oil reservoirs. At present, microseismic technology, tracer technology, and pressure monitoring technology can all be used to analyze the pressure channeling of interlayer fractures in fracturing construction. However, the results obtained by single application of one of the three

methods are not accurate. By analyzing the advantages and limitations of the three methods, a comprehensive application of the three methods can better describe the actual fracturing operation effect and fracture morphology.

Geologic features

The No. 58 platform studied in this paper is a typical thin interbedded shale oil reservoir. The "Sweet Spot" can be divided into seven sub-layers from top to bottom, and the oil layers are mainly distributed in the first, second, and third sub-layers. The average effective porosity of the oil layer is 8.36%, and the average permeability is 0.0047mD. The platform has a total of eight wells in the well area, and the three-dimensional development deployment mode is adopted. The well spacing is 200 m, and each well has undergone fracturing operations. The average fracturing process has 40 stages, the average cluster spacing is 5.8 m, and the average interval is 46 m. In this paper, pressure interference analysis was carried out on thin interbedded shale oil fracturing fractures in platform No. 58.

Longitudinal interference analysis and identification with different fracture monitoring methods

Microseismic technology

Microseismic monitoring technology can inversely locate the focal position through the study of the focal mechanism in the process of monitoring the fracture propagation behavior of reservoir fracturing, and determine the formation process, fracture orientation, length, and other information of fractures (Chunyan et al., 2018; Salishchev et al., 2020). Well 5 and Well 3 were selected for research. The vertical microseismic monitoring data of Well 5 shows that the upper fracture height is 20 m and the lower fracture height is 24 m. The vertical microseismic monitoring data of Well 3 shows that the upper fracture height is 18 m and the lower fracture height is 24 m. Well 5 and Well 3 are in the second sub-layer with an average layer thickness of 10.4 m. The thickness of the upper adjacent layer, the first sub-layer, is 5.9 m, and the thickness of the lower adjacent layer, the third sub-layer, is 8.6 m. By comparing the vertical thickness of the second layer and its adjacent layers, it is easy to conclude that the fracture pressures of Well 5 and Well 3 have vertically interfered with the first, second, and third sub-layers (Wu et al., 2017; Vadim et al., 2018; Xiong et al., 2019; Zhang et al., 2019).

Tracer technology

The tracer enters the formation synchronously with the fracturing fluid during the fracturing process. During backflow after fracturing, the backflow fluid is intensively sampled at a certain time interval to obtain the tracer backflow curve. The purpose of fracturing effect evaluation can be achieved by interpreting the tracer backflow curve (Ruixiang et al., 2007; Lingtao et al., 2022). Tracers were injected into Well 3 located in the second sub-layer, and then they were detected in Well 2 located in the first sub-layer and Well 4 located in the third sub-layer. This indicates that the fractures have connected the first, second, and third sub-layers. Well 5 and Well 6 are close to Well 4 and vertically located in the same layer; tracers were also detected in them. Meanwhile, the fracture morphology in the fracturing stage is characterized by analyzing the tracer breakthrough curve (BTC) of fracturing fluid recovery (Li et al., 2016). When tracers were injected into Well 4, the tracer production in Well 3 would decrease with time, indicating that the vertical fractures that connect the third and the second sub-layers might close. According to the identification results of fracture pressure interference based on tracer monitoring data (Lisa et al., 2019; Abdulaziz et al., 2020; Fu et al., 2020; Zhao et al., 2020), we could conclude that the fracture pressures of Well 3 have vertically interfered with the first, second, and third sub-layers.

Pressure monitoring technology

In the process of fracturing construction, the initiation and extension of hydraulic fractures in three-dimensional space are related to construction pressure. The decline speed of the bottom hole (wellhead) pressure after the pump is stopped can reflect the filtration property of the formation. Therefore, the purpose of fracturing effect evaluation can be achieved by analyzing the change in fracturing pressure. Well 3 was selected as the monitoring well to study the dynamic pressure changes of adjacent wells during the fracturing operation. The results showed that the pressures of Wells 1, 2, 4, 5, and 6 were significantly increased. The noticeable pressure increases of Well 1 in the upper, first sub-layer indicated that the pressure of Well 3 had interfered with the upper oil layer. The pressure of Wells 4, 5, and 6 located in the third sub-layer also increased significantly, indicating that the pressure of Well 3 had interfered with the lower, third sub-layer. In summary, the identification results of fracture pressure interference based on pressure interference monitoring data (Shahbazi et al., 2015; Escobar et al., 2021; Seth et al., 2021) suggested that the fracture pressures of Well 3 have vertically interfered with the first, second, and third sub-layers.

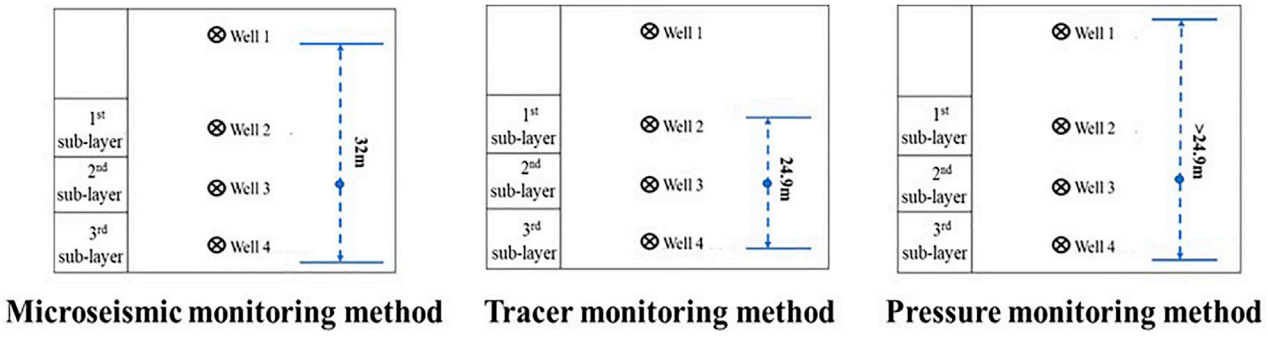

FIGURE 1
Comparative analysis of different identification methods.

Comparative analysis of different identification methods

Taking Wells 1, 2, 3, and 4 as examples, the analysis results of the three analysis methods of fracture pressure interference are shown in Figure 1.

The comparison results showed that the tracer monitoring method was the most accurate to analyze and identify fracture pressure interference. When tracers were injected into a certain well and could be detected in other wells, it was clear that these wells were connected and there were inter-well interferences. The microseismic monitoring method could locate the approximate locations of fractures with pressure interferences, but the predicted ranges were generally wider than the actual ones. The pressure monitoring technology could roughly generate the spread ranges of fracture pressure interference based on the dynamic pressure changes of adjacent wells, but the generated ranges were generally broader than the ones given by the tracer monitoring method. Though the tracer monitoring method showed the highest accuracy, its detection results can be sensitive to the locations of tracer injection and detection wells; for example, for layers without detection wells, the inter-well connectivity can be hard to identify. Therefore, to generate a more comprehensive fracture pressure interference report, the three methods should always be used together. Take the tracer monitoring method as the main body, use the microseismic monitoring method generated specific fracture ranges as constraints, and conduct further analysis by referring to the monitored pressure data in actual fracturing operations. Synthetical applications of the three methods are beneficial to the effective analysis and identification of interlayer fracture pressure interference. Furthermore, the fracture morphology in thin interbedded shale oil fracturing and the actual fracturing effect can be more accurately characterized and evaluated.

Conclusion

(1) The tracer monitoring method was the most accurate to analyze and identify fracture pressure interference. The scope of the microseismic monitoring method and pressure monitoring technology is wider than that given by the tracer monitoring method.
(2) Synthetic applications of the three methods are beneficial to the effective analysis and identification of interlayer fracture pressure interference. In addition, the fracture morphology in thin interbedded shale oil fracturing and the actual fracturing effect can be more accurately characterized and evaluated.

Author contributions

YC: investigation and research,conceptualization, writing—Original draft preparation, data curation XZ: resources, translation LH: modify analysis GS: supervision, typesetting.

Funding

This work was supported by the Open Fund of Hubei Key Laboratory of Drilling and Production Engineering for Oil and Gas (Yangtze University) (ID: YQZC202203), the Scientific Research Development Fund of Yangtze University.

Conflict of interest

The authors declare that the research was conducted in the absence of any commercial or financial relationships that could be construed as a potential conflict of interest.

Publisher's note

References

Al-Qasim, A., Kokal, S., Hartvig, S., and Huseby, O. (2020). Subsurface monitoring and surveillance using inter-well gas tracers. *Upstream Oil Gas Technol.* 3 (C), 100006. doi:10.1016/j.upstre.2020.100006

Aleksandrov, V., Kadyrov, M., Ponomarev, A., Drugov, D., and Bulgakova, I. (2018). Microseismic multistage formation hydraulic fracturing (MFHF) monitoring analysis results. *Key Eng. Mat.* 785, 107-117. doi:10.4028/www.scientific.net/KEM.785.107

Chunyan, C., Zhiruo, C., Enhao, L., Hu, L., Liu, Y., and Chen, P. (2018). Research progress of hydraulic fracturing technology and microseismic monitoring technology. *Sci. Technol. Inf.* 16 (28), 68–70. doi:10.16661/j.cnki.1672-3791.2018.28.068

Du, J., Liu, H., Ma, D., Fu, J., Wang, Y., and Zhou, T. (2014). Discussion on effective development techniques for continental tight oil in China. *petroleum Explor. Dev.* 41 (02), 198–205. (In Chinese). doi:10.1016/S1876-3804(14)60025-2

Escobar, F. H., Prada, E. F., and Suescún-Díaz, D. (2021). Interpretation of pressure interference tests for wells connected by a large hydraulic fracture. *J. Pet. Explor. Prod. Technol.* 11 (8), 3255–3265. doi:10.1007/s13202-021-01249-4

Feng, Q., Xu, S., Xing, X., Zhang, W., and Wang, S. (2020). Advances and challenges in shale oil development: A critical review. *Adv. Geo-Energy Res.* 4 (4), 406–418. doi:10.46690/ager.2020.04.06

Fu, Y., and Dehghanpour, H. (2020). How far can hydraulic fractures go? A comparative analysis of water flowback, tracer, and microseismic data from the horn river basin. *Mar. Petroleum Geol.* 115, 104259. (Pre-publish). doi:10.1016/j.marpetgeo.2020.104259

Li, J., Pei, Y., Jiang, H., Zhao, L., Li, L., Zhou, H., et al. 2016. Tracer flowback based fracture network characterization in hydraulic fracturing. Paper presented at the Abu Dhabi International Petroleum Exhibition & Conference, Abu Dhabi, UAE, November 7–10.

Lingtao, M., Wenhui, B., Bumin, G., Shen, J., and Sun, H. (2022). Research progress of tracer technology in fracturing effect evaluation. *Appl. Petrochem. field* 41 (3), 123–124. doi:10.3969/j.issn.1673-5285.2022.03.001

Liu, R., Jiang, Y., Huang, N., and Sugimoto, S. (2018). Hydraulic properties of 3D crossed rock fractures by considering anisotropic aperture distributions. *Adv. Geo-Energy Res.* 2 (2), 113–121. doi:10.26804/ager.2018.02.01

Lu, M., Su, Y., Zhan, S., and Almrabat, A. (2020). Modeling for reorientation and potential of enhanced oil recovery in refracturing. *Adv. Geo-Energ. Res.* 4 (1), 20–28. doi:10.26804/ager.2020.01.03

Meng, M., Chen, Z., Liao, X., Wang, J., and Shi, L. (2020). A well-testing method for parameter evaluation of multiple fractured horizontal wells with non-uniform fractures in shale oil reservoirs. *Adv. Geo-Energy Res.* 4 (2), 187–198. doi:10.26804/ager.2020.02.07

Puneet, S., Ripudaman, M., Ashish, K., and Sharma, M. M. (2021). Analyzing pressure interference between horizontal wells during fracturing. *J. Petroleum Sci. Eng.* 204, 108696. doi:10.1016/j.petrol.2021.108696

Ringel, L. M., Somogyvári, M., Jalali, M., and Bayer, P. (2019). Comparison of hydraulic and tracer tomography for discrete fracture network inversion. *Geosciences* 9 (6), 274. doi:10.3390/geosciences9060274

Ruixiang, Y., Taisheng, Z., and Weisheng, Z. (2007). Oilfield tracer technology [J]. *Ind. water Treat.* 27 (8), 12–15. doi:10.3969/j.issn.1005-829X.2007.08.004

Salishchev, M. V., Shirnen, A. A., Khamadaliev, D. M., and Chaplygin, D. A. 2020. Logging, well testing and microseismic fracture geometry investigations: Mistakes, lessons learnt and challenges. Paper presented at the SPE Russian Petroleum Technology Conference, Virtual, October 26–29.

Seewald, J. S. (2003). Organic-inorganic interactions in petroleum-producing sedimentary basins. *Nature* 426 (6964), 327–333. doi:10.1038/nature02132

Shahbazi, S., Maarefvand, P., and Gerami, S. (2015). Investigation on flow regimes and non-Darcy effect in pressure test analysis of horizontal gas wells. *J. Petroleum Sci. Eng.* 129, 129. doi:10.1016/j.petrol.2015.02.034

Sheng, G. L., Su, Y. L., and Wang, W. D. (2019). A new fractal approach for describing induced-fracture porosity/permeability/compressibility in stimulated unconventional reservoirs. *J. Petroleum Sci. Eng.* 179, 855–866. doi:10.1016/j.petrol.2019.04.104

Sheng, G. L., Zhao, H., Su, Y., Javadpour, F., Wang, C., Zhou, Y., et al. (2020). An analytical model to couple gas storage and transport capacity in organic matter with noncircular pores. *Fuel* 268, 117288. doi:10.1016/j.fuel.2020.117288

Sonnenberg, S. A., and Pramudito, A. (2009). Petroleum geology of the giant elm coulee field, williston basin. *Am. Assoc. Pet. Geol. Bull.* 93 (9), 1127–1153. doi:10.1306/05280909006

Surdam, R. C., Boese, S., and Crossey, L. J. (1982). Role of organic and inorganic reactions in development of secondary porosity in sandstones. *AAPG Bull.* 66 (5), 635. doi:10.1306/03B5A214-16D1-11D7-8645000102C1865D

Surdam, R. C., and Crossey, L. J. (1985). Organic-inorganic reactions during progressive burial: Key to porosity and permeability enhancement and preservation. *Philosophical Trans. R. Soc. Lond. Ser. A, Math. Phys. Sci.* 315 (1531), 135–156. doi:10.1098/rsta.1985.0034

Tan, P., Jin, Y., Han, K., Zheng, X., Hou, B., Gao, J., et al. (2017). Vertical propagation behavior of hydraulic fractures in coal measure strata based on true triaxial experiment. *J. Petroleum Sci. Eng.* 158, 398–407. doi:10.1016/j.petrol.2017.08.076

Wu, F., Yan, Y., and Yin, C. (2017). Real-time microseismic monitoring technology for hydraulic fracturing in shale gas reservoirs: A case study from the southern sichuan basin. *Nat. Gas. Ind. B* 4 (1), 68–71. doi:10.1016/j.ngib.2017.07.010

Xiong, W. (2019). Application of micro-seismic monitoring technology in fracturing and water injection development of horizontal wells with low permeability and thin layer. *IOP Conf. Ser. Earth Environ. Sci.* 252 (5), 052018. doi:10.1088/1755-1315/252/5/052018

Zhang, A., Yang, Z., Li, X., Xia, D., Zhang, Y., Luo, Y., et al. (2020). An evaluation method of volume fracturing effects for vertical wells in low permeability reservoirs. *Petroleum Explor. Dev.* 47 (02), 441–448. (In Chinese). doi:10.1016/s1876-3804(20)60061-1

Zhang, B., Tian, X., Ji, B., Zhao, J., Zhu, Z., and Yin, S. (2019). Study on microseismic mechanism of hydro-fracture propagation in shale. *J. Petroleum Sci. Eng.* 178, 711–722. doi:10.1016/j.petrol.2019.03.085

Zhou, D., and Zhang, G. (2020). A review of mechanisms of induced fractures in SC-CO2 fracturing. *Petroleum Sci. Bull.* 5 (02), 239–253. (In Chinese). doi:10.3969/j.issn.2096-1693.2020.02.021

frontiers | Frontiers in Earth Science

TYPE Original Research
PUBLISHED 16 September 2022
DOI 10.3389/feart.2022.990684

OPEN ACCESS

EDITED BY
Jianlin Zhao,
ETH Zürich, Switzerland

REVIEWED BY
Zhiming Chen,
China University of Petroleum, China
Qinglin Shan,
Shandong University of Science and Technology, China
Hun Lin,
Chongqing University of Science and Technology, China

*CORRESPONDENCE
Ren Zongxiao,
zxren@xsyu.edu.cn

SPECIALTY SECTION
This article was submitted to Geochemistry, a section of the journal Frontiers in Earth Science

RECEIVED 10 July 2022
ACCEPTED 17 August 2022
PUBLISHED 16 September 2022

CITATION
Jiaming Z, Zongxiao R, Guiyi Z, Zhenhua P, Minjing C, Liang W, Erbiao L and Xinggang M (2022), Study on flow model of multi-stage fracturing horizontal well in stress-denpendent dual medium reservoir.
Front. Earth Sci. 10:990684.
doi: 10.3389/feart.2022.990684

Study on flow model of multi-stage fracturing horizontal well in stress-denpendent dual medium reservoir

Zhang Jiaming[1], Ren Zongxiao[2,3]*, Zhang Guiyi[4], Peng Zhenhua[5], Chen Minjing[6], Wang Liang[2], Lou Erbiao[7] and Meng Xinggang[2]

[1]CNPC Economics and Technology Research Institute, BeiJing, China, [2]College of Petroleum Engineering, Xi'an Shiyou University, Xi'an, China, [3]Xi'an Shiyou University Shanxi Key Laboratory of Well Stability and Fluid and Rock Mechanics in Oil and Gas Reservoirs, Xi'an, China, [4]Engineering Technology Research Institute Xibu Drilling Engineering Company, Karamay, China, [5]Sinopec Northwest China Petroleum Bureau, Urumqi, China, [6]Xi'an Traffic Engineering Institute, Xi'an, China, [7]Research Institute of Oil and Gas Engineering, Tarim Oilfield Company, PetroChina, Korla, China

Often with abundant of natural fracture, Carbonate reservoirs are characterized with the stress sensitive and dual media. Mostly, its flow model solved by numerical method. In this paper, the semi-analytical solution for this problem is presented: firstly, the point source function considering stress sensitivity in infinite dual medium reservoir is obtained in Laplace space by Perturbation Transformation and Laplace Transformation; Secondly, the Laplace space solution of multi-stage fracturing horizontal well in infinite plate reservoir is obtained by Image Principle and Superposition Principle; Finally, the spacial solution of multi-stage fracturing horizontal well is obtained by Stehfest numerical inversion and perturbation inverse transformation. The calculation results show that the flow regime of multi-stage fracturing horizontal well can be divided into six stages: I- linear flow, II-first radial flow, III-double radial flow, IV-radial flow of natural fracture system, V-channeling flow regime and VI-radial flow of the whole system. The impact of stress sensitivity of formation permeability on linear flow is lower, and mainly affecting the last five flow regimes, and the dimensionless pressure drop derivative curve tends to rise in the later stage of development, showing the characteristics of closed boundary. In this paper, when the reservoir stress sensitivity is not considered, the calculation results will produce a large error, and the wrong well test interpretation will be obtained.

KEYWORDS

stress-sensitivity, dual media, source function, fracturing horizontal well, flow regime

1 Introduction

Most carbonate reservoirs are rich in natural fractures, which were first described by Barenblatt et al. (1960) (Barenblatt and Zheltov, 1960). They assume that there are two flow systems in reservoir:matrix and fracture, and matrix provides main storage space; then fracture is main flow channel. The system is evenly distributed in the fracture system, and the flow rate between them is proportionate to pressure difference. Warren and Root (1962) (Warren and Root, 1963) Based on Barenblatt (Barenblatt and Zheltov, 1960) established the double well test model of heavy medium reservoir; It provides a theoretical basis for well test analysis of natural fractured reservoir. Later, scholars (Kazemi, 1969; De Swaan, 1976) established the flow equations of unsteady channeling flow between matrix and fracture system, and these models laid the foundation for the study of dual medium flow. Based on these models, scholars (Ozkan, 1988; Ozkan and Raghavan, 1991; Chen and Raghavan, 1996; El-Banbi and Wattenbarger, 1998; Bello and Wattenbarger, 2010; Brown et al., 2011; Zhao et al., 2014; Chen et al., 2015; Jia et al., 2015; Luo and Tang, 2015) established unsteady pressure models for vertical wells, horizontal wells, staged fracturing horizontal wells and volumetric fracturing horizontal wells. However, these models assume that the permeability of fracture system and matrix system is fixed, and the permeability stress sensitivity effect is not considered.

Stress sensitive effect refers to that compression of rock causes the reduction of porosity, permeability due to the pressure decrease increase confining pressure as production of oil wells. Since the early 1950s, foreign scholars (Fatt and Davis, 1952; Fatt, 1953; Wyble, 1958; Gray et al., 1963) have studied the stress sensitivity effect of single medium through lab experiments; It is found that the influence of rock stress sensitivity on permeability is greater than that on porosity. In 1971, Vairogs (Vairogs et al., 1971) carried out stress sensitivity experiments on rock samples of different initial permeability (0.04md ~ 191md) and different properties (whether with micro-fractures and shale zones). The experimental results show that the lower the initial permeability is, the greater the stress sensitivity effect is; The existence of micro-fractures and shale zones aggravate the stress sensitivity effect. Stress sensitivity has a great impact on reservoir flow law and oil well productivity, and can reduce the production of oil wells by 50% (Vairogs and Rhoades, 1973). Pedrosa and Petrobras (1986) (Pedrosa, 1986) found that the change of rock sample permeability was exponentially related to the pressure drop based on the stress sensitivity experiment; The permeability modulus is proposed and the quantitative relationship between permeability and pressure to drop is established. Then, an analytical model of unsteady pressure under the fixed production condition of infinite stress sensitive reservoir is established by perturbation transformation. The calculation results show that with the progress of production, the dimensionless bottom hole pressure will rise like the influence of “closed boundary”. After that, scholars (Zhang and Ambastha, 1994; Chin et al., 2000; Franquet et al., 2004; Raghavan and Chin, 2004; Guo et al., 2005; Ali and Sheng, 2015; Wang and Marongiu-Porcu, 2015) conducted a lot of research on the flow law of stress sensitive reservoir. The research results show that in stress sensitive reservoir, if the change of permeability with pressure is not considered, it will cause large errors. However, the above calculation models are based on single heavy medium reservoir.

Vairogs et al, (1971) conducted stress sensitivity experiments on fractured reservoirs, scholars (Jia-Jyun et al., 2010; Cho et al., 2012; Han et al., 2013) also conducted stress sensitivity experiments on dual media reservoirs. The experimental results show that stress sensitivity has a great influence on permeability in dual medium reservoir. Scholars (Tong et al., 1999; Su et al., 2000; Tong et al., 2001; Tong et al., 2002; Tong and Zhang, 2003; MA et al., 2007) established the flow control equation considering the influence of stress sensitivity based on the dual medium flow model, and solved the model by numerical method. So far, no scholar has given a semi analytical solution to the flow model based on Kazemi, (1969) dual medium reservoir considering the influence of stress sensitivity. Based on Kazemi (Kazemi, 1969) dual medium model, this paper applies Pedrosa (Pedrosa, 1986) permeability calculation formula; The flow model of dual media reservoir considering stress sensitivity is established. Then, through perturbation transformation and Laplace transformation, the point source function of infinite dual medium reservoir considering stress sensitivity is obtained in Laplace space. Secondly, the Laplace space solution of staged fracturing horizontal well in infinite plate reservoir is obtained by image principle and superposition principle. Finally, the spatiotemporal solution of staged fractured horizontal wells is obtained through Stehfest (Stehfest, 1970) numerical inversion and perturbation inverse transformation.

2 Physical model description

Dual media reservoir is composed of matrix system and fracture system, which provides main reservoir space; The fracture system provides a channel for fluid flow. Kazemi (Kazemi, 1969) gives a simplified schematic diagram of dual media reservoir, as shown in Figure 1.

Assume that there is a point source in the infinite dual medium reservoir, which is infinitely small on the reservoir

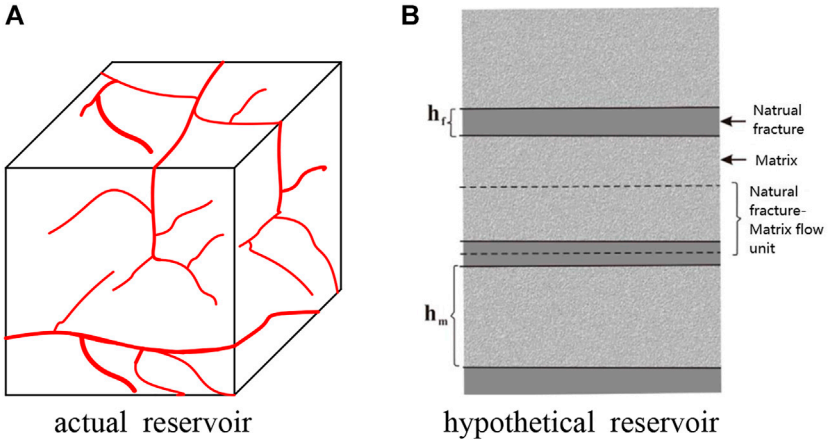

FIGURE 1
Schematic diagram of dual medium reservoir. **(A)** Actual reservoir; **(B)** Hypothetical reservoir.

scale; Large enough on the micro scale. When t = 0, the generated production at this point is $\tilde{q}$, and the fluid flow is caused near this point due to the output of liquid.

Assumption of the mode.

a. The reservoir is composed of matrix system and fracture system. The flow between the two systems is unsteady channeling flow, and the matrix system is evenly distributed in the fracture system;
b. Matrix system is the main storage space and fracture system is the main flow channel; All oil well production comes from the inflow of fracture system;
c. Considering the permeability sensitivity of fracture system, the permeability of matrix system is assumed to be constant;
d. There is a point source in the reservoir in production, the initial pressure of the reservoir is, and the temperature is constant during production;
e. The fluid in the reservoir can be either oil or gas. When the gas pressure is expressed by pseudo pressure, the form of flow control equation is consistent with that of oil; Therefore, the model established in this paper is also applicable to gas reservoirs.

The flow model of formation pressure change caused by the output of fluid at the point source is established below.

3 Establishment of point source function for infinite stress sensitive dual media reservoir

3.1 Flow in matrix system

The flow control equation of matrix system is:

$$\begin{cases} \dfrac{k_m}{\mu}\dfrac{\partial^2 p_m}{\partial z^2} = \phi_m c_m \dfrac{\partial p_m}{\partial t} \\ p_m(z,0) = p_i \\ \left.\dfrac{\partial p_m}{\partial z}\right|_{z=0} = 0 \\ p_m|_{z=h_m/2} = p_f \end{cases} \tag{1}$$

If the dimensionless parameter in Appendix 1 is introduced, Eq. 1 can be dimensionless as:

$$\begin{cases} \dfrac{\partial^2 \Delta p_m}{\partial z_D^2} = \dfrac{3(1-\omega)}{\lambda}\dfrac{\partial \Delta p_m}{\partial t_D} \\ \Delta p_m(z_D,0) = 0 \\ \left.\dfrac{\partial \Delta p_m}{\partial z_D}\right|_{z_D=0} = 0 \\ \Delta p_m|_{z_D=1} = \Delta p_f \end{cases} \tag{2}$$

Laplace transform Eq. 2 to obtain:

$$\begin{cases} \dfrac{d^2 \Delta \bar{p}_m}{dz_D^2} = \dfrac{3(1-\omega)}{\lambda} s\Delta \bar{p}_m \\ \dfrac{d\Delta \bar{p}_m}{dz_D}(z_D = 0, s) = 0 \\ \Delta \bar{p}_m(z_D = 1, s) = \Delta \bar{p}_f \end{cases} \tag{3}$$

The general solution of Eq. 3 is expressed as

$$\Delta \bar{p}_m = A\cosh\sqrt{\frac{3}{\lambda}(1-\omega)s}\cdot z_D + B\sinh\sqrt{\frac{3}{\lambda}(1-\omega)s}\cdot z_D \tag{4}$$

Substitute in the boundary conditions and simplify

$$\Delta\bar{p}_m = \Delta\bar{p}_f \frac{\cosh\sqrt{\frac{3(1-\omega)s}{\lambda}}\cdot z_D}{\cosh\sqrt{\frac{3(1-\omega)s}{\lambda}}} \tag{5}$$

The derivative of Eq. 5, then the derivation of $\bar{p}_m$ is obtained:

$$\left(\frac{d\Delta\bar{p}_m}{dz_D}\right)_{z_D=1} = \Delta\bar{p}_f\sqrt{\frac{3(1-\omega)s}{\lambda}}\tanh\sqrt{\frac{3(1-\omega)s}{\lambda}} \tag{6}$$

The calculation formula of channeling flow from matrix system to fracture system is (Nanba, 1991):

$$Q_m = \frac{2}{h_m}\frac{Ak_m}{\mu V_m}\left(\frac{\partial\Delta p_m}{\partial z_D}\right)_{z_D=1} \tag{7}$$

Laplace transform equation (7) to obtain:

$$\bar{Q}_m = \frac{2k_m}{\mu h_m}\left(\frac{A}{V}\right)_m\left(\frac{d\bar{p}_m}{dz_D}\right)_{z_D=1} \tag{8}$$

Eq. 6 is introduced into Eq. 8 and simplified to:

$$\bar{Q}_m = \Delta\bar{p}_f C_Q \tag{9}$$

The expression of C_Q in Eq. 9 is:

$$C_Q = \frac{k_m}{\mu}\left(\frac{2}{h_m}\right)^2\sqrt{\frac{3(1-\omega)s}{\lambda}}\tanh\sqrt{\frac{3(1-\omega)s}{\lambda}} \tag{10}$$

3.2 Flow model of fracture system

The flow control equation of fracture system is

$$\frac{1}{r^2}\frac{\partial}{\partial r}\left(r^2\frac{\partial\Delta p_f}{\partial r}\right) - \frac{\mu}{k_f}Q_m = \frac{(\phi c_t)_f\mu}{k_f}\frac{\partial\Delta p_f}{\partial t} \tag{11}$$

Considering the stress sensitivity of fracture system, fracture permeability can be expressed as (Pedrosa, 1986):

$$k_f = k_{if}e^{-\alpha\left(p_i-p_f\right)} \tag{12}$$

Substitute equation (12) into equation (11):

$$\frac{1}{r^2}\frac{\partial}{\partial r}\left(r^2\frac{\partial\Delta p_f}{\partial r}\right) - \frac{\mu}{k_{if}e^{-\alpha\left(p_i-p_f\right)}}Q_m = \frac{(\phi c_t)_f\mu}{k_{if}e^{-\alpha\left(p_i-p_f\right)}}\frac{\partial\Delta p_f}{\partial t} \tag{13}$$

If the dimensionless parameter in Annex A is introduced, Eq. 13 is dimensionless as follows:

$$e^{-\alpha\Delta p_f}\frac{1}{r_D^2}\frac{\partial}{\partial r_D}\left(r_D^2\frac{\partial\Delta p_f}{\partial r_D}\right) - \frac{\mu L^2}{k_{if}}Q_m = \omega\frac{\partial\Delta p_f}{\partial t_D} \tag{14}$$

Eq. 14 is a strongly nonlinear partial differential equation, and perturbation transformation is introduced:

$$\Delta p_f = -\frac{\ln(1-\alpha\eta)}{\alpha} \tag{15}$$

Eq. 15 is substituted into Eq. 14 and simplified to:

$$\frac{1}{r_D^2}\frac{\partial}{\partial r_D}\left(r_D^2\frac{\partial\eta}{\partial r_D}\right) - \frac{\mu L^2}{k_{if}}Q_m = \frac{\omega}{(1-\alpha\eta)}\frac{\partial\eta}{\partial t_D} \tag{16}$$

The neutralization η and $1/(1-\alpha\eta)$ in formula (16) is written as a power series in the form of:

$$\eta = \eta_0 + \alpha\eta_1 + \alpha^2\eta_2 + \alpha^3\eta_3 + \ldots \tag{17}$$

$$\frac{1}{1-\alpha\eta} = 1 + \alpha\eta + \alpha^2\eta^2 + \alpha^3\eta^3 + \ldots \tag{18}$$

Due to the low permeability modulus α, scholars Yeung et al. (Yeung et al., 1993) believe that the 0-order perturbation solution fully meets the needs of engineering calculation. Take Eq. 17–18 and substitute the 0-order perturbation transformation into Eq. 16 and simplify it to:

$$\frac{1}{r_D^2}\frac{\partial}{\partial r_D}\left(r_D^2\frac{\partial\eta_0}{\partial r_D}\right) - \frac{\mu L^2}{k_{if}}Q_m = \omega\frac{\partial\eta_0}{\partial t_D} \tag{19}$$

By Laplace transformation of Eq. 19 and combining with the initial condition equation (B-12), it is simplified as follows:

$$\frac{1}{r_D^2}\frac{d}{dr_D}\left(r_D^2\frac{d\bar{\eta}_0}{dr_D}\right) - \frac{\mu L^2}{k_{if}}\bar{p}_f C_Q = \omega s\bar{\eta}_0 \tag{20}$$

Eq. 9 is substituted into Eq. 20 and simplified to:

$$\frac{1}{r_D^2}\frac{d}{dr_D}\left(r_D^2\frac{d\bar{\eta}_0}{dr_D}\right) - \left[\omega + \frac{\lambda}{3s}\sqrt{\frac{3(1-\omega)s}{\lambda}}\tanh\sqrt{\frac{3(1-\omega)s}{\lambda}}\right]s\bar{\eta}_0 = 0 \tag{21}$$

Then:

$$f(s) = \omega + \frac{\lambda}{3s}\sqrt{\frac{3(1-\omega)s}{\lambda}}\tanh\sqrt{\frac{3(1-\omega)s}{\lambda}}$$

Then Eq. 21 can be written as:

$$\frac{d^2\bar{\eta}_0}{dr_D^2} + \frac{2}{r_D}\frac{d\bar{\eta}_0}{dr_D} - sf(s)\bar{\eta}_0 = 0 \tag{22}$$

Then:

$$g = r_D\bar{\eta}_0 \tag{23}$$

Then equation (22) can be transformed into:

$$\frac{d^2g}{dr_D^2} - sf(s)g = 0 \tag{24}$$

Eq. 24 is a conventional unary differential equation, and it is easy to obtain the general solution. Then, the solution of the equation can be obtained based on the initial conditions and boundary conditions (for specific steps, see reference (Ren et al., 2017)). Through the mirror image principle, the calculation

formula of unsteady pressure of vertical fractured wells in plate reservoir is as follows:

$$\bar{\eta}_{D0} = \bar{q}_D \int_{x_{wD}-L_{Df}}^{x_{wD}+L_{Df}} K_0\left(\sqrt{(x_D-\xi)^2+(y_D-y_{wD})^2}\sqrt{sf(s)}\right)d\xi \tag{25}$$

4 Unsteady pressure model of staged fracturing horizontal well in infinite closed plate reservoir

Considering the mutual interference between fractures, according to the superposition principle, the dimensionless pressure drop $\bar{\eta}_{D0i}$ of any fracture expressed as:

$$\bar{\eta}_{D0i} = \sum_{j=1}^{N} \bar{q}_{fDj}\bar{\eta}_{D0i,j} \tag{26}$$

In formula (26), $\bar{q}_{fDj}$ is the dimensionless rate of the j_{th} fracture; $\bar{\eta}_{D0i,j}$ is the dimensionless pressure drop of the j_{th} fracture at the i_{th} fracture (this value can be calculated by Eq. 25).

Without considering the flow resistance of fractures, then:

$$\bar{\eta}_{D0i} = \bar{\eta}_{wD} \quad i1, 2, \ldots, N \tag{27}$$

$\bar{\eta}_{wD}$ is the dimensionless pressure drop at the bottom of horizontal well in Eq. 27

The sum of dimensionless production of each fracture is 1, which is expressed as:

$$\sum_{j=1}^{N} \bar{q}_{fDj} = 1/s \tag{28}$$

Eqs. 26–28 are written in matrix form as follows:

$$\begin{bmatrix} \bar{\eta}_{D01,1} & \bar{\eta}_{D01,2} & \cdots & \bar{\eta}_{D01,N} & -1 \\ \bar{\eta}_{D02,1} & \bar{\eta}_{D02,2} & \cdots & \bar{\eta}_{D02,N} & -1 \\ \vdots & \vdots & \ddots & \vdots & \vdots \\ \bar{\eta}_{D0N,1} & \bar{\eta}_{D0N,2} & \cdots & \bar{\eta}_{D0N,N} & -1 \\ 1 & 1 & \cdots & 1 & 0 \end{bmatrix} \begin{bmatrix} \bar{q}_{fD1} \\ \bar{q}_{fD2} \\ \vdots \\ \bar{q}_{fD,N} \\ \bar{\eta}_{wD} \end{bmatrix} = \begin{bmatrix} 0 \\ 0 \\ \vdots \\ 0 \\ 1/s \end{bmatrix} \tag{29}$$

There are unknowns in Eq. 29, including $\bar{q}_{fDj}$ $(j = 1, 2, \ldots, N)$ and $\bar{\eta}_{wD}$ the number of equations is N+1 as well. Therefore, the equations are solvable, and the solution of the unknown in Laplace space can be obtained by Gauss Jordan elimination method. Using Stehfest (Stehfest, 1970) numerical inversion, Laplace space solution can be transformed into space solution η_{wD}. Then, the dimensionless bottom hole pressure is obtained from the perturbation inverse transformation (15).

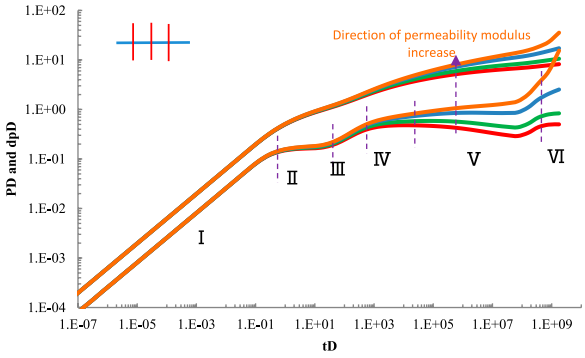

FIGURE 2
well test curves of three vertical fracture horizontal.

5 Analysis of calculation results of pressure model of staged fracturing horizontal well in dual medium reservoir

5.1 Flow regime divisions of staged fracturing horizontal wells in stress sensitive reservoirs

There are three vertical fractures with equal spacing and length in the stress sensitive dual medium reservoir. When the fracture half length $L_{fD} = 6$, spacing $L_{fD} = 6$, storage capacity ratio $\omega = 0.1$, cross to flow coefficient $\lambda = 10^{-8}$ and permeability modulus α are 0, 0.05, 0.1 and 0.12 respectively, the initial pressure of the reservoir is 34.5 MPa and the production is 15.8 m^3/d. The relationship curve between dimensionless bottom hole pressure drop, dimensionless pressure drop derivative and dimensionless time in the double logarithmic coordinate system is shown in Figure 2.

According to the relationship curve between dimensionless pressure drop derivative and time in Figure 2, the flow of staged fracturing horizontal well reservoir in stress sensitive dual medium reservoir can be divided into six flow regimes. I is linear flow. Because the reservoir pressure drop is small, the reservoir stress sensitivity has little effect on this stage. The reservoir fluid flows into the artificial fractures linearly, and the slope of the pressure drop derivative curve in Figure 2 is 0.5. The reservoir only uses the area between the artificial fractures. II. The first radial flow. In this flow process, there is no mutual interference between artificial fractures, and the slope of the corresponding pressure drop derivative

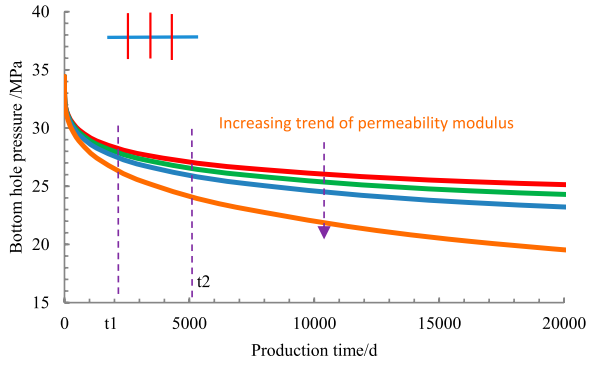

FIGURE 3
Sensitivity analysis of permeability modulus to BHP.

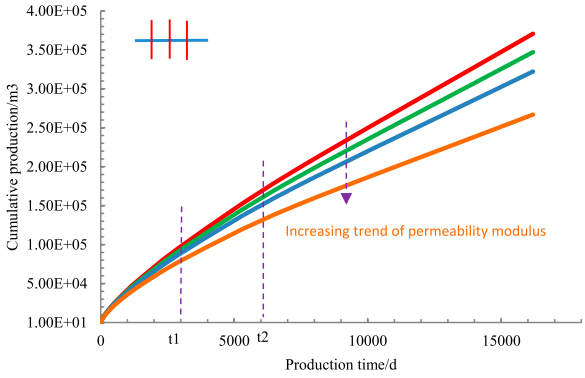

FIGURE 4
Influence of permeability modulus on cumulative production of fractured horizontal Wells.

is almost 0. It is known from the curve in Figure 2 that the reservoir pressure drop is affected by stress sensitivity. III. double radial flow, mutual interference between artificial fractures has occurred; The reservoir pressure decreases further, and the greater the permeability modulus, the higher the well test curve. IV radial flow in natural fracture system. V. in the stage of channeling flow, there is channeling flow from bedrock system to fracture system in dual medium reservoir; This stage shows a "groove" on the dimensionless pressure derivative curve. The position and depth of the "groove" are affected by the cross flow coefficient and storage capacity ratio respectively. At this time, the influence of stress sensitivity on bottom hole pressure is very obvious. VI for the radial flow of the whole system, the well test curve rises significantly with the increase of permeability modulus; It shows the characteristics of closed boundary influence (Huang et al., 2015; Ren et al., 2017; Ren et al., 2019a).

5.2 Effect of permeability modulus on bottom hole pressure and oil well production

Other data are the same as 4.1, when the permeability modulus α is 0, 0.05, 0.1 and 0.2 respectively; The relationship curve between bottom hole flow pressure and production time is shown in Figure 3.

It can be seen from Figure 3 that when the production of fractured horizontal wells remains unchanged, the greater the permeability modulus, the greater the bottom hole differential pressure required to produce the same production. At times t1 (2000 days), the maximum bottom hole flow pressure is 28.5 MPa and the minimum bottom hole flow pressure is 26.3MPa; The difference between them is 2.2 MPa. At t2 time (5000 days), the maximum bottom hole flow pressure is 27.3 MPa and the minimum bottom hole flow pressure is 24.2mpa; The difference between them is 3.1Mpa. Through the comparison of bottom hole flow pressure data at two times (it can also be seen from the curve trend in the figure), with the progress of production, the stress sensitivity has a greater and greater impact on bottom hole flow pressure (Ren et al., 2016; Ren et al., 2019b; Ren et al., 2019c).

The bottom hole flowing pressure is 24MPa, and other data are consistent with 4.1. When the permeability modulus α is 0, 0.05, 0.1 and 0.2 respectively; The relationship curve between cumulative production and production time of fractured horizontal wells is shown in Figure 4.

It can be seen from Figure 4 that when the production differential pressure on horizontal wells remains unchanged, the greater the permeability modulus, the smaller the cumulative production of horizontal wells. The maximum cumulative production at t1 time (3000 days) is 9.9×10^4 m^3, with a minimum cumulative yield of 8.1×10^4 m^3; The difference is 1.8×10^4 m^3。 The maximum cumulative yield at t2 time (6000 days) is 1.6×10^5 m^3, with a minimum cumulative production of 1.25×10^5 m^3. The difference between the two is 3.5×10^4 m^3。 Through the comparison of the accumulated production data onto two moments, it can be seen that the stress sensitivity has an increasing influence on the accumulated production of horizontal Wells with the progress of production.

5.3 Sensitivity analysis of wellbore storage factor

Other data are consistent with 4.1. When wellbore storage factor is 0.1, 0.5, 2, 5, respectively, the well test curve of fractured horizontal well is shown in Figure 5. It can be seen from Figure 5 that the larger the wellbore storage factor, the longer the wellbore

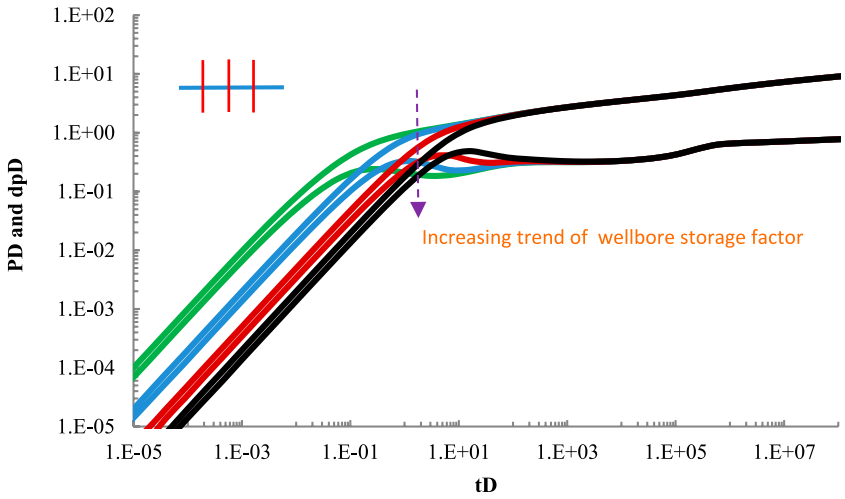

FIGURE 5
Sensitivity analysis of cross-flow coefficient.

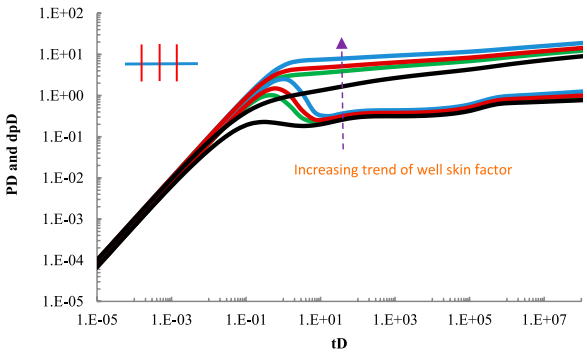

FIGURE 6
Sensitivity analysis of cross-flow coefficient.

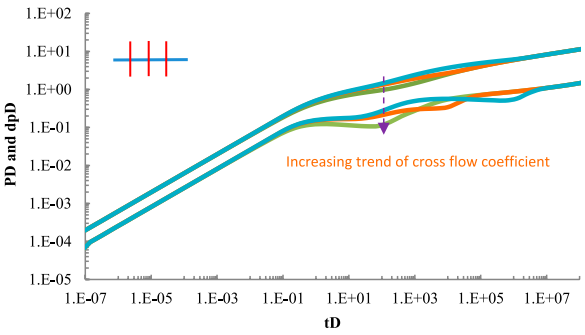

FIGURE 7
Sensitivity analysis of cross-flow coefficient.

storage phase lasts. Wellbore storage factor has little influence on other seepage stages.

5.4 Sensitivity analysis of well skin factor

Other data are consistent with 4.1. When well skin factor is 0.5,1,3,5, respectively, the well test curve of fractured horizontal well is shown in Figure 6. As can be seen from Figure 6, the larger the skin coefficient of oil well, the longer the duration of transition flow phase and the shorter the duration of radial flow phase, and the larger the dimensionless pressure drop.

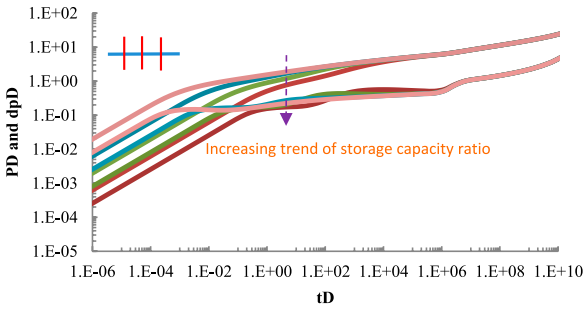

FIGURE 8
Sensitivity analysis of storage ratio.

5.5 Sensitivity analysis of cross flow coefficient

Other data are consistent with 4.1. When the cross flow coefficient is 10^{-6} , 10^{-4} , 10^{-3} respectively, the well test curve of fractured horizontal well is shown in Figure 7.

The larger the cross flow coefficient, the faster the liquid supply speed of matrix to the fracture system, and the earlier the channeling stage appears. The position of "groove" in Figure 7 is closer to the left. However, because the total liquid volume in the matrix system is certain, the dimensionless pressure drop curve tends to be consistent in the later stage of development.

5.6 Sensitivity analysis of storage capacity ratio

Other data are consistent with 4.1. When the storage capacity ratio is 0.0001,0.001,0.01, 0.1, the well test curve of fractured horizontal well is shown in Figure 8.

It can be seen from Figure 8 that the storage capacity ratio has a great impact on most production stages; With the increase of storage capacity ratio, the dimensionless pressure drop decreases and the duration of channeling becomes shorter and shorter; The dimensionless pressure drop derivative curve shifts to the right as a whole. Compared with the reservoir with low reservoir volume ratio, when the pressure of fracture system decreases, the reservoir with high reservoir volume ratio can quickly increase the pressure of fracture system; The pressure drop of fracture system changes little, so the "groove" duration of dimensionless pressure drop derivative is shorter.

6 Conclusion

Based on Kazemi's dual medium flow model, the flow equation of dual medium reservoir considering stress sensitivity is established in this paper. The equation is a strongly nonlinear partial differential equation, which is linearized by introducing perturbation transformation; Then, a series of processing methods such as Laplace transform and image principle are applied to establish the non-point source function of infinite plate reservoir considering stress sensitivity. In the process of writing, the following conclusions are drawn:

1) Based on area source function and superposition principle; The unsteady pressure model of staged fracturing horizontal well under stress sensitive dual medium reservoir is established. According to the calculation, the flow period of staged fracturing horizontal well can be divided into six regimes: I is linear flow, II is first radial flow, III is double radial flow, IV is radial flow of natural fracture system, V is channeling flow regime, and VI is radial flow of the whole system.
2) With the increase of permeability stress sensitivity, the well test curve moves upward gradually. The stress sensitivity has little effect on the linear flow regime, and the dimensionless pressure drop derivative curve tends to rise in the later stage of development, showing the influence characteristics of closed boundary (see Figure 2); If the influence of permeability stress sensitivity is not considered in well test analysis, wrong well test interpretation results will be obtained. Through the calculation and analysis in part 4.2, it is known that the permeability stress sensitivity has a great impact on the bottom hole flow pressure and oil well production.
3) The sensitivity analysis of cross flow coefficient and storage capacity ratio of dual media reservoir is carried out respectively. The results show that the larger the cross flow coefficient is, the earlier the channeling stage appears. The storage capacity ratio has a great influence on the first five flow regimes. With the increase of storage capacity ratio, the duration of channeling flow becomes shorter and shorter.

The development of carbonate reservoir is greatly affected by stress sensitivity, which can not be ignored in model calculation. The semi analytical model established in this paper provides a very useful method for quickly predicting the productivity of staged fracturing horizontal wells in stress sensitive reservoirs, understanding the flow law of fractured horizontal wells, and evaluating and analyzing the fracturing effect.

Data availability statement

The original contributions presented in the study are included in the article/supplementary material, further inquiries can be directed to the corresponding author.

Author contributions

ZJ—Conceptualization, Methodology, Investigation, Formal Analysis, Writing—Original Draft; RZ——Conceptualization, Funding Acquisition, Resources, Supervision, Writing—Review & Editing. Others—Visualization, Writing—Review & Editing.

Funding

This work is funded by National Natural Science Foundation of China (Grant No. 51804258, 51974255), Natural Science Basic Research Program of Shaanxi Province (Grant No.2019JQ-807, 2020JM-544, 2018JM-5054, 2019JM-141), and the Youth Innovation Team of Shaanxi Universities. Scientific Research Program Funded by Shaanxi Provincial Education Department (Program No.22JS029).

Conflict of interest

Author ZG was employed by Engineering Technology Research Institute Xibu Drilling Engineering Company. Author LE was employed by Research Institute of Oil and Gas Engineering, Tarim Oilfield Company.

The remaining authors declare that the research was conducted in the absence of any commercial or financial relationships that could be construed as a potential conflict of interest.

Publisher's note

References

Ali, T. A., and Sheng, J. J. (2015). *Evaluation of the effect of stress-dependent permeability on production performance in shale gas reservoirs*. West Virginia USA: Society of Petroleum Engineers. doi:10.2118/177299-MS

Barenblatt, G. I., and Zheltov, Yu. P. (1960). Fundamental equations of filtration of homogeneous liquids in fissured rocks, " soviet physics. *Doklady* 5, 522. doi:10.1016/0021-8928(60)90107-6

Bello, R. O., and Wattenbarger, R. A. (2010). "Multi-stage hydraulically fractured horizontal shale gas well rate transient analysis," in Paper presented at the North Africa Technical Conference and Exhibition (Cairo Egypt: Society of Petroleum Engineers). doi:10.2118/126754-MS

Brown, M., Ozkan, E., Raghavan, R., and Kazemi, H. (2011). Practical solutions for pressure transient responses of fractured horizontal wells in unconventional Shale reservoirs. *SPE Reserv. Eval. Eng.* 14 (3), 663–676. doi:10.2118/125043-PA

Chen, C., and Raghavan, R. (1996). A multiply-fractured horizontal well in a rectangular drainage region. *SPE 37072* 2 (04), 455–465. doi:10.2118/37072-PA

Chen, Z., Liao, X., Zhao, X., Lv, S., and Zhu, L. (2015). A semianalytical approach for obtaining type curves of multiple-fractured horizontal wells with secondary-fracture networks. *Soc. Petroleum Eng.* 21 (02), 538–549. doi:10.2118/178913-PA

Chin, L. Y., Raghavan, R., and Thomas, L. K. (2000). "Fully coupled geomechanics and fluid-flow analysis of wells with stress-dependent permeability,", 32–45. doi:10.2118/58968-PA

Cho, Y., Ozkan, E., and Apaydin, O. G. (2012). *Pressure-Dependent natural-fracture permeability in shale and its effect on shale-gas well production*. USA: Society of Petroleum Engineers. doi:10.2118/159801-MS

De Swaan, O., A. (1976). Analytic solutions for determining naturally fractured reservoir properties by well testing. *Soc. Petroleum Eng.* 16 (03), 117–122. doi:10.2118/5346-PA

El-Banbi, A. H., and Wattenbarger, R. A. (1998). "Analysis of linear flow in gas well production," in Proceeding Paper presented at the SPE Gas Technology Symposium, (Alberta Canada: Society of Petroleum Engineers). doi:10.2118/39972-MS

Fatt, I., and Davis, T. H. (1952). The reduction in permeability with overburden pressure. *Trans. AIME* 195, 329. doi:10.2118/952329-G

Fatt, I. (1953). The effect of overburden pressure permeability on relative permeability. *AIME* 198, 325. doi:10.2118/953325-G

Franquet, M., Ibrahim, M., Wattenbarger, R. A., and Maggard, J. B. (2004). Effect of pressure dependent permeability in tight gas reservoirs, transient radial flow in Proceeding Paper presented at the Canadian International Petroleum Conference (Calgary Alberta: Petroleum Society of Canada). doi:10.2118/2004-089

Gray, D. H., Fatt, I., and Bergarnini, G. (1963). The effect of stress on permeability of sandstone cores. *Soc. Petroleum Eng. J.* 3, 95–100. doi:10.2118/531-pa

Guo, X., Li, Y., Du, Z., and Shu, Z. (2005). "Numerical modelling for simulating coupled flow in stess-sensitive gas reservoirs," in Proceding Petroleum Society of Canada. Petroleum Society of Canada, 2005–2064. doi:10.2118/2005-064

Han, G., Gutierrez, M., and Schmitz, P. (2013). *Stress-Dependent flow, mechanical, and acoustic properties for an unconventional oil reservoir rock*. USA: Society of Petroleum Engineers. doi:10.1190/URTEC2013-177

Huang, T., Guo, X., and Chen, F. (2015). Modeling transient flow behavior of a multiscale triple porosity model for shale gas reservoirs. *J. Nat. Gas Sci. Eng.* 23, 33–46. doi:10.1016/j.jngse.2015.01.022

Jia, P., Cheng, L., Huang, S., and Liu, H. (2015). Transient behavior of complex fracture networks. *J. Petroleum Sci. Eng.* 132, 1–17. ISSN 0920-4105. doi:10.1016/j.petrol.2015.04.041-

Jia-Jyun, D., Jui-Yu, H., Wen-Jie, W., Shimamoto, T., Hung, J. H., Yeh, E. C., et al. (2010). Stress-dependence of the permeability and porosity of sandstone and shale from TCDP Hole-A. *Int. J. Rock Mech. Min. Sci.* 47 (7), 1141–1157. ISSN 1365-1609. doi:10.1016/j.ijrmms.2010.06.019

Kazemi, H. (1969). Pressure transient analysis of naturally fractured reservoirs with uniform fracture distribution. *Soc. Petroleum Eng.* 9 (04), 451–462. doi:10.2118/2156-A

Luo, W., and Tang, C. (2015). Pressure-Transient analysis of multiwing fractures connected to a vertical wellbore. *Soc. Petroleum Eng.* 20 (02), 360–367. doi:10.2118/171556-PA

Ma, X., Tong, D., and Huawei, H. (2007). Non-Darcy flow analysis of fluid in deformed fractal reservoir with double porosity[J]. *Chin. J. Comput. Phys.* 02, 197–202.

Nanba, T. (1991). *Numerical simulation of pressure transients in naturally fractured reservoirs with unsteady-state matrix-to-fracture flow*. Japan: Society of Petroleum Engineers. doi:10.2118/22719-MS

Ozkan, E., and Raghavan, R. (1991). New solutions for well test analysis problems : Part1 analytical considerations. *SPEFE* 6 (03), 359–368. doi:10.2118/18615-PA

Ozkan, E. (1988). *Performance of horizontal wells*. Tulsa. OK: U. of Tulsa. PhD dissertation.

Pedrosa, O. A., Jr. (1986). Pressure transient response in stress-sensitive formations." in Proceeding Paper presented at the SPE California Regional Meeting (Oakland: SPE California Regional Meeting), 15115 MS. doi:10.2118/15115-MS

Raghavan, R., and Chin, L. Y. (2004). Productivity changes in reservoirs with stress-dependent permeability. *Soc. Petroleum Eng.* 7 (04), 308–315. doi:10.2118/88870-PA

Ren, Z., Wu Dandan, L., et al. (2016). Semi-analytical model for transient pressure behavior of complex fracture networks in tight oil reservoirs [J]. *J. Nat. Gas Sci. Eng.* 33, 497–508.doi:10.1016/j.jngse.2016.09.006

Ren, Z., Wu, X., and Han, G. (2017). Transient pressure behavior of multi-stage fractured horizontal wells in stress-sensitive tight oil reservoirs[J]. *J. Petroleum Sci. Eng.* 157., 1197. doi:10.1016/j.petrol.2017.07.073

Ren, Z., Yan, R., Huang, X., Liu, W., Yuan, S., Xu, J., et al. (2019). The transient pressure behavior model of multiple horizontal wells with complex fracture networks in tight oil reservoir. *J. Pet. Sci. Eng.* 173, 650–665. doi:10.1016/j.petrol.2018.10.029

Ren, Z., Du, K., and Shi, J. (2019). Semi-analytical coupled model of transient pressure behavior for horizontal well with complex fracture networks in tight oil reservoirs[J]. *Math. Problems Eng.* 12, 231–245.doi:10.1155/2019/6524105

Ren, Z., Wu, X., and Han, G. (2019). Transient pressure behavior of multi-stage fractured horizontal well in stress-sensitive coal seam[J]. *Int. J. Oil Gas CoalTechnology* 15, 45–52. doi:10.1016/j.petrol.2017.07.073

Stehfest, H. (1970). Algorithm 368: Numerical inversion of Laplace transforms [D5]. *Commun. ACM* 13 (1), 47–49. doi:10.1145/361953.361969

Su, Y., Luan, Z., and Zhang, Y. (2000). A study on development characteristics for deformed reservoir[J]. *Acta Pet. Sin.* 02, 51. doi:10.7623/syxb200002010

Tong, D., and Zhang, H. (2003). Flow analysis of fluid in fractal reservoir with deformed double porosity medium[J]. *J. Univ. Petroleum* 04, 76China. doi:10.1007/BF02974893

Tong, D., Zhou, D., and Chen, Q. (1999). An approximate analytical study of fluids flow in fractal reservoir with pressure-sensitive formation permeability. *[J].Petroleum Explor. Dev.* 03, 73

Tong, D., Chen, Q., and Zong, G. (2001). Exact solution and pressure transient analysis for the flow problem of fluids flow in a bounded fractal reservoir with double porosity [J]. *Acta Pet. Sin.* 03, 58–62. doi:10.7623/syxb200103012

Tong, D., Jiang, D., and Wang, R. (2002). Generalized flow analysis of fluid in deformed reservoir with double-porosity media[J]. *Chin. J. Appl. Mech.* 02, 141

Vairogs, J., and Rhoades, V. W. (1973). Pressure transient tests in formations having stress-sensitive permeability. *Soc. Petroleum Eng.* 25 (08), 965–970. doi:10.2118/4050-PA

Vairogs, J., Hearn, C. L., Dareing, D. W., and Rhoades, V. W. (1971). Effect of rock stress on gas production from low permeability reservoirs. *J. Petroleum Technol.* (23), 1161–1167. doi:10.2118/3001-pa

Wang, H., and Marongiu-Porcu, M. (2015). Impact of shale-gas apparent permeability on production: Combined effects of non-Darcy flow/gas-slippage, desorption, and geomechanics. *Soc. Petroleum Eng.* 18 (04), 495–507. doi:10.2118/173196-PA

Warren, J. E., and Root, P. J. (1963). The behavior of naturally fractured reservoirs. *Sot. Pet. Eng.* 3, 245–255. doi:10.2118/426-PA

Wyble, D. O. (1958). Effect of applied pressure on conductivity, porosity and permeability of sandstones. *Trans. AIME* 213, 430. doi:10.2118/1081-G

Yeung, K., Chakrabarty, C., and Zhang, X. (1993). An approximate analytical study of aquifers with pressure-sensitive formation permeability. *Water Resour. Res.* 29 (10), 3495–3501. doi:10.1029/93wr01493

Zhang, M. Y., and Ambastha, A. K. (1994). New insights in pressure-transient analysis for stress-sensitive reservoirs." in ProceedingPaper presented at the SPE Annual Technical Conference and Exhibition. New Orleans, Louisiana: Society of Petroleum Engineers. doi:10.2118/28420-MS

Zhao, Y. L., Zhang, L. H., Luo, J. X., and Zhang, B. N. (2014). Performance of fractured horizontal well with stimulated reservoir volume in unconventional gas reservoir. *J. Hydrol. X.* 512, 447–456. doi:10.1016/j.jhydrol.2014.03.026

Appendix A Definition of dimensionless variables

The dimensionless variables introduced are:

$$p_{Dj} = \frac{2\pi k_{if} h\left(p_i - p_j\right)}{\mu Q} \quad j = f/m \tag{A-1}$$

$$q_D = \frac{\tilde{q}L}{Q} \tag{A-2}$$

$$t_D = \frac{k_{if} t}{(\phi c)_{f+m} \mu L^2} \tag{A-3}$$

$$z_D = \frac{2z}{h_m} \tag{A-4}$$

$$\lambda = \frac{12 k_m L^2}{k_{if} h_m^2} \tag{A-5}$$

$$\omega = \frac{(\phi c)_f}{(\phi c)_{f+m}} \tag{A-6}$$

Glossary

Parameter definition

α :permeability modulus,MPa^{-1}

c total comprehensibility, MPa^{-1}

g : Conversion function

h : length, m

H : length, m

k : permeability,m^2

k_{if} :Initial permeability of natural fracture,m^2

l :horizontal well length,m

L_f :half length of fracture,m

L :reference length,m

p :pressure,MPa

Δp :difference from initial formation pressure,MPa

p_i :initial formation pressure, MPa

$\tilde{q}$:point source instantaneous rate, m^3/s;

Q : production rate, m^3/s;

s: Laplace variable

S: conversion function

t: time, s;

V :ratio of each system to total reservoir volume

x, y, z: variables in Cartesian coordinate system,m

z_e :height of oil columu,m

ϕ :porosity

μ :oil viscosity, Pa·s

ω :storage ratio

λ :channel flow

σ :shape factor

subscript

m represent the matrix system

f represents the fracture system

D is dimensionless

w is location of point source

i j is hydraulic fracture

frontiers | Frontiers in Earth Science

TYPE Original Research
PUBLISHED 20 September 2022
DOI 10.3389/feart.2022.965743

OPEN ACCESS

EDITED BY
Jianlin Zhao,
ETH Zürich, Switzerland

REVIEWED BY
Gang Liu,
Taizhou University, China
Andreas Hermann,
University of Edinburgh,
United Kingdom

*CORRESPONDENCE
Ming Zhang,
zm9792@xsyu.edu.cn

SPECIALTY SECTION
This article was submitted to Geochemistry, a section of the journal Frontiers in Earth Science

RECEIVED 10 June 2022
ACCEPTED 26 August 2022
PUBLISHED 20 September 2022

CITATION
Zhang M, Zhao B, Li J, Li T and Li J (2022), Comparison of CO_2, N_2, CO, H_2S, CH_4, and H_2O adsorptions onto sI methane hydrate surface.
Front. Earth Sci. 10:965743.
doi: 10.3389/feart.2022.965743

Comparison of CO_2, N_2, CO, H_2S, CH_4, and H_2O adsorptions onto sI methane hydrate surface

Ming Zhang[1,2]*, Baoli Zhao[3], Jiahua Li[1,2], Tiantai Li[1,2] and Jian Li[2]

[1]College of Petroleum Engineering, Xi'an Shiyou University, Xi'an, China, [2]Shaanxi Cooperative Innovation Center of Unconventional Oil and Gas Exploration and Development, Xi'an Shiyou University, Xi'an, China, [3]No. 2 Gas Production Plant, PetroChina Changqing Oilfield Company, Yulin, China

By employing molecular dynamic (MD) and density functional theory (DFT) calculations, the adsorptions of CO_2, N_2, CO, H_2S, CH_4, and H_2O onto methane hydrate (MH) surface are compared in this work. The methane hydrate planes of (001) and (110) and various cleaving sites are compared with cleavage energies. MH(001) has more tendency to form when compared with MH(110) in thermodynamics. Two different terminations of MH(001) surfaces are compared, and MH(001)-I (terminated with CH_4+H_2O) leads to more negative adsorption energies when compared with MH(001)-II (terminated with H_2O only). The priority sequence of the adsorptions can be queued as: H_2O > H_2S > CO_2 > N_2 > CH_4 > CO. Namely, CO_2, N_2, and H_2S have potential to replace CH_4 in methane hydrate. The interfacial hydrogen bond and electronic interactions are clarified for the adsorptions of CO_2, N_2, and H_2S. The hydrogen bonds tend to form between O-H atom pairs of CO_2-H_2O, N-H atom pairs of N_2-H_2O, and S-H and H-O atom pairs of H_2S-H_2O, respectively. The bonds are mainly contributed from the dispersion interaction between the O-2*p* in CO_2 and H-1*s* in H_2O, N-2*p* in N_2 and H-1*s* in H_2O, S-3*p* in H_2S and H-1*s* in H_2O, and H-1*s* in H_2S and O-2*p* in H_2O, respectively.

KEYWORDS

methane hydrate (MH), adsorption priority, interfacial bonding, hydrogen bonds, DFT calculations

1 Introduction

In the last few decades, natural gas clathrate, especially methane hydrate (MH), has attracted attention from a wide range of academic communities (Kvenvolden, 1988; Sloan, 2003; Walsh et al., 2009; Lunt et al., 2011). Methane hydrates are ice-like inclusion compounds that are composed of water (H_2O) and methane (CH_4) molecules, and CH_4 guest molecules are encapsulated in the hydrogen-bonded water cages (Sloan, 2003). Compared with other fossil fuels, methane hydrate generates lower CO_2 emissions per unit of energy, which makes it a promising energy source to mitigate global warming (Lunt et al., 2011; Phrampus and Hornbach, 2012).

Up to now, nine different polymorphs are reported for MH's structures, which includes three cubic (sI, sII, and sIII), one hexagonal (sH), one orthorhombic (sIV), two monoclinic (sV and sVI) and two tetragonal (sT and sK) structures (Cao et al., 2017; Huang et al., 2018).

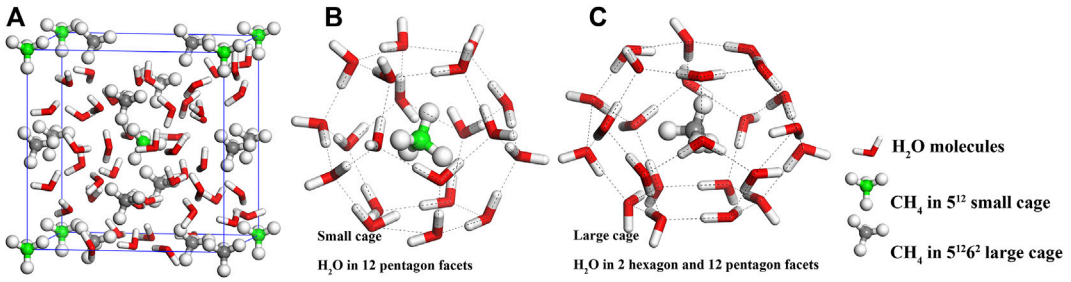

FIGURE 1
Atomic structure of cubic sI-MH **(A)**. The spheres with white, green (grey), and red colors denote H, C, and O atoms, and C atoms in green and grey depict the carbon atoms of CH_4 in 5^{12} small water cage **(B)** and $5^{12}6^2$ large water cage **(C)**, respectively.

Among these polymorphs, Cubic sI structure (sI-MH) predominates in the Earth's natural environments (Sloan, 2003). Under room temperature, structure type sI is stable below 120 MPa (Shu et al., 2011). Eight water cages (two 5^{12} small cages and six $5^{12}6^2$ large cages) are contained in sI-MH, in which eight methane molecules are trapped, and the ideal H_2O:CH_4 ratio is 5.75. The 5^{12} small cage can be regarded as formed with water molecules in the positions of 12 pentagons, while the $5^{12}6^2$ large cage can be regarded as formed with water molecules in the positions of 12 pentagons and two hexagons (Figure 1).

Compared with conventional natural gas sources, MH's exploitation is more challenging. Dissociating or untrapping CH_4 molecules from H_2O cages is the fundamental problem. Thermal stimulation and depressurization are commonly proposed as exploitation techniques (Chong et al., 2016). However, they change the reservoir's conditions, which makes it no longer thermodynamically stable, which facilitates dissociating CH_4. Inhibitor injection usually employs ethylene glycol (EG) as an inhibitor. However, the inhibitor's required concentration is as high as around 30 wt.% (Chong et al., 2016). In recent years, replacing CH_4 with CO_2 (and/or N_2) in methane hydrate is also proposed as an encouraging avenue (Cha et al., 2015; Zhang et al., 2017a; Zhang et al., 2017b; Okwananke et al., 2018; Matsui et al., 2020). In the replacing process, the adsorption of CO_2 (N_2) onto MH surface can be regarded as the first step. Meanwhile, various small gas molecules might also compete in the adsorption. For example, CO and H_2S gases are commonly associated with MH reservoirs, replacing CH_4 from MH with CO_2 (or N_2) is potentially affected by the adsorptions of CO and H_2S. Meanwhile, the condensation of MH can be viewed as an adverse process of CH_4 dissociation, which can be also regarded as the adsorptions of CH_4 and H_2O onto the MH surface. Therefore, the competition derived from these small gas molecules' adsorptions should be considered. The interfacial bonding mechanism between CO_2, N_2 and MH surface is also interesting to be clarified. Unfortunately, the correlated content has been insufficiently reported in the literature.

In this work, by employing MD and DFT methods, the adsorptions of several kinds of gas molecules (i.e., CO_2, N_2, CO, H_2S, CH_4, and H_2O) onto sI-MH surface are investigated. Their adsorption priorities are confirmed based on the energetic data and the interfacial electronic interactions are also discussed.

TABLE 1 Parameters employed in the DFT-D TS scheme.

Atom	C_6 (eV·Å^6)	R_0 (Å)	α (Å^3)
H	3.8839	1.6404	0.6668
C	27.8447	1.8997	1.7782
N	14.4601	1.7675	1.0966
O	9.3214	1.6881	0.8002
S	80.0686	2.0426	2.9044

2 Methodology and details

2.1 Computation parameters

In the present work, MD and DFT calculations are conducted by employing FORCITE and CASTEP (Clark et al., 2005) codes in the Materials Studio package. The forcefield of COMPASS (Sun, 1998; McQuaid et al., 2004) and pseudopotential of GGA-PBE are employed in both calculations, respectively. The atom cores and valence electrons of H $1s^1$, C $2s^22p^2$, N $2s^22p^3$, O $2s^22p^4$, S $3s^23p^4$, and cutoff energy of 450 eV and k-points spacing around 0.03 Å^{-1} are adopted. To better describe the inter-atomic bonding effect, the van der Waals dispersion corrections (DFT-D, TS scheme (Tkatchenko and Scheffler, 2009), $sR = 0.94$ and $d = 20$) are deployed in all DFT of the calculations. The parameters C_6, R_0, α are listed in Table 1.

2.2 Calculation of bulk methane hydrate

The cubic cell of bulk sI-MH (Figure 1) contains 46 H_2O and eight CH_4 molecules. Its oxygen lattice has the space group of *Pm-3n* (Kirchner et al., 2004). After DFT geometry optimization,

TABLE 2 Calculated results and previous data of sI-MH unit cell.

Items	Present work[a]	Exp. data	Cal. data
Lattice parameter *a* (Å)	11.306	11.877, Kirchner et al., (2004)	11.830, Cox et al., (2014)
		11.88, Kirchner et al., (2004)	11.56, Martos-Villa et al., (2013)
r (O-H) in H_2O (Å)	1.110	—	0.983, Wang et al., (2020)
r (C-H) in CH_4 (Å)	1.140	—	1.094, Wang et al., (2020)

[a]The results of present work are obtained after DFT-D geometry optimization.

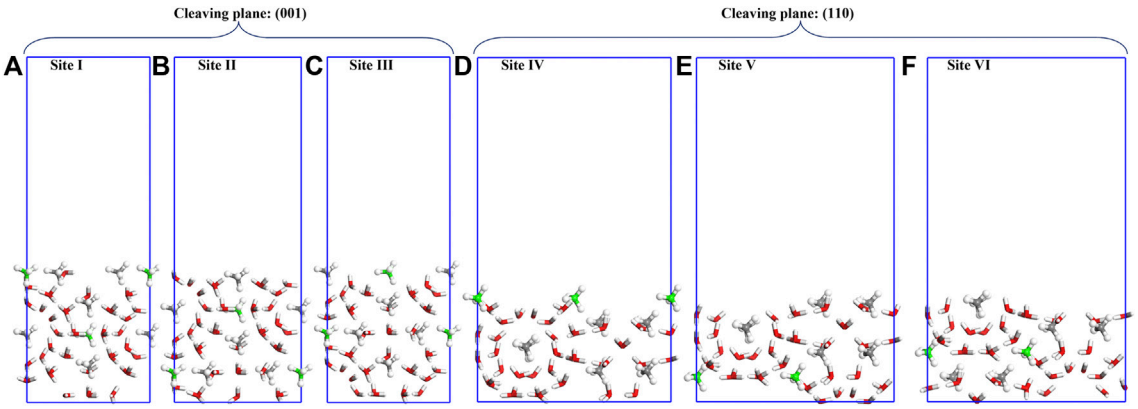

FIGURE 2
Cleaved slabs along (001) and (110) planes of sI-MH with 20Å vacuum in depth: **(A–F)** are cleaved slabs along different sites (Sites-I to Site-VI). The white, grey (green), and red spheres denote H, C, and O atoms, and CH_4 with grey and green C atoms are from large and small water cages, respectively.

the lattice parameters of sI-MH unit cell and diatomic lengths are summarized in Table 2. Some previous experimental and theoretical data are also listed as references. Our results agree well with these data.

2.3 Cleavage energy and surface models

Under the theorem of thermodynamics, for any condensed materials, their facet (or plane) with minimum excess energy tends to be the surface contacting with other matters (e.g., air, liquid, vacuum, or other condensed phases). In the present work, cleavage energy is employed to determine the energetically-favored surface of sI-MH. The low-index planes of the methane hydrate surface are mentioned in the literature, such as (001) (Hu et al., 2021a; Liao et al., 2022) and (110) (Liang et al., 2011; Cox et al., 2018). Consequently, both planes are specifically discussed in the present work.

Two different cleaving planes (i.e., (001) and (110) planes) are considered (as shown in Figure 2). For cleaving plane (001), three sites (denoted as Site I, II and III) are compared; while for cleaving plane (110), two sites (denoted as Site IV and V) are examined.

TABLE 3 Calculated cleavage energies (E_{cl}) along (001) and (110) planes of sI-MH.

Cleaving planes	(001)			(110)		
Cleaving sites	I	II	III	IV	V	VI
E_{cl} (J/m^2)	0.697	0.963	0.804	0.850	0.715	0.820

The cleavage energy (E_{cl}) can be estimated as:

$$E_{cl} = \frac{1}{A}\left(E_{sI-MH}^{\text{cleaved slab}} - E_{sI-MH}^{\text{bulk}}\right) \quad (1)$$

,

where A denotes the surface area, $E_{sI-MH}^{\text{cleaved slab}}$ a and E_{sI-MH}^{bulk} are the total energies of the cleaved slab and bulk unit cell. Because the cleaved slab and bulk unit cell have the same number of molecules (46 H_2O and 8CH_4), the difference $E_{sI-MH}^{\text{cleaved slab}} - E_{sI-MH}^{\text{bulk}}$ can denote the excess energy of cleaved slab.

The cleavage energies (E_{cl}) are calculated as shown in Table 3. Cleaving along (001) at Site-I requires the lowest

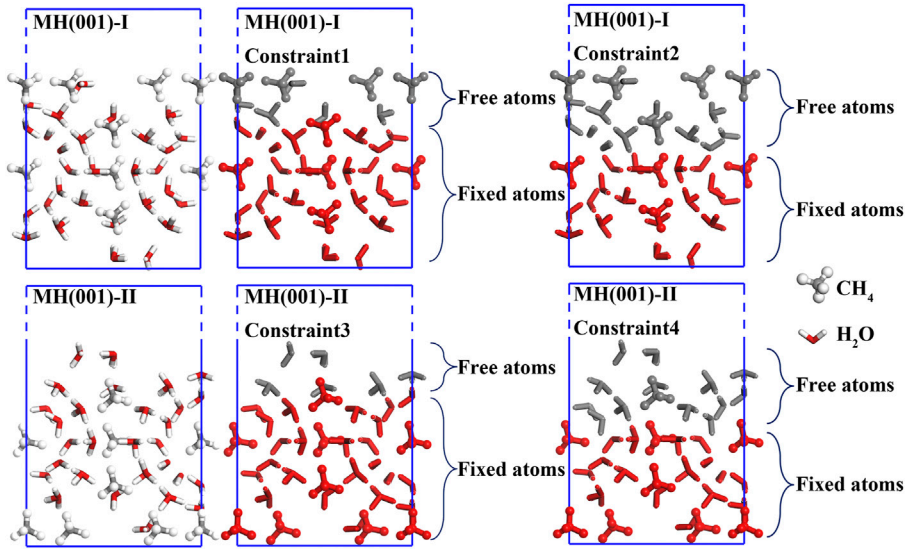

FIGURE 3
Constraint conditions of MH(001)-I and MH(001)-II surface models.

TABLE 4 Calculated energy differences (ΔE) between initial and optimized surface models of sI-MH.

Surface models	Relaxation and constraints	Energy (eV)	ΔE (eV)[a]
MH(001)-I	Unrelaxed	−23342.4083	—
	Relaxed with Constraint1	−23343.6995	1.2911
	Relaxed with Constraint2	−23344.2991	0.5997
MH(001)-II	Unrelaxed	−23342.4083	—
	Relaxed with Constraint3	−23343.6864	1.2781
	Relaxed with Constraint4	−23344.1706	0.4842

[a]Energy differences (ΔE) are values of ($E_{\text{Unrelaxed}}$—$E_{\text{Relaxed with Constraint1}}$), ($E_{\text{Relaxed with Constraint1}}$—$E_{\text{Relaxed with Constraint2}}$), ($E_{\text{Unrelaxed}}$—$E_{\text{Relaxed with Constraint3}}$), and ($E_{\text{Relaxed with Constraint3}}$—$E_{\text{Relaxed with Constraint4}}$), respectively.

cleavage energy. Consequently, bulk methane hydrate is more likely to be cleaved in this case. However, cleaving the bulk sI-MH cell along (001) at Site-I will simultaneously generate two surfaces with distinct terminations. Namely, the top and bottom surfaces depicted in Figure 2A will be created simultaneously. For both surfaces, one is terminated with H_2O+CH_4 and the other is terminated with H_2O only. For simplicity, both surfaces are denoted as MH(001)-I and MH(001)-II, respectively. It is difficult to determine their energetic priorities. Therefore, the both surfaces are considered in following interfacial calculations.

The MH(001)-I and MH(001)-II surface models are established with areas of 11.31 × 11.31 Å^2. A vacuum layer (20Å in thickness) is inserted to avoid the imaginary interaction between the top and bottom sides. The same number of molecules (46 H_2O and 8CH_4) are included in both surface models.

First, the surface models are fully relaxed within DFT-D frame. During the relaxations, the inner atoms are fully constrained to mimic the bulk-like interior. To determine optimal constraint conditions, different constraints are compared for both surface models (as shown in Figure 3).

The energies of initial and optimized models are listed in Table 4. According to our calculated results, the energy deviation between optimized models with Constraint1 and Constraint2 conditions is merely around -0.6 eV. Likewise, the energy deviation between Constraint3 and Constraint4 conditions is also less than −0.5 eV. Consequently, it is evidenced that, for surface models MH(001)-I and MH001)-II, Constraint2 and Constraint4 are adequate to guarantee the calculations' accuracy. MH(110)-I and MH(001)-II with Constraint2 and Constraint4 are employed as substrates in the following adsorption simulations (interface models).

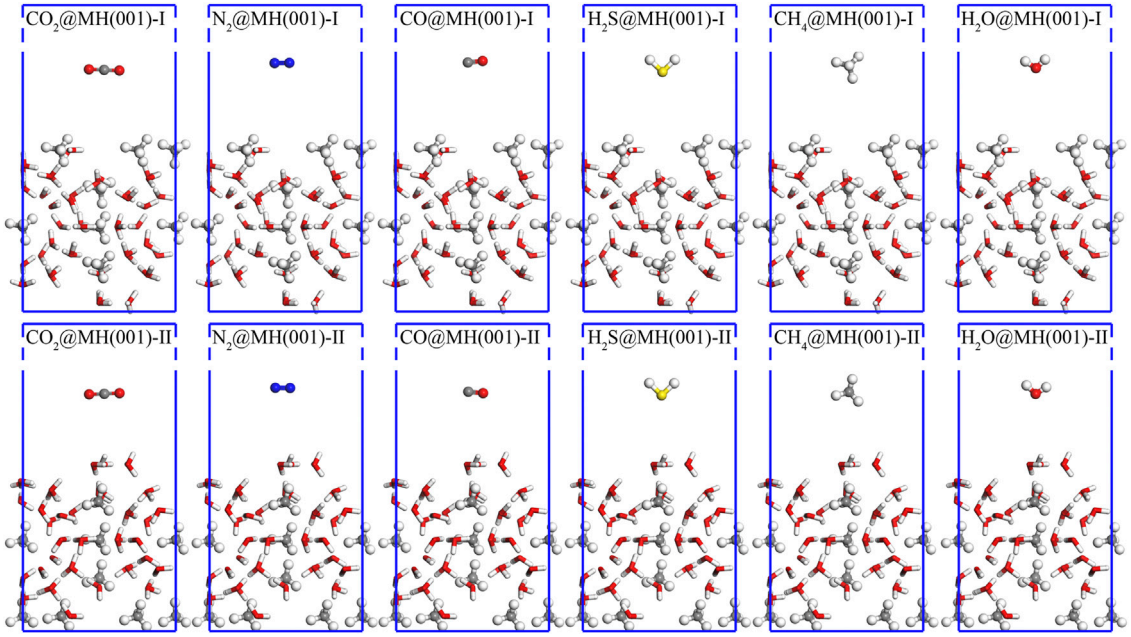

FIGURE 4
Initial interface models for the adsorptions of CO_2, N_2, CO, H_2S, CH_4, and H_2O over MH(001)-I and MH(001)-II substrates. The white, grey (green), red, blue, and yellow spheres denote H, C, O, N, and S atoms, respectively.

2.4 Interface models and adsorption simulations

By arbitrarily putting single molecule (CO_2, N_2, CO, H_2S, CH_4 and H_2O) over MH(110)-I and MH(110)-II surfaces, the initial distance between the molecule and surface is roughly 10 Å, and 12 interface models are established. These initial models (Figure 4) are treated as starting points of the adsorption processes.

For the initial interface models, MD geometry optimization is first implemented to achieve an intermediate configuration. On this basis, DFT-D relaxation is continued to reach the final configuration. The final relaxed models are treated as the equilibrium states of adsorption processes.

3 Results and discussion

3.1 Equilibrium model and adsorption energies

By sequentially conducting geometry optimizations with MD and DFT-D methods, the final equilibrium interface models are as shown in Figure 5.

Based on these final models, the adsorption energies (E_{ad}) can be ascertained as (Zhu et al., 2017):

$$E_{ad} = E_{\text{final interface}} - (E_{\text{surface}} + E_{\text{molecule}}) \quad (2)$$

where $E_{\text{final interface}}$, E_{surface}, and E_{molecule} denote the total energies of final interface slab, surface slab, and adsorbed gas molecules. The calculated adsorption energies (E_{ad}) are listed in Table 5.

The previous E_{ad} data of these six molecules are hardly retrieved. The adsorption energy of H_2O on the ice Ih basal plane were calculated around -59 kJ/mol (Thierfelder et al., 2006). By using the MD method, the adsorption energy of a single water molecule during MH's formation could be as high as −84.14 kJ/mol (Cox et al., 2018). The adsorption energies of single CH_4 and CO_2 into hydrate cage cavities were estimated as 46.31 kJ/mol and 36.66 kJ/mol with DFT method, respectively. The adsorption energy was estimated as large as −61.48 kJ/mol the adsorption energy of amino acids over (001) surface by employing DFT calculations (Hu et al., 2021b). These data are close to our results. Therefore, our results are reasonable and acceptable.

First, the adsorption energies for the six different molecules are all negative. This means that these adsorptions are all exothermal and spontaneous processes onto MH(001) substrate.

Second, a greater E_{ad} value implies a larger heat release for the adsorption process. Therefore, a greater E_{ad} value implies a stronger driving force to facilitate the adsorption's spontaneous occurrence. Consequently, the priority order of these adsorption processes can be queued as: H_2O > H_2S > CO_2 > N_2 > CH_4 > CO. The adsorptions of H_2O and CH_4 can be

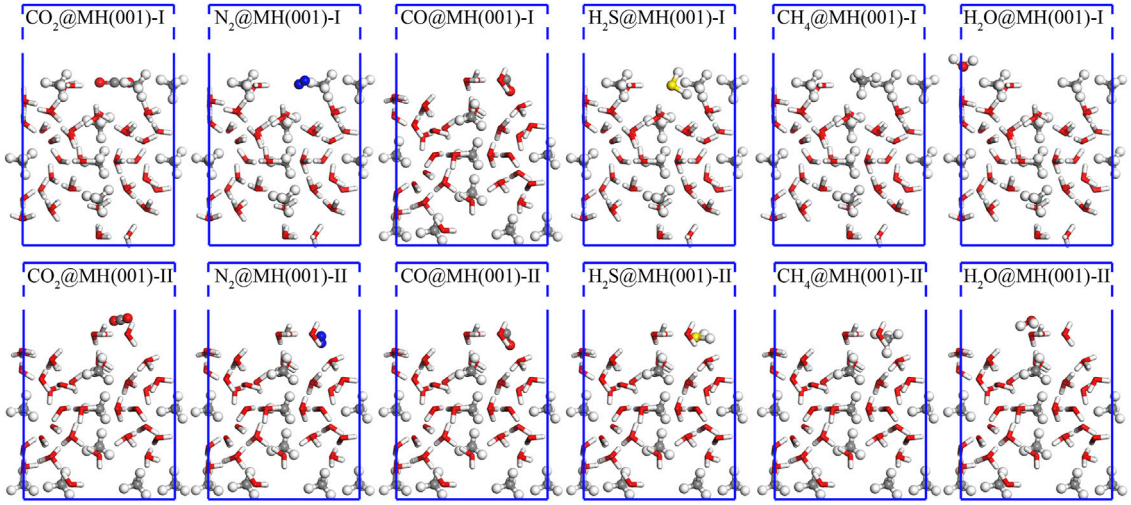

FIGURE 5
Final equilibrium interface models for the adsorptions of CO_2, N_2, CO, H_2S, CH_4, and H_2O over MH(001)-I and MH(001)-II substrates. The white, grey (green), red, blue, and yellow spheres denote H, C, O, N, and S atoms, respectively.

TABLE 5 Calculated adsorption energies (E_{ad}) of CO_2, N_2, CO, H_2S, CH_4, and H_2O onto MH(001)-I and MH(001)-II substrates.

Adsorbed molecules	E_{ad} onto different substrates (kJ/mol)		Average values (kJ/mol)
	MH(001)-I	MH(001)-II	
CO_2	−27.63	−25.51	−26.57
N_2	−28.94	−13.85	−21.39
CO	−15.34	−10.76	−13.05
H_2S	−53.80	−33.76	−43.78
CH_4	−21.52	−19.91	−20.72
H_2O	−51.57	−49.23	−50.40

regarded as the condensation of MH. The condensation process of H_2O is most prevalent. Importantly, the adsorptions of H_2S, CO_2 and N_2 are more privileged when compared with the condensation of CH_4, This implies that the molecules H_2S, CO_2 and N_2 have potential to be employed to replace CH_4 in MH. Meanwhile, the CO molecule has the least tendency to adhere onto MH(001) surface, and CH_4 will be hardly replaced with CO.

3.2 Interfacial configuration and electronic interaction

3.2.1 Interfacial diatomic distance

Our calculation results demonstrate that the molecules of CO_2, N_2, and H_2S can spontaneously adhere onto MH(001)-I surface. Their equilibrium atomic configurations are illustrated as Figure 5 and Figure 6.

The absorbed molecules have closer distance to the H atoms of H_2O molecules than to the CH_4 molecules of MH(001) surface. The diatomic distances between the adsorbed molecules and the closest H_2O molecules are labeled in Figure 6. These distances fall into the range of 1.8–3.0 Å, which corresponds to the hydrogen bond lengths in a previous study (Jendi et al., 2015). Therefore, hydrogen bonds are likely formed between these atom pairs.

3.2.2 Electronic interactions

The interfacial electron interactions of the absorbed CO_2, N_2, and H_2S molecules with the MH(001) surface are examined. Based on the equilibrium interface models, partial density of states (PDOS; as shown in Figure 7) and electron orbitals are employed to clarify the adsorption binding.

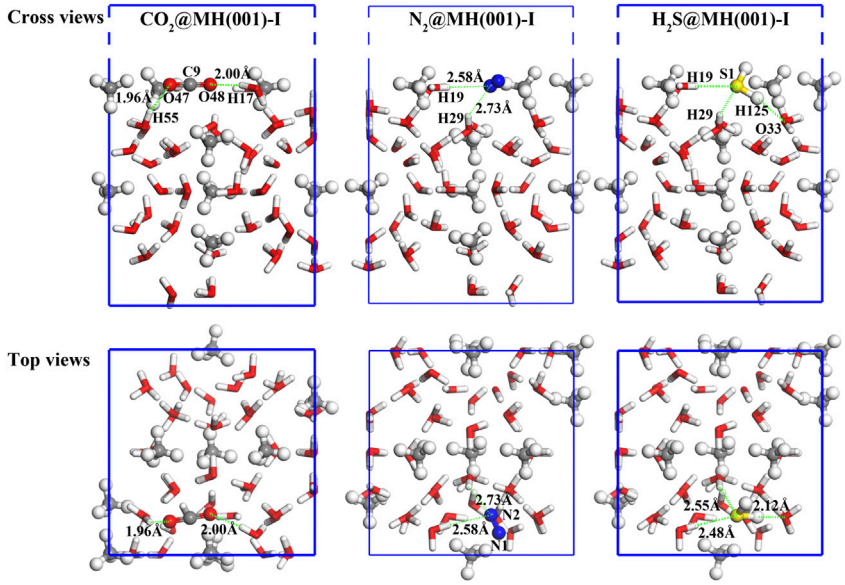

FIGURE 6
Final adsorption models of CO_2, N_2, and H_2S molecules, the green-dashed lines denote the interfacial bonds, and spheres with white, red, blue, yellow, and grey colors denote H, O, N, S, and C atoms, respectively.

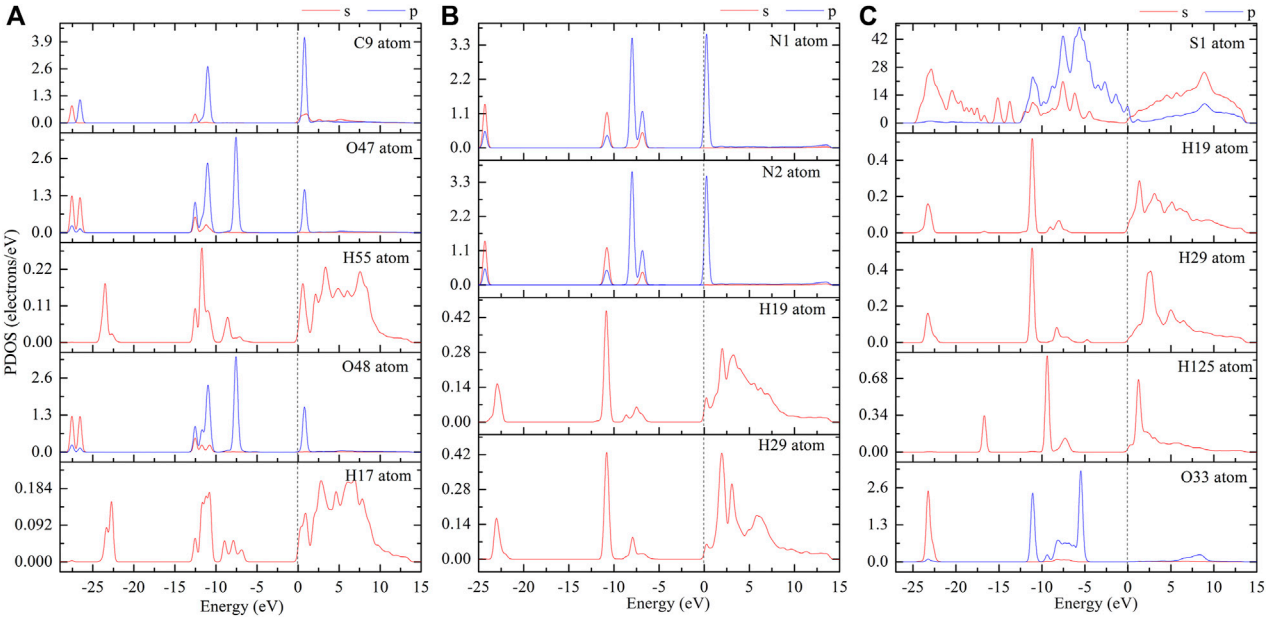

FIGURE 7
PDOS curves of absorbed CO_2 **(A)**, N_2 **(B)**, and H_2S **(C)** on MH(001) surface (please refer to the atom names in Figure 6).

The H-bonding effect mainly comes from the dispersion interactions of the interfacial electrons. Based on the PDOS curves, one can note that there are resonant peaks between the interfacial atoms, especially between the H atoms of H_2O and the O atoms of CO_2 (or N atoms of N_2, S, and H atoms of H_2S).

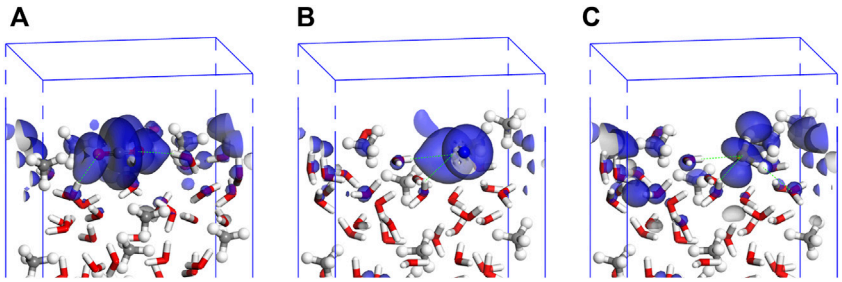

FIGURE 8
Interfacial electronic orbitals of absorbed CO_2 **(A)**, N_2 **(B)**, and H_2S **(C)** on MH(001) surface (energy level range: −1~1 eV).

The dispersion interactions are mainly contributed from the electrons with orbitals around the Fermi level. Therefore, the orbital images for the interfacial models of CO_2, N_2, and H_2S molecules are depicted in the energy range from −1 eV to +1 eV (Figure 8).

By combining the PDOS curves and the orbital images, it can be confirmed that, for the adsorptions of CO_2, N_2, and H_2S molecules, the interfacial H-bonds forms between the interfacial atoms. For the absorbed CO_2 molecule, the bonds will form mainly between O-2*p* in CO_2 and H-1*s* in H_2O. Similarly, for the absorbed N_2 molecule, the bonds will form mainly between N-2*p* in N_2 and H-1*s* in H_2O. However, for the absorbed H_2S molecule, the bonds will form not only between S-3*p* in H_2S and H-1*s* in H_2O but also between H-1*s* in H_2S and O-2*p* in H_2O.

4 Summary

In the present work, by utilizing MD and DFT computations, the adsorptions of CO_2, N_2, CO, H_2S, CH_4, and H_2O onto methane hydrate surface are investigated. The methane hydrate planes of (001) and (110), and various cleaving sites are compared with cleavage energies. The sI-MH(001) is more likely to exist comparing with MH(110). Two (001) surfaces of MH(001)-I and MH(001)-II with different terminations (CH_4+H_2O and H_2O only, respectively) are compared by examining the adsorption energies of these molecules. The molecules tend to adhere onto the surface MH(001)-I (termination CH_4+H_2O) with more negative adsorption energy. The priority order of these molecules' adsorptions can be queued as: H_2O > H_2S > CO_2 > N_2 > CH_4 > CO. So, CO_2, N_2, and H_2S have potential to replace the CH_4 in methane hydrate. The interfacial bonds and electronic interactions of these three molecules are narrowly investigated with PDOS and electron orbital. The interfacial H-bonds forms between the interfacial atoms for the adsorptions of CO_2, N_2, and H_2S. For the absorbed CO_2 molecule, the bonds will form mainly between O-2*p* in CO_2 and H-1*s* in H_2O. Similarly, for the absorbed N_2 molecule, the bonds will form mainly between N-2*p* in N_2 and H-1*s* in H_2O. However, for the absorbed H_2S molecule, the bonds will form not only between S-3*p* in H_2S and H-1*s* in H_2O but also between H-1*s* in H_2S and O-2*p* in H_2O.

Data availability statement

The raw data supporting the conclusion of this article will be made available by the authors, without undue reservation.

Author contributions

MZ: conceptualization, methodology, and software; BZ: data curation and writing—original draft; JhL: validation and investigation; TL: supervision; JnL: writing—review and editing.

Acknowledgments

The authors acknowledge the financial support from the Youth Innovation Team of Xi'an Shiyou University (Grant No. 2019QNKYCXTD04). Support from the Center for High Performance Computing of Northwestern Polytechnical University is also gratefully appreciated.

Conflict of interest

BZ was employed by the company No. 2 Gas Production Plant, PetroChina Changqing Oilfield Company.

The remaining authors declare that the research was conducted in the absence of any commercial or financial relationships that could be construed as a potential conflict of interest.

Publisher's note

References

Cao, X., Huang, Y., Jiang, X., Su, Y., and Zhao, J. (2017). Phase diagram of water–methane by first-principles thermodynamics: Discovery of MH-IV and MH-V hydrates. *Phys. Chem. Chem. Phys.* 19, 15996–16002. doi:10.1039/c7cp01147d

Cha, M., Shin, K., Lee, H., Moudrakovski, I. L., Ripmeester, J. A., and Seo, Y. (2015). Kinetics of methane hydrate replacement with carbon dioxide and nitrogen gas mixture using *in situ* NMR spectroscopy. *Environ. Sci. Technol.* 49, 1964–1971. doi:10.1021/es504888n

Chong, Z. R., Yang, S. H. B., Babu, P., Linga, P., and Li, X. (2016). Review of natural gas hydrates as an energy resource: Prospects and challenges. *Appl. Energy* 162, 1633–1652. doi:10.1016/j.apenergy.2014.12.061

Clark, S. J., Segall, M. D., Pickard, C. J., Hasnip, P. J., Probert, M. I. J., Refson, K., et al. (2005). First principles methods using CASTEP. *Z. fur Kristallogr. - Cryst. Mater.* 220, 567–570. doi:10.1524/zkri.220.5.567.65075

Cox, S. J., Taylor, D. J. F., Youngs, T. G. A., Soper, A. K., Totton, T. S., Chapman, R. G., et al. (2018). Formation of methane hydrate in the presence of natural and synthetic nanoparticles. *J. Am. Chem. Soc.* 140, 3277–3284. doi:10.1021/jacs.7b12050

Cox, S. J., Towler, M. D., Alfè, D., and Michaelides, A. (2014). Benchmarking the performance of density functional theory and point charge force fields in their description of sI methane hydrate against diffusion Monte Carlo. *J. Chem. Phys.* 140, 174703. doi:10.1063/1.4871873

Hu, Y., Wang, S., and He, Y. (2021). Interaction of amino acid functional group with water molecule on methane hydrate growth. *J. Nat. Gas Sci. Eng.* 93, 104066. doi:10.1016/j.jngse.2021.104066

Hu, Y., Wang, S., Yang, X., and He, Y. (2021). Examination of amino acid inhibitor effect in methane hydrate dissociation via molecular dynamics simulation. *J. Mol. Liq.* 325, 115205. doi:10.1016/j.molliq.2020.115205

Huang, Y., Li, K., Jiang, X., Su, Y., Cao, X., and Zhao, J. (2018). Phase diagram of methane hydrates and discovery of MH-VI hydrate. *J. Phys. Chem. A* 122, 6007–6013. doi:10.1021/acs.jpca.8b02590

Jendi, Z. M., Servio, P., and Rey, A. D. (2015). Ideal strength of methane hydrate and ice Ih from first-principles. *Cryst. Growth Des.* 15, 5301–5309. doi:10.1021/acs.cgd.5b00829

Kirchner, M. T., Boese, R., Billups, W. E., and Norman, L. R. (2004). Gas hydrate single-crystal structure analyses. *J. Am. Chem. Soc.* 126, 9407–9412. doi:10.1021/ja049247c

Kvenvolden, K. A. (1988). Methane hydrate - a major reservoir of carbon in the shallow geosphere? *Chem. Geol.* 71, 41–51. doi:10.1016/0009-2541(88)90104-0

Liang, S., Rozmanov, D., and Kusalik, P. G. (2011). Crystal growth simulations of methane hydrates in the presence of silica surfaces. *Phys. Chem. Chem. Phys.* 13, 19856–19864. doi:10.1039/c1cp21810g

Liao, B., Wang, J., Han, X., Wang, R., Lv, K., Bai, Y., et al. (2022). Microscopic molecular insights into clathrate methane hydrates dissociation in a flowing system. *Chem. Eng. J.* 430, 133098. doi:10.1016/j.cej.2021.133098

Lunt, D. J., Ridgwell, A., Sluijs, A., Zachos, J., Hunter, S., and Haywood, A. (2011). A model for orbital pacing of methane hydrate destabilization during the Palaeogene. *Nat. Geosci.* 4, 775–778. doi:10.1038/ngeo1266

Martos-Villa, R., Francisco-Márquez, M., Mata, M. P., and Sainz-Díaz, C. I. (2013). Crystal structure, stability and spectroscopic properties of methane and CO_2 hydrates. *J. Mol. Graph. Model.* 44, 253–265. doi:10.1016/j.jmgm.2013.06.006

Matsui, H., Jia, J., Tsuji, T., Liang, Y., and Masuda, Y. (2020). Microsecond simulation study on the replacement of methane in methane hydrate by carbon dioxide, nitrogen, and carbon dioxide–nitrogen mixtures. *Fuel* 263, 116640. doi:10.1016/j.fuel.2019.116640

McQuaid, M. J., Sun, H., and Rigby, D. (2004). Development and validation of COMPASS force field parameters for molecules with aliphatic azide chains. *J. Comput. Chem.* 25, 61–71. doi:10.1002/jcc.10316

Okwananke, A., Yang, J., Tohidi, B., Chuvilin, E., Istomin, V., Bukhanov, B., et al. (2018). Enhanced depressurisation for methane recovery from gas hydrate reservoirs by injection of compressed air and nitrogen. *J. Chem. Thermodyn.* 117, 138–146. doi:10.1016/j.jct.2017.09.028

Phrampus, B. J., and Hornbach, M. J. (2012). Recent changes to the Gulf Stream causing widespread gas hydrate destabilization. *Nature* 490, 527–530. doi:10.1038/nature11528

Shu, J., Chen, X., Chou, I. M., Yang, W., Hu, J., Hemley, R. J., et al. (2011). Structural stability of methane hydrate at high pressures. *Geosci. Front.* 2, 93–100. doi:10.1016/j.gsf.2010.12.001

Sloan, E. D. (2003). Fundamental principles and applications of natural gas hydrates. *Nature* 426, 353–359. doi:10.1038/nature02135

Sun, H. (1998). Compass: An *ab initio* force-field optimized for condensed-phase ApplicationsOverview with details on alkane and benzene compounds. *J. Phys. Chem. B* 102, 7338–7364. doi:10.1021/jp980939v

Thierfelder, C., Hermann, A., Schwerdtfeger, P., and Schmidt, W. G. (2006). Strongly bonded water monomers on the ice Ih basal plane: Density-functional calculations. *Phys. Rev. B* 74, 045422. doi:10.1103/physrevb.74.045422

Tkatchenko, A., and Scheffler, M. (2009). Accurate molecular van der Waals interactions from ground-state electron density and free-atom reference data. *Phys. Rev. Lett.* 102, 073005. doi:10.1103/physrevlett.102.073005

Walsh, M. R., Koh, C. A., Sloan, E. D., Sum, A. K., and Wu, D. T. (2009). Microsecond simulations of spontaneous methane hydrate nucleation and growth. *Science* 326, 1095–1098. doi:10.1126/science.1174010

Wang, H., Zhu, X., Cao, J., Qin, X., Yang, Y., Niu, T., et al. (2020). Density functional theory studies of hydrogen bonding vibrations in sI gas hydrates. *New J. Phys.* 22, 093066. doi:10.1088/1367-2630/abb54c

Zhang, L., Kuang, Y., Zhang, X., Song, Y., Liu, Y., and Zhao, J. (2017). Analyzing the process of gas production from methane hydrate via nitrogen injection. *Ind. Eng. Chem. Res.* 56, 7585–7592. doi:10.1021/acs.iecr.7b01011

Zhang, L., Yang, L., Wang, J., Zhao, J., Dong, H., Yang, M., et al. (2017). Enhanced CH_4 recovery and CO_2 storage via thermal stimulation in the CH_4/CO_2 replacement of methane hydrate. *Chem. Eng. J.* 308, 40–49. doi:10.1016/j.cej.2016.09.047

Zhu, B., Zhang, L., Xu, D., Cheng, B., and Yu, J. (2017). Adsorption investigation of CO2 on g-C3N4 surface by DFT calculation. *J. CO2 Util.* 21, 327–335. doi:10.1016/j.jcou.2017.07.021

frontiers | Frontiers in Earth Science

TYPE Opinion
PUBLISHED 21 September 2022
DOI 10.3389/feart.2022.1007620

OPEN ACCESS

EDITED BY
Qingbang Meng,
China University of Geosciences, China

REVIEWED BY
Zhiming Chen,
China University of Petroleum, China
Wendong Wang,
China University of Petroleum, China

*CORRESPONDENCE
Jinghua Liu,
liujh2019@yangtzeu.edu.cn
Guanglong Sheng,
shenggl2019@yangtzeu.edu.cn

SPECIALTY SECTION
This article was submitted to Geochemistry, a section of the journal Frontiers in Earth Science

RECEIVED 30 July 2022
ACCEPTED 02 September 2022
PUBLISHED 21 September 2022

CITATION
Yang Y, Liu J, Sheng G, Du F and Zheng D (2022), Analysis of the influence of CO_2 pre-injection during hydraulic fracturing on enhanced oil recovery in shale reservoirs. *Front. Earth Sci.* 10:1007620. doi: 10.3389/feart.2022.1007620

Analysis of the influence of CO_2 pre-injection during hydraulic fracturing on enhanced oil recovery in shale reservoirs

Yage Yang[1,2], Jinghua Liu[1,2]*, Guanglong Sheng[1,2]*, Fengshuang Du[1,2] and Da Zheng[3]

[1]Hubei Key Laboratory of Drilling and Production Engineering for Oil and Gas, Yangtze University, Wuhan, China, [2]School of Petroleum Engineering, Yangtze University, Wuhan, China, [3]Research Institute of Petroleum Exploration & Development, PetroChina, Beijing, China

KEYWORDS

hydraulic fracturing, CO_2 pre-injection, reservoir pressure, stimulated reservoir volume, fracturing stimulation

1 Introduction

Hydraulic fracturing was first developed in North America, resulting in a multi-stage horizontal well and multi-layer vertical well volume fracturing technology, and has been commonly used in reservoir reconstruction. However, hydraulic fracturing will cause a lot of waste of water resources, and the treatment of flowback fluids requires high cost (Wang et al., 2012; Lu et al., 2016; Rao et al., 2021). Supercritical CO_2 has attracted much attention due to its high mobility and low intermolecular interaction. Using CO_2 fracturing can effectively avoid the above problems by show more effectively increase the reservoir pressure and reduce the damage to the reservoir (King, 1983; Bryant and Monger, 1988; Yost et al., 1993; Xie and Hou, 2009). However, CO_2 fracturing needs a large number of supercritical CO_2, which is expensive and not easily accessible.

Since the first application of CO_2 fracturing technology in the United States in the 1980s, CO_2 fracturing technology has entered a stage of rapid development (Gupta and Bobier, 1998; Wei et al., 2019; Chen et al., 2020). A large number of CO_2 pre-injection experiments during hydraulic fracturing have been carried out, and field applications have been carried out in oilfields, which have achieved good results in increasing production (Liu et al., 2014; Zhou et al., 2019). In 1990, CO_2 sand fracturing, N_2 foam fracturing and N_2 fracturing were carried out in 15 gas wells in Kentucky, United States. The production data show that the cumulative gas production of CO_2 sand fracturing wells in 37 months is 2 times that of N_2 fracturing wells and 5 times that of N_2 foam fracturing wells. In 2014, an oil well in Oklahoma was fractured by CO_2. The daily oil production after fracturing was 2.7 t, and the oil production increased to 3.3 t/d after 1 month. CO_2 fracturing technology has been applied in 25 wells of tight oil reservoir, and the average daily production of single well is 1.7 t higher than that of adjacent wells. But up to now, there is still a lack of discussion on the mechanisms of CO_2 pre-injection to increase reservoir energy and production. Therefore, this paper aimed at investigating the interaction between pre-injected CO_2 and the reservoir fluid/rock/energy, providing reference for further confirming the mechanism of enhancing production and improving the fracturing effect.

2 Effect of CO_2 on rocks and fluids in reservoirs

The study on the interaction of injected CO_2 with reservoir rocks and fluids is of great significance for fracturing and reservoir reconstruction using CO_2. The influence of injected CO_2 on reservoirs is mainly reflected in four aspects, namely, improving physical properties of matrix, influence on fluid, improving stimulation effect and increasing reservoir pressure.

2.1 Effect of CO_2 on reservoir rocks

The improvement of reservoir properties by CO_2 is mainly reflected in the influence of porosity and permeability of rock, the change of reservoir wettability, plugging removal, and inhibition of clay expansion.

2.1.1 Changes of porosity and permeability

On the one hand, when the CO_2 dissolution mechanism dominates, the porosity and permeability of rock will increase with the injection of CO_2. When rocks and reservoir water contact with CO_2, CO_2 aqueous solution will produce new pores or broaden primary pores in the dissolution of organic matter or minerals, and the dissolution will increase with the increase of temperature and immersion time (Ross et al., 1981; Pokrovsky et al., 2005). Zou et al. (2021) conducted an experiment on the change of pore structure of shale reservoirs after immersion in CO_2 aqueous solution for 24 h under simulated reservoir temperature/pressure conditions (80°C, 20 MPa), and the rock matrix sample was soaked for 24 h. A large number of dissolved pores appeared, the porosity

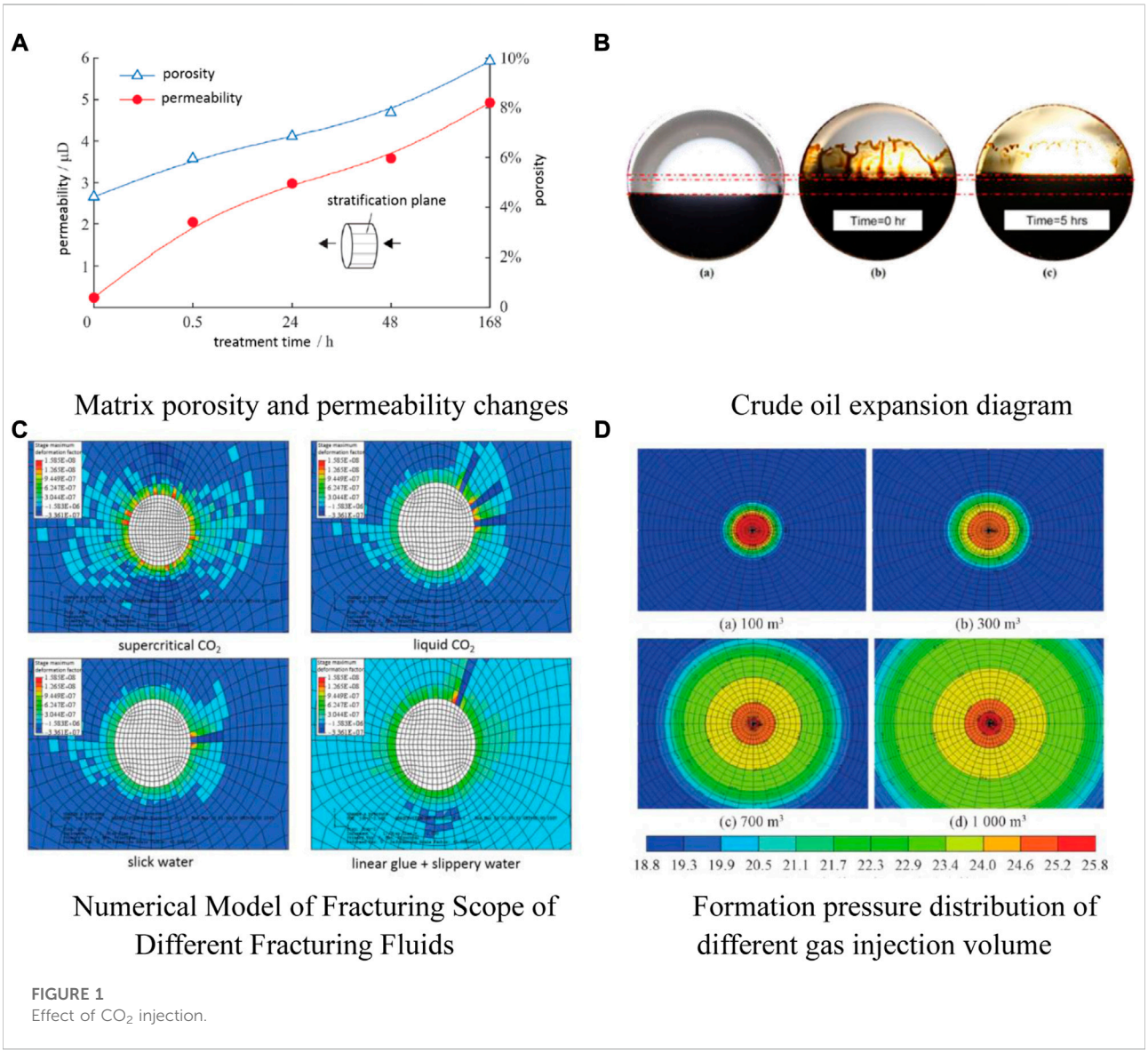

FIGURE 1
Effect of CO_2 injection.

was increased by 6.9%, and the permeability was increased from 0.23 μD to 2.98 μD. Experiments have proven that CO_2 can greatly increase the porosity and permeability, which is beneficial to increase production after fracturing.

On the other hand, when CO_2 adsorption expansion is dominant, CO_2 injection will reduce rock porosity and permeability. The interaction of CO_2, brine, and rock will form mineral crystals, which grow and precipitate in pores (Xu et al., 2005; Lahann et al., 2013). An experimental study by Kumar et al. (2015) showed that the adsorption of CO_2 in micropores may cause adsorption-induced swelling, thereby closing existing natural fractures and reducing fluid flow capacity. The change of pore structure is significantly affected by CO_2, and it is necessary to conduct targeted research on shale in practical applications.

2.1.2 Change of wettability

CO_2 can change reservoir wettability (Chiquet et al., 2005; Zhang et al., 2018). The injection of CO_2 will form carbonate in the reservoir, and the acid reacts with the minerals in the reservoir to generate new minerals, thereby changing the wettability of the solid wall of the liquid phase. The strong hydrophilicity of the reservoir is conducive to improving the injectivity of subsequent water flooding, and thus improving the recovery efficiency. Yao et al. (2017) proved that after injection of CO_2 into the reservoir, the wetting contact angle decreased and the hydrophilicity of the reservoir increased.

2.1.3 Deblocking and inhibiting clay swelling

In shale reservoirs, the reduction of the pH value of reservoir water can inhibit the expansion of clay. In carbonatite and sandstone, partial plugging can be relieved to restore oil well production. In the experiments by Zhang et al. (2020), the aqueous solution was slightly acidic owing to CO_2 dissolution, and the formation water dissolved CO_2 and interacted with the formation matrix to relieve plugging and inhibit clay swelling.

2.2 Effect of CO_2 on fluid

The influence of CO_2 on fluid is mainly reflected in the influence of extraction rate, density, expansion, gas solubility, surface tension, and irreducible water saturation.

2.2.1 Effect on mass transfer of oil

CO_2 enhances the extraction capacity of crude oil (Ding et al., 2019). It is difficult for CO_2 to get miscible with crude oil at first contact, so pre-injection of CO_2 can achieve multi-contact with oil, and the extraction effect of CO_2 on crude oil is continuously enriched to realize the miscibility. CO_2 has strong extraction ability for C2-C5 components of crude oil, but weak extraction ability for heavy components and methane. Liu et al. (2021) determined the extraction rate of crude oil by CO_2 at different pressures. Results show that CO_2 density was positively correlated with pressure. When the pressure reaches 40 MPa, the extraction rate can reach 85.2%. The experiment showed that CO_2 significantly enhanced the extraction rate of crude oil, as shown in Figure 1A.

2.2.2 Effect on oil density

Dissolving CO_2 in crude oil will increase the density of crude oil. With the increase of CO_2 content, more supercritical CO_2 contacts with crude oil, and the density of crude oil increases with the increase of CO_2 content (Abedini and Torabi, 2014). Su et al. (2021) injected 45% mole fraction of CO_2 into crude oil in the oil expansion experiment, and the oil density was increased by 8.78% from 0.7341 to 0.7986 g/cm^3 at 20 MPa.

2.2.3 Effect on oil expansion

CO_2 has a high expansion effect on crude oil. The specific volume, reservoir volume factor and compressibility coefficient of crude oil increase after CO_2 injection, which increases the compressibility of crude oil and further improves the productivity of oil wells (Nobakht et al., 2008), as shown in Figure 1B. Su et al. (2021) conducted crude oil expansion experiment, and found that when the mole fraction of CO_2 in crude oil was increased from 0 to 0.45%, the specific volume, reservoir volume factor, and compressibility coefficient of crude oil were increased by 2.53, 30.06, and 41.54%, respectively. Zhang et al. (2020) injected CO_2 into crude oil, and the expansion coefficient of crude oil increased from 1.00 to 1.19 after adding 45% CO_2. The above experiments have demonstrated that CO_2 can significantly enhance the elastic energy of reservoir.

2.2.4 Effect on gas solubility

The injection of CO_2 can effectively improve the gas solubility of crude oil. The higher the viscosity of crude oil is, the more obvious the viscosity reduction effect will be. Lower viscosity can increase its mobility, which is conducive to the production of crude oil. Shi and Zhao (2020) found that the average dissolved gas-oil ratio of the oil samples increased from 13.5 to 18.05, an increase of 4.52, accounting for 33.41% of the dissolved gas-oil ratio of total oil samples. The data show that CO_2 injection into crude oil can effectively enhance the gas solubility of crude oil and improve the gas solubility of crude oil.

2.2.5 Effect on oil-water surface tension

CO_2 can reduce the oil-water interfacial tension and reduce the viscosity of crude oil. CO_2 was injected into the reservoir in advance and CO_2 was contacted with crude oil many times, which improved the physical properties of crude oil, enhanced the mobility of crude oil and finally reached the miscibility. This will greatly reduce crude oil viscosity, improve displacement efficiency and increase production. The high-pressure PVT experiments conducted by Yang et al. (2009) showed that when the oil-water mixed solution was saturated with CO_2, the interfacial tension can be reduced by about 33%. Reducing the surface tension can reduce the adhesion work that needs to be overcome to strip oil from the rock surface, making the oil adhered to the rock surface and pores easier to be extracted.

2.2.6 Effect on irreducible water saturation

Injecting CO_2 increases irreducible water saturation (Liu et al., 2020). With the injection of CO_2, the dissolved gas volume of reservoir water increase. Some of the irreducible water that occupies the oil flow channel becomes mobile water, which makes the oil flow out and thus improves the recovery efficiency. Zhao et al. (2011) conducted the reservoir water injection CO_2 expansion experiment, and found that when the injection pressure was 27 MPa, irreducible water saturation increased from 36.3 to 41.11%.

2.3 Improving stimulated effect

Improving stimulated effect by CO_2 is mainly reflected in reducing initiation pressure and increasing fracture complexity.

2.3.1 Reducing initiation pressure

Supercritical CO_2 can reduce the rupture pressure of rocks. Since supercritical CO_2 has good diffusion and permeability, supercritical CO_2 fracturing reduces the effective stress of surrounding rock by increasing pore pressure, which makes the initiation pressure lower than hydraulic fracturing (Tudor et al., 1994; Ito, 2008; Zou et al., 2018; Deng et al., 2022), as shown in Figure 1C. Ding et al. (2018) analyzed the fracturing mechanism of supercritical CO_2 fracturing based on the rock fracture criterion of linear elastic model. The calculated data indicated that the rupture pressure by using supercritical CO_2 was reduced by 75.5%. Wang et al. (2019) experimentally demonstrated that the initiation pressure of supercritical CO_2 fracturing rock is 15% lower than that of liquid CO_2 under the same conditions, which is about half of that of hydraulic fracturing.

2.3.2 Increasing fracture complexity

Supercritical CO_2 has the effect of slippage and diffusion, which makes its liquidity have certain nonlinear characteristics. CO_2 can enter the tiny pores and fracture tips that water and fracturing fluid cannot enter during the propagation, promoting the opening of natural weak surface and increasing the complexity of fractures (Zou et al., 2018; Sheng et al., 2019; Tudor et al., 1994; Ito, 2008). Su et al. (2019) combined with physical simulation and numerical simulation, and found that the volume strain increment produced by supercritical CO_2 fracturing is higher than that of hydraulic fracturing, the fracture conplexity and fracture surface roughness after fracturing are also larger, and the fracture morphology is more complex (Zhou et al., 2016).

2.4 Enhancing reservoir pressure

Injection of CO_2 can effectively increase reservoir pressure, which is conducive to production. CO_2 has strong injection, good diffusion, strong production-increasing effect, wide range of pressure spread. Equal velocity injection of liquid carbon dioxide and water, the pressure-increasing effect of CO_2 injection is twice that of water injection (Singh, 2018; Xiao, 2018). Zhang et al. (2020) found that with the increase of CO_2 injection rate, the radius of miscible zone increased gradually. Due to the rapid propagation of CO_2 pressure, the reservoir pressure increases rapidly, as shown in Figure 1D, and the pressure can be maintained above 29 MPa in the reservoir near the wellbore.

3 Conclusion and foresight

CO_2 pre-injection during hydraulic fracturing can affect the physical properties of the reservoir, increase the porosity and permeability of the rock and improve the wettability of the reservoir, which is conducive to improving the subsequent water flooding injection capacity. CO_2 injection enhances the flow capacity of crude oil by using the effect of CO_2 injection on the fluid, making it easier for crude oil to be recovered. It also reduces initiation pressure, increases fracture complexity and increases formation pressure. Combined with water-based fracturing fluid, the fractures were further propagated and effectively supported.

At present, the mechanism of CO_2 pre-injection during hydraulic fracturing on reservoir has not been comprehensive considered in the fracture propagation simulation and production dynamic simulation. In the future, all of the mechanism should be considered for the accuracy and efficiency of experimental and theory research.

Author contributions

CRediT author statement YY: Investigation and research, Conceptualization, Writing—Original draft preparation JL: Resources, Translation GS: Supervision, Modify analysis FD: Typesetting.

Funding

Supported by Open Fund of Hubei Key Laboratory of Drilling and Production Engineering for Oil and Gas (Yangtze University) (ID: YQZC202203).

Conflict of interest

The authors declare that the research was conducted in the absence of any commercial or financial relationships that could be construed as a potential conflict of interest.

Publisher's note

References

Abedini, A., and Torabi, F. (2014). On the CO_2 storage potential of cyclic CO_2 injection process for enhanced oil recovery. *Fuel* 124, 14–27. doi:10.1016/j.fuel.2014.01.084

Bryant, D. W., and Monger, T. G. (1988). Multiple-contact phase behavior measurement and application with mixtures of CO_2 and highly asphaltic crude. *SPE Reserv. Eng.* 3 (02), 701–710. doi:10.2118/14438-pa

Chen, H., Liu, X., and Jia, N. (2020). Prospects and key scientific issues of CO2 near-mis cible flooding. *Petroleum Sci. Bull.* 03, 392–401. doi:10.3969/j.issn.2096-1693.2020.03.033

Chiquet, P., Broseta, D., and Thibeau, S. (2005). "Capillary alteration of shaly caprocks by carbon dioxide (SPE94183)," in 67th EAGE Conference & Exhibition, Madrid, Spain, June 13–16, 2005 (European Association of Geoscientists & Engineers). cp-1-00041.

Deng, H., Sheng, G., Zhao, H., Meng, F., Zhang, H., Ma, J., et al. (2022). Integrated optimization of fracture parameters for subdivision cutting fractured horizontal wells in shale oil reservoirs. *J. Petroleum Sci. Eng.* 212, 110205. doi:10.1016/j.petrol.2022.110205

Ding, M., Wang, Y., Han, Y., Gao, M., and Wang, R. (2019). Interactions in bypassed oil-CO_2 systems and their utilization in enhancing the recovery of bypassed oil[J]. *Fuel* 237, 1068–1078. doi:10.1016/j.fuel.2018.10.019

Ding, Y., Ma, X., and Ye, L. (2018). *Rock breaking mechanism of CO2 and fracturing technology*. Qingdao, China: Elsevier BV.

Gupta, D. V. S., and Bobier, D. M. (1998). "The history and success of liquid CO_2 and CO_2/N2 fracturing system," in SPE Gas Technology Symposium, Calgary, Alberta, Canada, March 15–18, 1998. SPE 40016: Society of Petroleum Engineers.

Ha, S. J., Choo, J., and Yun, T. S. (2018). Liquid CO_2 fracturing: Effect of fluid permeation on the breakdown pressure and cracking behavior. *Rock Mech. Rock Eng.* 51 (11), 3407–3420. doi:10.1007/s00603-018-1542-x

Ito, T. (2008). Effect of pore pressure gradient on fracture initiation in fluid saturated porous media: Rock. *Eng. Fract. Mech.* 75 (7), 1753–1762. doi:10.1016/j.engfracmech.2007.03.028

King, S. R. (1983). "Liquid CO_2 for the stimulation of low-permeability reservoirs," in SPE/DOE Low Permeability Gas Reservoirs Symposium, Denver, Colorado, March 14–16, 1983. OnePetro.

Kumar, H., Elsworth, D., Liu, J., Pone, D., and Mathews, J. P. (2015). Permeability evolution of propped artificial fractures in coal on injection of CO_2. *J. Petroleum Sci. Eng.* 133, 695–704. doi:10.1016/j.petrol.2015.07.008

Lahann, R., Mastalerz, M., Rupp, J. A., and Drobniak, A. (2013). Influence of CO_2 on new albany shale composition and pore structure. *Int. J. Coal Geol.* 108, 2–9. doi:10.1016/j.coal.2011.05.004

Liu, H., Wang, F., Zhang, J., and Meng, S. (2014). Fracturing with carbon dioxide: Application and development trend. *Petroleum Explor. Dev.* 41 (4), 513–519. doi:10.1016/S1876-3804(14)60060-4

Liu, H., Zhu, Z., Patrick, W., Liu, J., Lei, H., and Zhang, L. (2020). Pore-scale numerical simulation of supercritical CO2 migration in porous and fractured media saturated with water. *Adv. Geo-Energy Res.* 4 (4), 419–434. doi:10.46690/ager.2020.04.07

Liu, J., Li, L., and Gao, M. (2021). Interaction between CO_2 and crude oil in low permeability reservoirs. *Oilfield Chem.* 38 (03), 464–469. doi:10.19346/j.cnki.1000-4092.2021.03.015

Lu, J., Nicot, J. P., Mickler, P. J., Ribeiro, L. H., and Darvari, R. (2016). Alteration of bakken reservoir rock during CO_2-based fracturing—an autoclave reaction experiment. *J. Unconv. Oil Gas Resour.* 14, 72–85. doi:10.1016/j.juogr.2016.03.002

Nobakht, M., Moghadam, S., and Gu, Y. (2008). Mutual interactions between crude oil and CO_2 under different pressures. *Fluid phase equilibria* 265 (1-2), 94–103. doi:10.1016/j.fluid.2007.12.009

Pokrovsky, O. S., Golubev, S. V., and Schott, J. (2005). Dissolution kinetics of calcite, dolomite and magnesite at 25 C and 0 to 50 atm pCO_2. *Chem. Geol.* 217 (3-4), 239–255. doi:10.1016/j.chemgeo.2004.12.012

Rao, X., Xu, Y., Liu, D., and Hu, Y. (2021). A general physics-based data-driven framework for numerical simulation and history matching of reservoirs. *Adv. Geo-Energy Res.* 5 (4), 422–436. doi:10.46690/ager.2021.04.07

Ross, G. D., Todd, A. C., and Tweedie, J. A. (1981). "The effect of simulated CO_2 flooding on the permeability of reservoir rocks," in *Enhanced oil recovery* (Amsterdam: Elsevier), 351–366.

Sheng, G., Su, Y., and Wang, W. (2019). A new fractal approach for describing induced-fracture porosity/permeability/compressibility in stimulated unconventional reservoirs. *J. Petroleum Sci. Eng.* 179, 855–866. doi:10.1016/j.petrol.2019.04.104

Shi, J., and Zhao, X. (2020). Effect of CO_2 on physical properties of crude oil. *China Petroleum Chem. Stand. Qual.* 40 (8), 117–118,120. doi:10.3969/j.issn.1673-4076.2020.08.056

Singh, H. (2018). Impact of four different CO2 injection schemes on extent of reservoir pressure and saturation. *Adv. Geo-Energy Res.* 2 (3), 305–318. doi:10.26804/ager.2018.03.08

Su, Y., Wang, C., and Li, L. (2021). Behavior of CO2 pre-fracturing fluid in tight reservoir. *Sci. Technol. Eng.* 21 (8), 3076–3081. doi:10.3969/j.issn.1671-1815.2021.08.014

Su, Z., Li, F., and Zhou, D. (2019). Hydraulic fracture propagation behavious and geometry under supercritical CO_2 fracturing in shale reservoirs. *Oil Gas Geol.* 40 (3), 616–625. doi:10.11743/ogg20190316

Tudor, R., Vozniak, C., and Peters, W. (1994). "Technical advances in liquid CO2 fracturing," in Annual Technical Meeting, Calgary, Alberta, June 11–14, 1994. OnePetro.

Wang, H., Li, G., and Shen, Z. (2012). A feasibility analysis on shale gas exploitation with supercritical carbon dioxide. *Energy Sources, Part A Recovery, Util. Environ. Eff.* 34 (15), 1426–1435. doi:10.1080/15567036.2010.529570

Wang, X., Sun, X., and Luo, P. (2019). Progress and application of CO2 fracturing technology for unconventional oil and gas[J]. *Lithologic Reservoirs* 31 (2), 1–7

Wei, Q., Hou, J., and Hao, H. (2019). Laboratory study of CO2 channeling characteristics in ultra-low-permeability oil reservoirs. *Petroleum Sci. Bull.* 02, 145–153. doi:10.3969/j.issn.2096-1693.2019.02.013

Xiao, S. (2018). *Research on carbon dioxide flooding technology in Fu Yang oilfield*. Daqing: Northeast Petroleum University.

Xie, P., Hou, G., and Han, J. (2009). Application of CO, fracturing technology in sulige gas field. *Fault-Block Oil Gas Field* 16 (5), 104–106.

Xu, T., Apps, J. A., and Pruess, K. (2005). Mineral sequestration of carbon dioxide in a sandstone–shale system. *Chem. Geol.* 217 (3-4), 295–318. doi:10.1016/j.chemgeo.2004.12.015

Yang, S., Hang, D., Sun, R., et al. (2009). CO_2 extraction for crude oil and its effect on crude oil viscosity. *J. Petroleum Sci. Eng. Nat. Sci. Ed.* 33 (4), 85–88. doi:10.3321/j.issn:1673-5005.2009.04.016

Yao, Z., Huang, C., and Ma, Y. (2017). Physical property variation law of CO_2 flooding reservoir, Yanchang Oilfield. *Fault-block Oilfield* 24 (1), 60–62. doi:10.6056/dkyqt201701014

Yost, A. B., Mazza, R. L., and Gehr, J. B. (1993). "CO2/Sand fracturing in devonian shales," in SPE Eastern Regional Meeting, Pittsburgh, Pennsylvania, November 2–4, 1993. OnePetro.

Zhang, K., Bai, X., and Liu, S. (2020). Energy enhancement effect and parameters optimization of CO_2 injection in tight oil reservoir. *Sci. Technol. Eng.* 20 (26), 10751–10758. doi:10.3969/j.issn.1671-1815.2020.26.029

Zhang, X., Wei, B., Shang, J., Gao, K., Pu, W., Xu, X., et al. (2018). Alterations of geochemical properties of a tight sandstone reservoir caused by supercritical CO_2-brine-rock interactions in CO_2-EOR and geosequestration. *J. CO_2 Util.* 28, 408–418. doi:10.1016/j.jcou.2018.11.002

Zhao, M., Li, J., and Wang, Z. (2011). Study on mechanism of CO_2 immiscible flooding in ultra-low permeability reservoir [J]. *Sci. Tech. Engg.* 11 (7), 1438–1440

Zhou, J., Hu, N. A. N., Xian, X., Zhou, L., Tang, J., Kang, Y., et al. (2019). Supercritical CO2 fracking for enhanced shale gas recovery and CO2 sequestration: Results, status and future challenges. *Adv. Geo-Energy Res.* 3 (2), 207–224. doi:10.26804/ager.2019.02.10

Zhou, J., Liu, G., Jiang, Y., Xian, X., Liu, Q., Zhang, D., et al. (2016). Supercritical carbon dioxide fracturing in shale and the coupled effects on the permeability of fractured shale: An experimental study. *J. Nat. Gas Sci. Eng.* 36, 369–377. doi:10.1016/j.jngse.2016.10.005

Zou, Y., Li, S., Ma, X., Zhang, S., Li, N., and Chen, M. (2018). Effects of CO_2–brine–rock interaction on porosity/permeability and mechanical properties during supercritical-CO_2 fracturing in shale reservoirs. *J. Nat. Gas Sci. Eng.* 49, 157–168. doi:10.1016/j.jngse.2017.11.004

Zou, Y., Li, Y., and Li, S. (2021). Influence of CO_2 pre-injection on fracture mophology and the petrophysical properties in shale fracturing. *Nat. Gas. Ind.* 41 (10). doi:10.3787/j.issn.1000-0976.2021.10.009

frontiers | Frontiers in Earth Science

TYPE Original Research
PUBLISHED 30 September 2022
DOI 10.3389/feart.2022.1016941

OPEN ACCESS

EDITED BY
Qingbang Meng,
China University of Geosciences
Wuhan, China

REVIEWED BY
Hao Xiong,
University of Oklahoma, United States
Kang Botao,
China National Offshore Oil
Corporation, China

*CORRESPONDENCE
Pin Jia,
jiapin1990@163.com

SPECIALTY SECTION
This article was submitted
to Geochemistry,
a section of the journal
Frontiers in Earth Science

RECEIVED 11 August 2022
ACCEPTED 25 August 2022
PUBLISHED 30 September 2022

CITATION
Jia P, Guo H, Wang Y, Peng C, Cheng L and Ke X (2022), COMSOL-based investigation of the characteristics of microscopic water flooding and residual oil distribution in carbonate reservoirs. *Front. Earth Sci.* 10:1016941.
doi: 10.3389/feart.2022.1016941

COMSOL-based investigation of the characteristics of microscopic water flooding and residual oil distribution in carbonate reservoirs

Pin Jia[1,2]*, Hongxin Guo[1,2], Yichen Wang[1,2], Cong Peng[1,2], Linsong Cheng[1,2] and Xianzhe Ke[1,2]

[1]State Key Laboratory of Petroleum Resources and Prospecting, China University of Petroleum, Beijing, China, [2]College of Petroleum Engineering, China University of Petroleum, Beijing, China

Carbonate reservoirs are rich in oil and gas reserves; thus, they have great exploitation potential. Therefore research on the microscopic mechanisms of carbonate reservoirs is of great significance. Based on the thin section images of core castings of typical Well 555 and its pore and fracture features in actual reservoirs, this study designed three kinds of images representing the pore and throat structure of real rocks by applying image stitching and binarization processing methods. A microscopic pore model of carbonate rocks was then established using COMSOL numerical simulation software. The microscopic water flooding characteristics and residual oil distributions of different schemes were observed by designing different fracture development forms. The fractures that developed in parallel main lines showed a more obvious influence on water flooding characteristics compared to fractures that developed in vertical main lines. The cluster residual oil was the main residual oil type in the early stage of water flooding in the pure matrix model. With the progress of water flooding, the continuous cluster residual oil gradually turned into mainly discontinuous porous and columnar residual oils. Vertical mainline fractures reduced the amount of residual oil in clusters and replaced it with columnar residual oil. In contrast, parallel main line fractures expanded the unswept area, with the residual oil appearing in contiguous clusters. This study microscopically analyzed the law and characteristics of water flooding in carbonate reservoirs to provide key theoretical support for enhancing oil recovery.

KEYWORDS

carbonate reservoir, numerical simulation, microscopic water flooding characteristics, residual oil, flow performance

Introduction

Approximately 40% of the world's total oil and gas reserves are carbonate reservoirs, with oil and gas production accounting for about 60% of the total production (Roehl and Choquette, 1985a; Roehl and Choquette, 1985b). By the end of 2013, 2P recoverable reserves of oil and gas in marine carbonate rocks accounted for approximately 37.3% of the global total recoverable reserves (Roehl and Choquette, 1985a; Roehl and Choquette, 1985b). Globally, carbonate reservoirs are mainly distributed in the northern hemisphere (Roehl and Choquette, 1985a; Roehl and Choquette, 1985b). Carbonate rocks are sedimentary rocks composed of carbonate minerals (calcite-calcium carbonate mineral, dolomite-calcium, and magnesium carbonate). Carbonate reservoirs are mainly composed of primary matrix pores and secondary fractures, pores, and caves including pore, karst cave, fracture, and pore types, as well as fracture-karst cave, pore-fracture, and fracture-pore types. Many scholars have studied the waterflooding development methods of carbonate rocks, including pressure retaining exploitation, steam huff and puff, combined top gas and edge water injection, bottom injection, and top production (buoyancy support), and well patterns with some strong areas and weak surfaces (Xue et al., 2016; Cui, 2018; Song and Li, 2018; Yuan et al., 2021). However, research is lacking on the microscopic mechanisms, which can guide understanding of the impact of pore structure changes on water flooding development to help inform the further development of residual oil.

Many experimental methods have been proposed to microscopically explore water flooding, including etching glass and other physical methods to characterize the microscopic pore structure. Some studies have applied the digital core method to scan the core, followed by numerical simulation to produce three-dimensional models of the cores to quantitatively analyze the water flooding process and draw corresponding conclusions.

The physical model of etched glass was first described in the 1950s to observe microscopic phenomena. In the early 1960s, Mattax and Kyte reported improved methods for observing microscopic displacement details and developed the first etched glass network model. Later, Davis and Jonesl improved the etched glass microscopic model by using photosensitive technology. In 1977, Bonnet and Lenormand reported a resin technique to control the network geometry. Mckellar and Wardlar then introduced the technique for making micro-models using glass mirrors. The 2D micro-model made by etching glass is the most common method reported in the literature. The pore structure of the micro-model prepared in this way is basically the same as that of the actual core; therefore, the experimental results are of more practical significance (Li, 1996). Using the simulation micro-model, Guo et al. (1990) reported that bound water mainly existed in three states in the hydrophilic: in the narrow throat; as a "dead end" with no exit, and as a film on the pore wall, especially on rough pore surfaces. In the oil-philic model, bound water mainly existed as granules or islands in large pores. In addition, Donalolson et al. used the etched glass model to analyze the distribution of residual oil. While it is not possible to measure production and other data or to analyze the characteristics of water flooding through physical experiments, microscopic numerical simulations may be able to overcome these challenges.

Regarding microscopic numerical simulation, previous studies have proposed the establishment of digital cores constructed using two general methods: physical experiments and numerical reconstruction (He). In the physical experiment method, the focused scanning method is used to inject stained epoxy resin into the pores of the core. A focusing scanner is then applied to scan the core section point by point, record the reflection of the light from the epoxy resin, and obtain the core image (Zhao, 2009). Although this approach can provide high-resolution images of two-dimensional cores, the experimental time is long and the pore structure of the cores is damaged (Zhang et al., 2012), which is not conducive for practical application. The CT scanning method can be used to distinguish the composition and spatial structure of core particles according to the different X-ray absorption characteristics of core components based on their densities, which allows the determination of the matrix and the pores of the core (Sheng et al., 2005). By constructing a digital pore network model, Zhao established a digital pore network model of asymmetric corrugated pore channels according to the actual core pore structure by considering the non-equidimensional characteristics of the pore-throat space. Du (2019) used micro-CT imaging and Avizo software to reconstruct the core in three dimensions, obtain the two-dimensional axial profile, and conduct numerical simulation analysis using COMSOL software.

In the study of microscopic water flooding law and residual oil, Mo et al. (2015) used CT imaging technology to analyze the microscopic pore structure and slow water flooding characteristics of low-permeability sandstone cores, and discussed the influence of limited water and flow rate on water-flooding characteristics of this material. Ouyang et al. (2019) analyzed the influence of factors such as permeability, pore-throat radius, structural seepage coefficient, and movable fluid saturation on oil displacement through the microscopic model of actual sandstone. Kang et al. (2019) also used a real sandstone model to study the microscopic water flooding characteristics of an actual reservoir and the residual oil occurrence under the two influencing factors of rock pore structure and clay wettability. However, quantitative analyses are limited regarding the types of residual oil and the reasons for the changes of microscopic residual oil in the process of water injection, which are critical for the re-development of residual oil.

The present study used COMSOL to establish a carbonate pore model. To explore the impact of fracture development patterns on water flooding characteristics and residual oil distribution of carbonate rocks, the design included pure

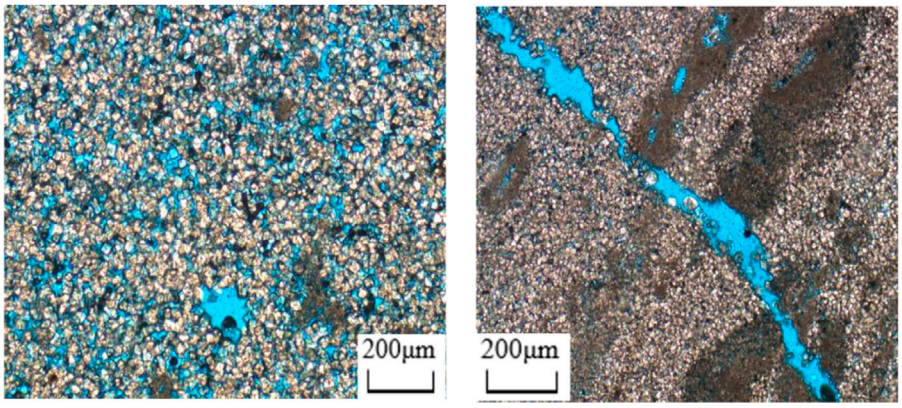

FIGURE 1
Thin section of the cast.

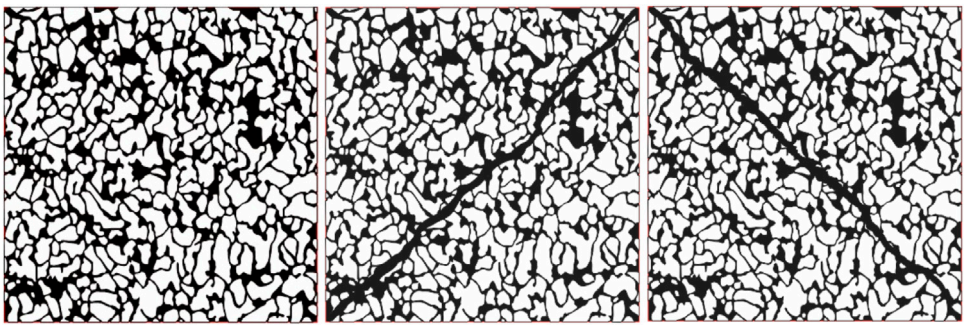

FIGURE 2
Binarization image.

matrix, vertical main line fracture, and parallel main line fracture models. The characteristics of water flooding under different schemes were analyzed from the perspectives of oil production, water production, injection pressure, and oil displacement efficiency. Finally, the formation mechanism of microscopic residual oil, residual oil types, and distribution rules of different schemes were analyzed and the effects of fracture morphology on residual oil distribution were studied.

Establishment and scheme design of the microscopic pore model

Scheme design and image processing

The carbonate reservoirs used in this study were based on the typical wells determined by casting thin sections, observing the casting thin sections, and selecting the appropriate test results of typical images (Figure 1). The image mosaicking and binarization processing method was used to design three representative rock pore-throat structure images (Figure 2); namely, the pure matrix type, vertical mainstream lines, and cracks parallel to the main line.

In COMSOL, water flooding was designed to be injected from the lower right pore-throat of the model and extracted from the upper left pore-throat. The water flooding characteristics and residual oil distribution were then observed. To obtain vectorized graphics, Algolab Photo Vector software was used for image processing (Figure 2). After processing, the identified pore contour was more accurate and the original pore structure could be restored, which reduced the subsequent graphics processing in COMSOL.

Physical field selection

We generally assume that the micropore fluid flow in laminar flow relatively conforms to Darcy's law. Considering that the

TABLE 1 Oil and water parameters.

	Density (kg/m^3)	Dynamic viscosity (mPa·s)
Oil phase	800	2.3
Water phase	950	2.3

TABLE 2 Parameter names.

Fluid properties	Name
Density	rho
Dynamic viscosity	eta

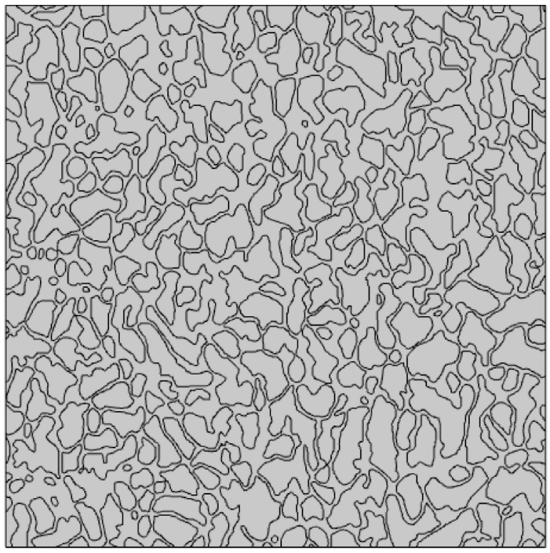

FIGURE 3
Matrix-type microscopic pore model.

object this study was two-phase oil-water, and the research scope was a two-dimensional plane flow, we selected a two-dimensional spatial dimension, two-phase flow as the physical field, and a laminar flow to meet the research purposes, reduce the calculation difficulty of the subsequent model, and improve the convergence of the model.

Model construction

The two-phase flow process of water flooding involves both oil and water. Thus, both oil and water parameters were added and re-determined as materials in COMSOL. The oil and water parameters are shown in Table 1. The names and specific values of density and viscosity were defined as possible in these parameters to facilitate data processing after the model calculation and the determination of the calculation formula. Table 2 shows the parameter names. Figure 3 shows the microscopic pore geometry model of the matrix carbonate rocks. The independent disconnected irregular shapes are rock skeletons and the interconnected channels are pores. The initial oil phase existed in the pore of the rock. The simulated water flooding process involved the injection and extraction of the water phase from the lower right and the upper left ends, respectively. Therefore, the initial water phase region was the lower right end. The interface between the water and oil phase areas was defined as the water inlet, with an outlet established at the upper left end.

Governing equations and boundary conditions of the oil and water two-phase

The four governing equations used by COMSOL for the study of two-phase flow problems are two fluid flow equations: the N-S equation (Naiver-Stokes equation, also known as momentum conservation equation) and a continuity equation (mass conservation equation), as well as two phase field-governing equations.

1) Momentum equation

The N-S equation (Yang, 2020) that controls the flow is expressed as Eqs 1, 2:

$$\frac{\delta\rho}{\delta t} + \nabla\times\left(\rho\vec{u}\right) = 0 \tag{1}$$

$$\rho\frac{\delta\vec{u}}{\delta t} + \rho\left(\vec{u}\times\nabla\right)\vec{u} = \nabla\left[-p\vec{\mathrm{I}} + \vec{K}\right] + \rho\vec{g} \tag{2}$$

where p is the fluid density, kg/m^3; $\vec{u}$ is the velocity vector, m/s; p is pressure, Pa; $\vec{K}$ is the viscous force tensor, Pa; and $\vec{g}$ is the acceleration due to gravity, N/kg.

The viscous stress tensor $\vec{K}$ is defined in Eq. 3.

$$\vec{K} = \mu\left(\nabla\vec{u} + \left(\nabla\vec{u}\right)^T\right) \tag{3}$$

2) Phase field equation

The phase field method tracks the interface of the two-phase flow by introducing a phase field variable ϕ, which is obtained by solving the phase field (Eq. 4).

$$\frac{\delta\varnothing}{\delta t} = \nabla\times\frac{\gamma\lambda}{\varepsilon_{pf}^2}\nabla\psi, \phi = phipf \tag{4}$$

$$\psi = -\nabla\times\varepsilon_{pf}^2\nabla\phi + \left(\phi^2 - 1\right)\phi + \frac{\varepsilon_{pf}^2}{\lambda}\delta f/\delta\phi, \psi = psi \tag{5}$$

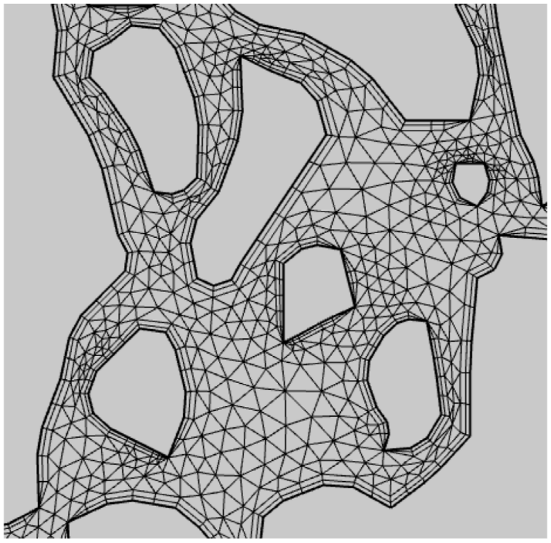

FIGURE 4
Local meshing.

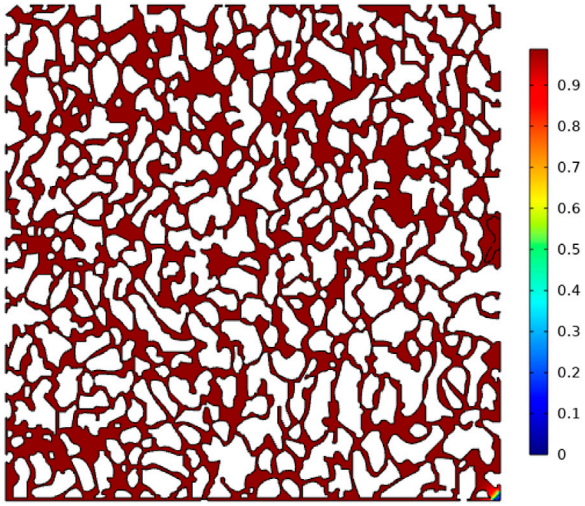

FIGURE 5
Initial oil-water distribution.

$$\lambda = \frac{3\varepsilon_{pf}\sigma}{\sqrt{8}}\gamma = x\varepsilon_{pf}^2 \tag{6}$$

where ϕ is the dimensionless phase field variable; λ is the mixed energy density, N; $\epsilon$is the coefficient related to the interface, m; and ψ is the free energy, J/m3.

3) Boundary conditions

The boundary conditions of the laminar flow phase field include inlet condition, outlet condition, wall wettability, initial condition, and surface tension. For the problem of water flooding, there exists an inlet of water phase and an outlet of oil-water two-phase. Oil and water flow from the inlet to the outlet due to a pressure difference. The model in this study adopted a constant flow inlet with an injection rate of 20 mm/s. The outlet condition was pressure, with a value of 0 Pa. In this study, as the glass in a real etching glass experiment is a water-biased wet material, the contact angle was set to $\frac{\pi}{3}$. The surface tension was set to 0.02 N/m.

Grid construction

The meshes in COMSOL include structured, unstructured, and boundary meshes. Reasonable meshing can not only improve the calculation efficiency but also its accuracy. The calculation in this study used a two-dimensional model. Unstructured grid cells not only met the accuracy requirements for the calculations but also minimized the calculation time.

Finally, a total of 83678 cells was considered, including 14900 edge cells and 10263 vertex cells. The average cell mass was 0.7082 and the grid area was 343.1 square millimeters. Figure 4 shows a partial grid setup.

Microscopic water flooding characteristics of carbonate reservoirs with different fracture forms

Pure matrix carbonate model

The size of the pure matrix model was 30 mm×30 mm, the initial pore pressure was 100 Pa, the porosity was approximately 38.14%, and the total transient solution step was 20 s. Because the model assessed two-dimensional plane flow, in consideration of the practical significance of the data, 1 mm thickness was added to the porous medium area during the calculation. Thus, the porous medium was near-cuboid (30 mm (X) ×30 mm (Y) ×1 mm (Z)), with an initial oil content of 343.05 mm^3.

Figure 5 illustrates the initial oil-water distribution, where red, blue, and white indicate the oil phase, the water phase, and the rock matrix, respectively, and the transition zone between the red and blue is the oil-water zone. After the calculations, the data were post-processed. The parameters such as the oil-water volume fraction, pressure, and flow velocity at each calculation step were then obtained and the corresponding images were drawn. Figure 6 shows from left to right the characteristics of the water drive front for injected PVs of 0.05, 0.19, and 0.34, respectively. In the first half of the water drive front, the front shows a piston

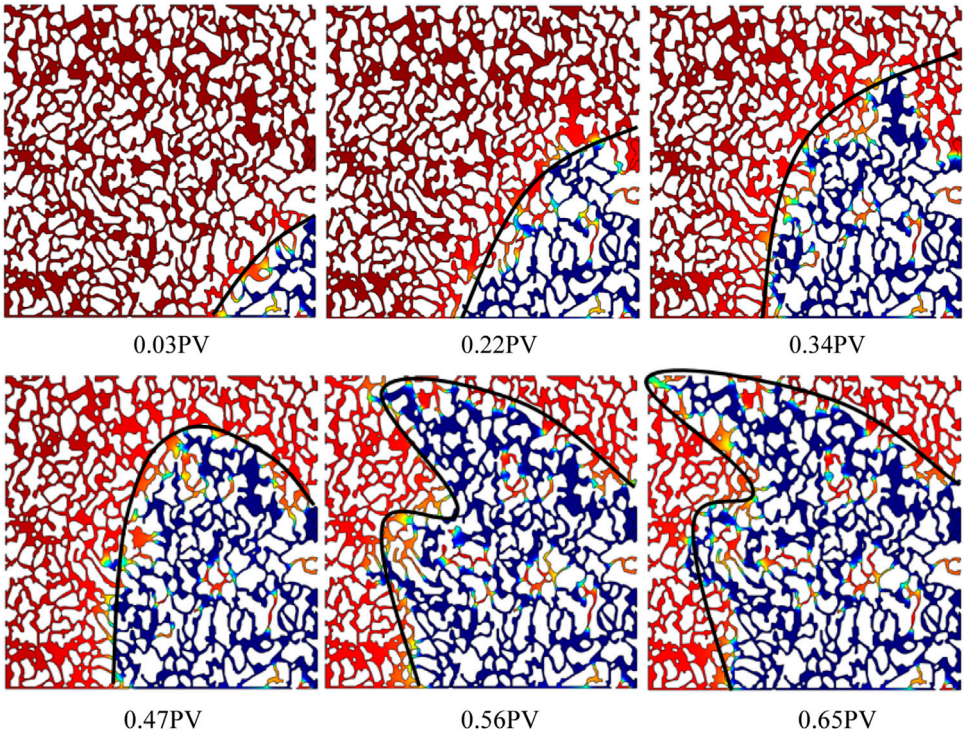

FIGURE 6
Water drive front of the matrix mode.

displacement state (Wang et al., 2018) and a relatively uniform displacement. Figure 7 shows from left to right the water drive front for injected PVs of 0.44, 0.52, and 0.68, respectively. The second half shows an obvious fingering phenomenon and water is injected into the outlet from the upper right. The fingering phenomenon is common in water flooding. After the injected water enters from the injection end, it always reaches the outlet end along the channel of least resistance and forms a dominant channel after connecting to the outlet end, which is known as the microscopic fingering phenomenon. With the continuous increase of injected PV value, the water drive front inrush also increases; in other words, with increasing injected PV value, the fluid flow in the fingered area becomes increasingly obvious while the flow in other areas is slow, generating a "concave" front shape.

Although the pure matrix model is relatively homogeneous as a whole, the fingering phenomenon still occurs in the water flooding process. The heterogeneity of the microscopic pore-throat structure, displacement velocity, and oil-water viscosity ratio are among the main explanations for microscopic fingering (Chen, 2017). In addition, displacement velocity and oil-water viscosity ratio are also important factors affecting the characteristics of the water drive front (Chen, 2017; Wang et al., 2018).

The output is calculated by integrating the output line at the outlet. The line integral is performed on the outlet line, and the expression required for integration is input. Formulas (7) and (8) are the expressions for oil and water production, respectively, with an assigned flowing fluid thickness of 1 mm. These calculations provide the oil and water production of the matrix model.

$$spf.U \times t \times pf.Vf2 \times 1[mm] \quad (7)$$

$$spf.U \times t \times pf.Vf1 \times 1[mm] \quad (8)$$

where spf.U is the fluid flow rate at the outlet, mm/s; t is time, s; Pf.Vf2 is the volume fraction of the oil phase; and Pf.Vf1 is the volume fraction of the aqueous phase.

Fracture vertical main line model

The pore volume of the vertical main fracture line model was 344.25 mm^3 and the porosity was approximately 38.25%, close to that of the pure matrix type. The other boundary conditions were the same as those of the pure matrix type. Figure 8 shows from left to right the characteristics of the water drive front for injected PVs of 0.06, 0.18, 0.28, 0.37, 0.46, and 0.51, respectively. When the shape of the water drive front was not close to the fracture of the vertical main line, it showed a uniform piston displacement. However, as the water drive front gradually approached the fracture, the fingering phenomenon became increasingly active until the water

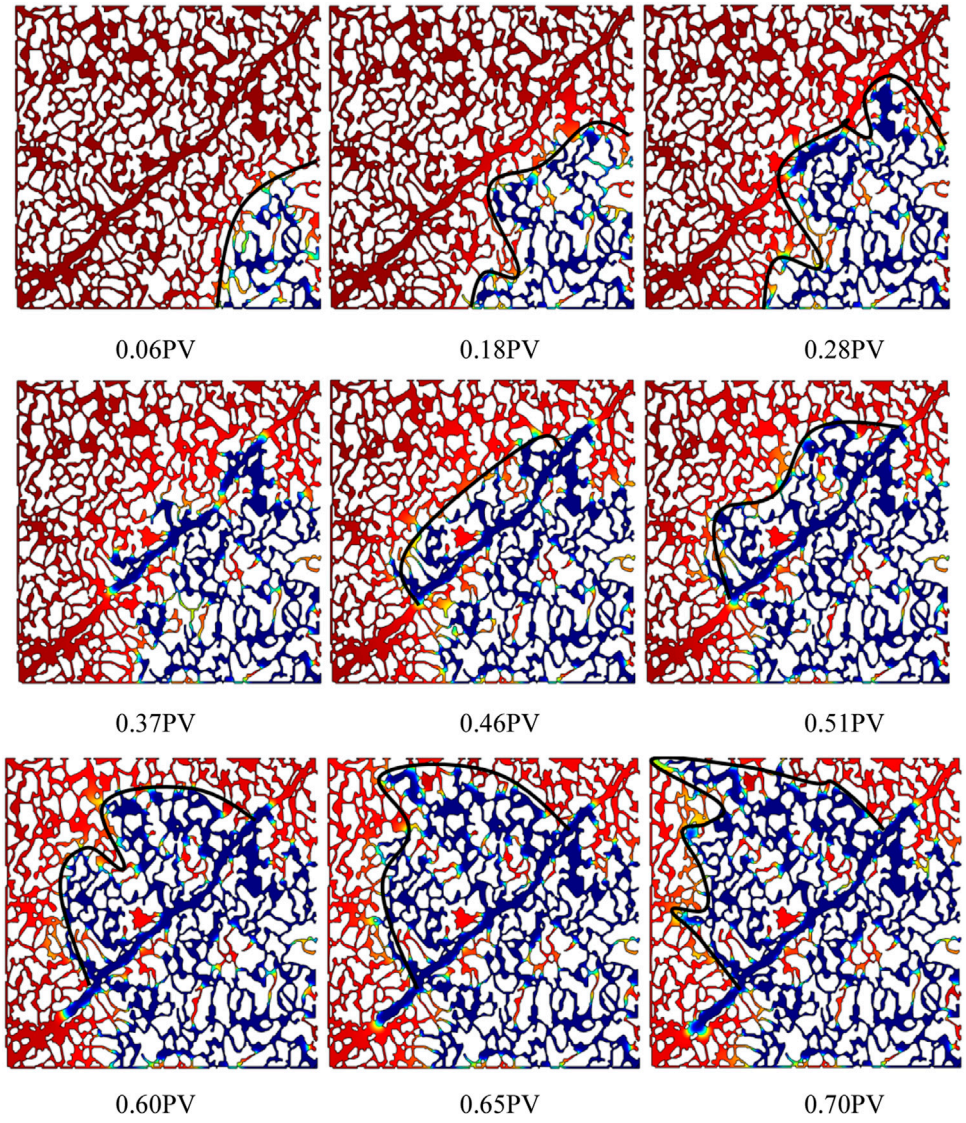

FIGURE 7
Water drive front of the parallel fracture mode.

drive front reached the fracture. When the water drive front reached the crack, it advanced first in the crack. When the pressure in the crack reached a certain level, the water in the crack continued to sweep forward through the crack. When the water drive front swept forward again, the water drive front again formed a uniform displacement shape. Figure 7 shows the morphology of the water drive front for injected PVs of 0.6, 0.65, and 0.7 respectively, showing the appearance of the fingering trend after a period of uniform displacement of the water drive front. At this time, while water expanded in the crack, it did not completely fill it due to the formation of the dominant channel.

Fracture parallel mainstream line model

The pore volume of the fracture parallel main line model was 341.23 mm^3, and the porosity was approximately 38%. The water drive front of the fracture parallel mainstream line model showed an obvious trend of advancing along the fracture. Figure 8 shows the characteristics of the water drive front for injected PVs of 0.04, 0.1, and 0.15, respectively. The water drive front always advanced along the fracture and quickly connected the inlet and outlet to form a dominant channel, hardly affecting the pores on either side of the fracture.

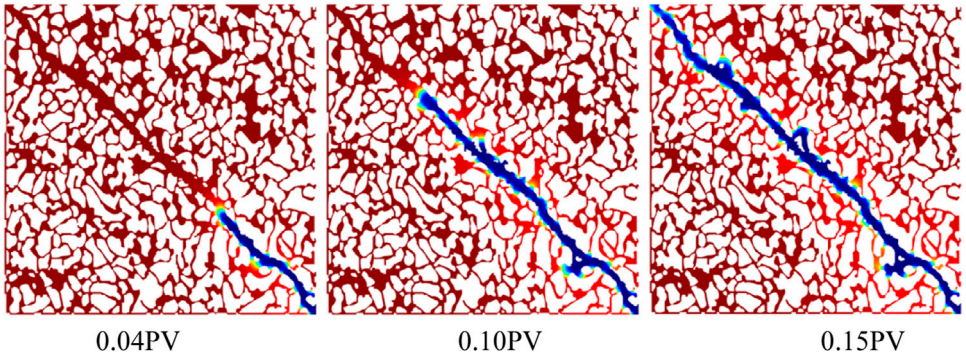

FIGURE 8
Water drive front of the vertical fracture mode.

Impact of fracture morphology on water flooding characteristics

Water emergence time

Figure 9 directly illustrates the impact of fractures on water emergence time. The water emergence time of the parallel fracture main line model was significantly shorter than those of the pure matrix and vertical fracture main line models. Water emergence occurred for injected PVs of <0.2. The water penetration time of the vertical main line model was slightly later than that of the pure matrix model. The cracks in the parallel main lines provided the channel with the least flow resistance for the potential difference between the inlet and outlet; thus, the injected water quickly reached the outlet along the cracks to form a flow advantage channel, resulting in a short water appearance time. Cracks perpendicular to the mainstream line model showed better breakthrough times compared to the pure matrix model of vertical water because the mainstream line delayed the micro means into the phenomenon of cracks. Therefore, the displacement front was rearranged and cracks in the time away from the cracks maintained a uniform displacement; thus, the micro situation was not as serious as in the pure matrix model.

Oil displacement efficiency

The model water flooding was divided into two stages. The first stage was the stable growth stage of oil displacement efficiency, while the second stage was the no-growth stage of oil displacement efficiency. Figure 10 shows the comparison of oil displacement efficiencies of the three different fracture morphology schemes. The oil displacement efficiency curve trends of the pure matrix model and the vertical mainstream fracture model were basically parallel, indicating that the vertical mainstream fracture had almost no influence on the change trend of oil displacement efficiency. The total displacement efficiency of the vertical mainline fracture model was better than that of the pure matrix model. The oil displacement efficiency of the fracture parallel main line model was smaller than that of the other two models because the premature water emergence time caused a sudden decline in the growth rate of the oil displacement efficiency at a relatively stable stage. The final displacement efficiency of the vertical fracture main line and pure matrix models were 78.9% and 72.3%, respectively, while the minimum displacement efficiency of the parallel fracture main line model was 18.1%.

Water content

Figure 11 shows the comparison of the water content curves of the three models. The change of water content was divided into two stages. The first stage was the slow increase of water content, in which the water produced was mainly droplets dispersed in the oil and membrane water flowing along the pore wall. The second stage was the rapid increase of water content, during which the water drive front reached the outlet end and more water is produced from the outlet, with a significant increase in the water content. The pure

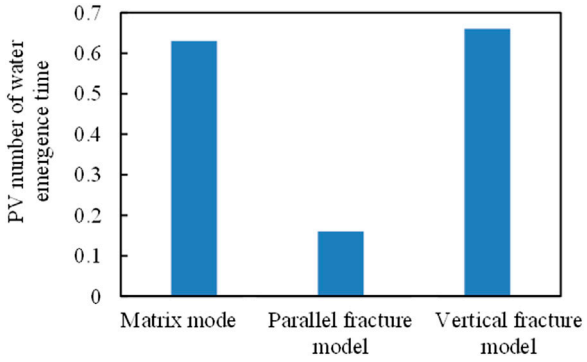

FIGURE 9
Water emergence time.

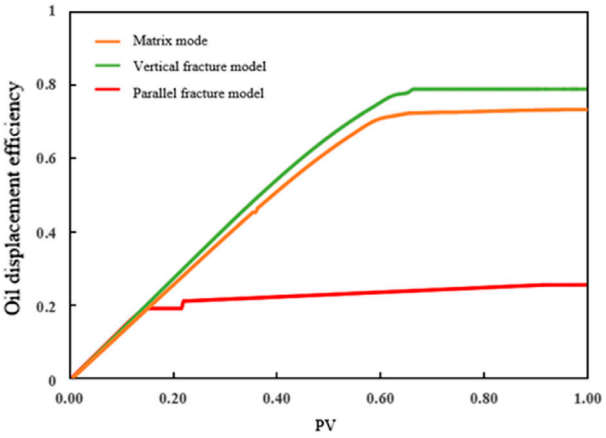

FIGURE 10
Oil displacement efficiency.

matrix model and the fracture vertical curves of the moisture content of the mainstream line model showed that the difference in the vertical fracture water cut curve in the middle period of the mainstream line model depended on the right side. For the same injection PV, perpendicular cracks in the mainstream line model showed lower moisture content than that of the pure matrix model; however, in the end, at 100% moisture content, the injection PVs were basically the same. Compared to the other two models, the water content curve of the parallel main line model is significantly shifted to the left and the first stage is significantly shorter compared to those of the other two models, indicating that the water content of the parallel main line model increased rapidly and reached 100% when the injected PV was very small.

Types and distributions of microscopic residual oil

When the water content in the pores increases, the residual oil in the pores still has a high exploitation value. However, at present, studies on residual oil have mostly focused on the macro static perspective (Jiang et al., 1999), with relatively few studies on micro dynamic residual oil. However, flowing residual oil is the main contributor to production (Yu et al., 2016).

Types and formation mechanism of residual oil

COMSOL identifies five main types of flow residual oil: clusters, porous, columnar (Figure 12), blockages trapped in "dead ends" (Wang et al., 2020), and contiguous clusters in areas untouched by injected water. Continuous clusters occur mainly because the injected water is not affected and remains in the corner of the model. Several oil-water interfaces and continuous-phase residual oil connect multiple pore throats in cluster residual oil, which is mainly caused by the flow of injected water around the pores and microscopic fingering. Porous residual oil has fewer than five oil-water interfaces and pore-throat residual oil in the discontinuous phase. Columnar residual oil shows two oil-water interfaces, mainly distributed in a single channel or, in the discontinuous phase, the "H" channel, with two oil-water interfaces (He and Zhang, 2006). The residual oil is trapped in a "dead end" with only one oil-water interface and only one connected pore throat.

The two main forms of injected water flow in water flooding in hydrophilic reservoirs are the movement of injected water from the middle of large pores with low resistance or the slow movement along the surface of pore rocks. If the inrush speed is greater than the wetting speed along the pore wall, the oil in small pores is easily trapped by the water. If the wetting rate along the pore wall is greater than the inrush rate in the large pore, oil droplets form in the large pores, and residual oil forms in large pores surrounded by many small pores.

The mechanical mechanisms of underground seepage mainly act through capillary, viscous, inertial, shear, and other forces (Hou et al., 2015; Zhang and Li, 2020). The results of microscopic etching glass experiments have summarized the main mechanism of forming microscopic residual oil morphology and distribution characteristics, including capillary, viscous, inertial, and shear force actions. Microscopic fingering is caused by viscosity differences; wall adhesion (oil-philic), micro-heterogeneous water drive flow, and crude oil cutoff due to abrupt pore-roar resistance.

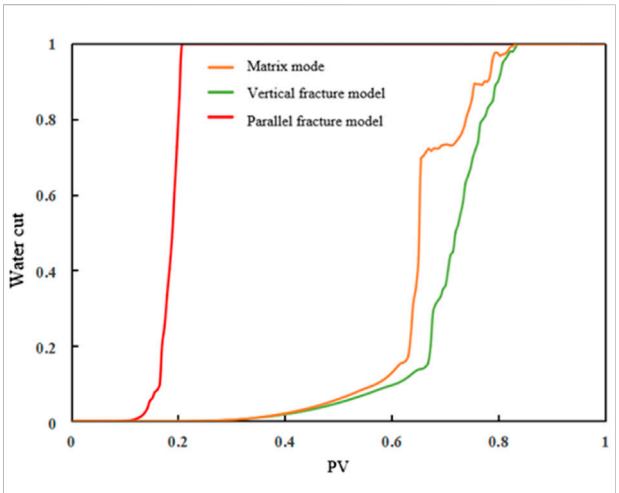

FIGURE 11
Moisture content.

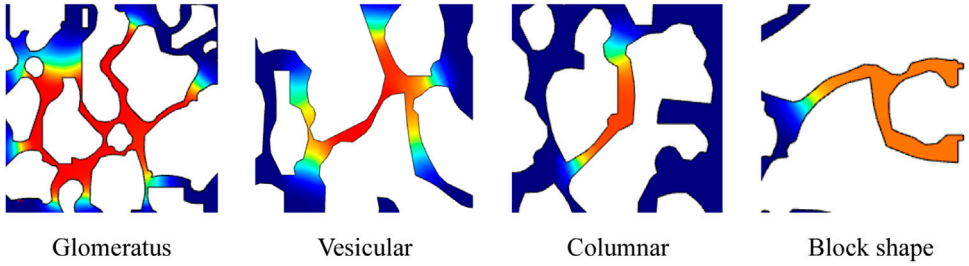

FIGURE 12
Residual oil types.

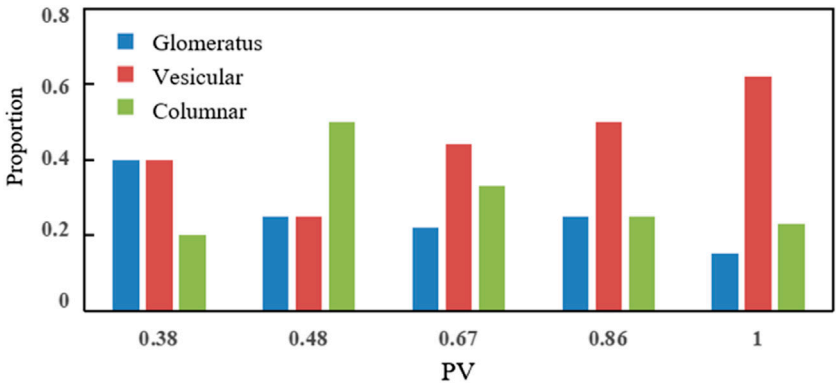

FIGURE 13
Residual oil distribution according to the matrix type.

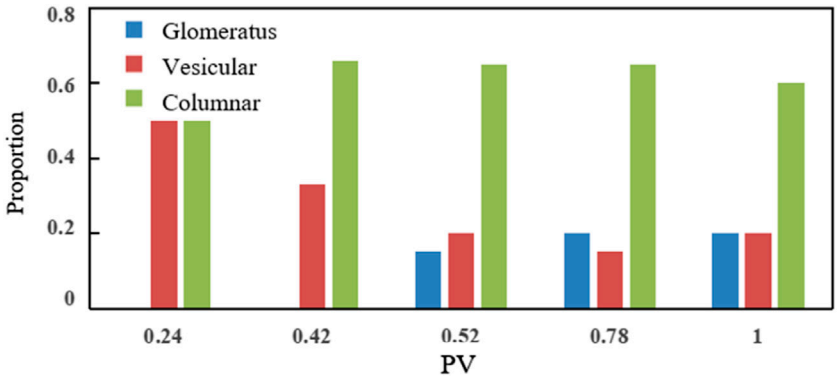

FIGURE 14
Distribution of residual oil types in the vertical fracture main line model.

Residual oils under different fracture development

For the pure matrix model, injected PVs of <0.5 in the early stage of water flooding resulted in a limited distribution of residual oil and there were no obvious laws. The type of residual oil was mainly affected by the microscopic pore structure. When the injected PV reached approximately 0.5, distribution patterns were observed (Figure 13). Initially, cluster and porous residual oils were the main types. Later, the proportions of porous and columnar residual oil increased and the more continuous cluster residual oil changed to porous and columnar residual oil. The distribution of residual oil in the plugging condition was basically unchanged.

The presence of vertical main line fractures reduced or eliminated the residual oil clusters in the early stage of water flooding (Figure 14). The residual oil was mainly column-like and clustered because the fractures inhibited the fingering phenomenon and reduced residual oil clusters. The clusters still appeared after a period of water flooding, although cracks delayed their emergence. Columnar residual oil was the main type throughout the whole process.

The residual oil in the fracture parallel main line model was mainly contiguous clusters in the unaffected area, with almost no other residual oil types.

The vertical main line fracture somewhat reduced the flow around the injected water and also reduced the cluster of residual oil formed by the flow around the injected water. A more discontinuous column of residual oil was formed, especially in the area near the fracture. At the same time, the vertical main line fracture increased the sweep area and reduced the area of the residual oil clustered on both sides. The parallel main line fracture reduced all residual oil types to clusters of continuous residual oil on both sides of the fracture. Therefore, in water flooding, the mainstream line should be avoided along the fracture direction and should instead be perpendicular to the fracture when using the well distribution method. The quantitative analysis of the type of residual oil to identify the main type will allow the selection of potential countermeasures to effectively enhance oil recovery.

Conclusion

This study established a microscopic carbonate pore model in the COMSOL numerical simulation software. The influence of different fracture morphology on water flooding characteristics and residual oil distribution was studied, and the variation of residual oil types with the number of injected PV in the water flooding process of different schemes was quantitatively characterized. The following conclusions were drawn:

1) Comparison of the effects of micro water drive characteristics between the pure matrix and vertical mainstream line crack models mainly showed an approximately 10% higher oil displacement efficiency for the vertical model compared to the pure matrix model. The main line model showed a water drive front near the crack, and then a fingering phenomenon, which changed again after leaving the crack. After a period of homogeneous displacement, the fingering phenomenon appeared again due to the microscopic heterogeneity of the pore structure. Injected water flowed along the fracture after entering the fracture, increasing the sweep area and slightly delaying the water emergence time of the vertical main line model of the fracture.
2) Parallel main line fractures not only reduced the production but also affected the water flooding characteristics. The water flooding front formed a dominant channel directly along the fracture to the outlet end, which decreased the water appearance time and further reduced the oil displacement efficiency, and improved the water cut, resulting in a significantly decreased production.
3) Clusters of residual oil were observed in the pure matrix model, along with early water drive was mainly residual oil. The continuous clusters of residual oil gradually became predominantly discontinuous vesicular and columnar residual oil. At the same time, both sides of the mainstream line showed clusters of residual oil in the unswept marginal area. This residual oil is generally more difficult to use than liquid oil.
4) Vertical main line fractures reduced the amount of residual oil in clusters, while the presence of fractures increased the sweep area and reduced the fingering and flow around the injected water, replacing it with columnar residual oil. Parallel main line fractures expanded the unswept area, with the residual oil appearing in contiguous clusters.

Data availability statement

The original contributions presented in the study are included in the article/Supplementary material. further inquiries can be directed to the corresponding author.

Author contributions

PJ, framework development; HG, simulation; YW, analysis of results; CP, writing manuscript; LC, project conception; XK, verification.

Funding

This study was partially supported by the National Natural Science Foundation of China (No. 52004307) and the Science Foundation of China University of Petroleum, Beijing (No. 2462018YJRC015).

Acknowledgments

We also acknowledge financial support from the Science and Technology Project of CNPC—major project (No. ZLZX 2020-02-04).

Conflict of interest

The authors declare that the research was conducted in the absence of any commercial or financial relationships that could be construed as a potential conflict of interest.

Publisher's note

All claims expressed in this article are solely those of the authors and do not necessarily represent those of their affiliated organizations, or those of the publisher, the editors, and the reviewers. Any product that may be evaluated in this article, or claim that may be made by its manufacturer, is not guaranteed or endorsed by the publisher.

References

Chen, M. (2017). *Quantitative description of micro-seepage mechanism in water drive reservoir [D]*. Chengdu China: Southwest Petroleum University.

Cui, H. (2018). Demonstration of steam huff-puff development in fracture-pore carbonate heavy oil reservoirs [J]. *Inn. Mong. Petrochem. Ind.* 44 (04), 98

Du, Y. (2019). *Numerical simulation of tight reservoir water drive front*. Daqing China: Northeast Petroleum University.

Guo, S., and Huang, Y. (1990). Simulation micromodel and its application in reservoir engineering [J]. *Acta Pet. Sin.* 11 (1), 49. doi:10.7623/syxb199001007

He, J., and Zhang, S. (2006). Study on micro-residual oil distribution in high water cut stage [J]. *J. Oil Gas Technol. J. Jianghan Petroleum Inst.* (04), 340.

He, L. *Study on pore structure of core based on geometric modeling [D]*. Beijing China: China University of Petroleum. (East China).

Hou, J., Zhang, F., Zhao, F., Song, W., Lu, Y., Guo, F., et al. (2015). Experimental study on micromechanism and system optimization of chemical flooding [J]. *Sci. Technol. Eng.* 15 (10), 72. doi:10.3969/j.issn.1671-1815.2015.10.014

Jiang, H., Gu, J., Chen, Y., Sun, M., and Ji, Z. (1999). Fine numerical simulation of residual oil distribution [J]. *J. Univ. Petroleum Ed. Nat. Sci.* (05), 31. doi:10.3321/j.issn:1000-5870.1999.05.009

Kang, Y., Wang, L., Fan, L., Huang, H., Yang, H., and Zhu, Y. (2019). Microscopic water flooding characteristics of Yan8 reservoir in B16 block of Yanwu Oilfield [J]. *Liaoning Chem. Ind.* 48 (12), 1234. doi:10.14029/j.cnki.issn1004-0935.2019.12.023

Li, K. (1996). *Fabrication and application of two-dimensional glass microsimulation model [J]*. Drilling and Production Technology.

Mo, S., He, S., Xie, Q., Luan, G., Gai, S., and Lei, G. (2015). Study on characteristics of low-velocity water flooding in low permeability sandstone by CT scanning [J]. *Sci. Technol. Rev.* 33 (05), 46. doi:10.3981/j.issn.1000-7857.2015.05.006

Ouyang, S., and Meng, Z. (2019). Analysis of micro-water flooding characteristics and influencing factors of ultra-low-ultra-low permeability reservoirs: A case study of chang 6 and chang 8 reservoirs in heshui area, ordos basin [J]. *Petroleum Geol. Eng.* 33 (03), 62. doi:10.3969/j.issn.1673-8217.2019.03.013

Roehl, P. O., and Choquette, P. W. (1985). *Introduction: Carbonate petroleum reservoirs[M]*. Berlin, Heidelberg, New York: Springer-Verlag, 1

Roehl, P. O., and Choquette, P. W. (1985). *Perspectives on world—class carbonate petroleum reservoirs[C]*. Tulsa: AAPG, 148. AAPG Memoir 69.

Sheng, Q., Shi, X., and Liu, W. (2005). Core CT three-dimensional imaging and multiphase displacement analysis system [J]. *CT Theory Appl. Res.* 14 (3), 8. CNKI:SUN:CTLL.0.2005-03-001

Song, X., and Li, Y. (2018). Ideas and countermeasures for waterflooding development of carbonate reservoirs in the Middle East [J]. *Petroleum Explor. Dev.* 45 (04), 679. doi:10.11698/PED.2018.04.13

Wang, C., Jiang, H., and Ma, M. (2020). Study on the variation of pore scale residual oil flow state based on microfluidic model [J]. *Bull. Petroleum Sci.*, 376. doi:10.3969/j.issn.2096-1693.2020.03.032

Wang, C., Cai, M., and Yi, J. (2018). Numerical simulation of water flooding front of tight reservoir [J]. *Chem. Eng.* 32 (12), 15. CNKI:SUN:HXGC.0.2018-12-006

Wang, D., Lu, H., and Chen, X. (2016). Accumulation system and distribution characteristics of large and medium-sized Marine carbonate oil and gas fields [J]. *Oil Gas Geol.* 37 (03), 363–371. doi:10.11743/ogg20160308

Xue, J., Liu, Y., and Zhu, W. (2016). Study on waterflood development mode of carbonate reservoir [J]. *J. Chongqing Univ. Sci. Technol. Nat. Sci. Ed.* 18 (01), 43. CNKI:SUN:CQSG.0.2016-01-014

Yang, Li (2020). *Study on Enhanced oil recovery by pore scale water flooding [D]*. Tianjin China: Tianjin University of Commerce.

Yu, C., Mi, L., Wang, C., Zhao, Y., Jiang, H., and Tian, Y. (2016). Study on micro-residual oil flow characteristics in ultra-high water cut stage of water drive reservoir [J]. *Fault-block Oil Gas Field* 23 (05), 592. doi:10.6056/dkyqt201605010

Yuan, S., Liu, W., Jiang, H., Zhao, L., and Wang, J. (2021). Development of fracture-vug carbonate reservoirs based on reservoir characteristics [J]. *Petroleum Geol. Recovery Effic.* 28 (01), 80. doi:10.13673/j.cnki.cn37-1359/te.2021.01.010

Zhang, Jihong, and Li, Xin (2020). Micro-displacement mechanism of residual oil in weak base ternary flooding [J]. *Coll. petroleum Eng. northeast petroleum Univ. Contemp. Chem. Eng.* 49 (04), 645. CNKI:SUN:SYHH.0.2020-04-037

Zhang, Li, Sun, Jianmeng, and Sun, Zhiqiang (2012). Application of digital core modeling method [J]. *J. Xi'an Shiyou Univ. Nat. Sci. Ed.* 27 (3), 35. doi:10.3969/j.issn.1673-064X.2012.03.007

Zhang, N., He, D., and Sun, Y. (2014). Distribution characteristics and controlling factors of global large carbonate oil and gas fields [J]. *China Pet. Explor.* 19 (06), 54. doi:10.3969/j.issn.1672-7703.2014.06.007

Zhao, L. *Study on quantitative description of microscopic residual oil after polymer flooding based on digital channel [D]*. Daqing China: Northeast Petroleum University.

Zhao, X. (2009). *Research on Reconstruction method of digital core and pore network model [D]*. Beijing China: China University of Petroleum.

frontiers | Frontiers in Earth Science

TYPE Original Research
PUBLISHED 09 January 2023
DOI 10.3389/feart.2022.1035702

OPEN ACCESS

EDITED BY
Qingbang Meng,
China University of Geosciences
Wuhan, China

REVIEWED BY
Jincheng Zhao,
Henan Polytechnic University, China
Junjian Zhang,
Shandong University of Science and
Technology, China

*CORRESPONDENCE
Teng Li,
liteng2052@163.com

SPECIALTY SECTION
This article was submitted to
Geochemistry,
a section of the journal
Frontiers in Earth Science

RECEIVED 03 September 2022
ACCEPTED 13 September 2022
PUBLISHED 09 January 2023

CITATION
Gao Y, Li T, Zhang Z, Yu J, Zhang Y, Li X and Zhao H (2023), Research on fluid mobility in tight-sandstone with a NMR fractal theory pore
classification method.
Front. Earth Sci. 10:1035702.
doi: 10.3389/feart.2022.1035702

Research on fluid mobility in tight-sandstone with a NMR fractal theory pore classification method

Yongli Gao[1], Teng Li[1]*, Zhiguo Zhang[2], Jian Yu[2], Yingke Zhang[2], Xuan Li[3] and Hui Zhao[3]

[1]College of Petroleum Engineering, Xi'an Shiyou University, Xi'an, Shaanxi, China, [2]PetroChina Changqing Oilfield Company, Xi'an, Shaanxi, China, [3]No.2 Oil Production Plant, PetroChina Changqing Oilfield Company, Qingyang, Gansu, China

The fluid mobility characteristics in the pores with various apertures for tight-sandstone would finally determine the fluid mobility and production of tight oil and gas reservoirs. In this study, the tight-sandstone core samples collected from Middle Jurassic Xishanyao Formation in Santanghu Basin were launched the fluid mobility measurements under various centrifugal speeds. With the NMR fractal theory pore classification method, the various types of pores in the tight-sandstone core samples were classified, and the fluid mobility in different types of pores were also investigated. The results show that the tights-sandstone core samples were significantly influenced by compaction, and the core samples are relatively dense, the mineral intergranular solution pores and colloidal intergranular pores are the main storage spaces. With a constant increase of the centrifugal speed, the fluid mobility increases continuously, and the fluid mobility for CTOS-19 features stronger than that of CTOS-7, which is related to the complexity of pore structure in tight-sandstone sample. Compared with the pore aperture in CTOS-19, the pore aperture in CTOS-7 is smaller, and the connectivity between the smaller and larger pores is poorer, leading to the poorer fluid mobility. Besides, the NMR fractal theory pore classification method also shows that the COTS-7 features more pore types than COTS-19, five and four types respectively. The type P2 and P3 pores are dominant in COTS-7 and CTOS-19 core samples, and the connectivity between type P2 and P3 pores contributes dominantly to the fluid mobility. With the NMR fractal theory pore classification method, the complexity of the distribution of fluid and fluid mobility in tight reservoirs could be studied quantitatively, and the results can efficiently guide the development of residual oil and gas in tight oil reservoirs.

KEYWORDS

tight-sandstone, fluid mobility, nuclear magnetic resonance, fractal, pore classification

Introduction

The development of tight-sandstone reservoirs is hot in the field of unconventional oil and gas in recent years. However, the nano-scale pores in the tight oil and gas reservoirs are developed with complex pore structures and strong microscopic heterogeneity. With a refined classification of pores in the tight-sandstone reservoirs, it could ensure the mobility and activation of geological fluids in different scale pore spaces, which would guide the development of tight oil and gas.

Tight-sandstone reservoir features various types, the structure and genesis of pores in tight-sandstone reservoir is complex, and the classification and identification of pores are the basis to study the reservoir characteristics, which is also the core content of reservoir space characterization. Currently, the study of the pores in the tight-sandstone mainly focus on the pore genesis, pore morphology, pore size, pore yield and matrix correlation, etc (Slatt and O'Neal, 2011; Loucks et al., 2012; Yu, 2013). Various measurements have been used to investigate the pore structure of tight-sandstone reservoir, such as scanning electron microscopy (SEM), atomic force microscope (AFM), focus-focused ion beam-electron SEM (FIB-SEM), nano-CT, transmission electron microscope (TEM), high-pressure mercury injection pressure (HMIP), constant-velocity mercury pressure (C-MP), low-temperature nitrogen adsorption (LP-N_2A), low-temperature carbon dioxide adsorption (LP-CO_2A), nuclear magnetic resonance (NMR), small-angle neutron scattering (SANS), small-angle X-ray scattering SAXS, ultra-small angular scattering USAS (Curtis et al., 2012; Javadpour et al., 2012; Melnichenko et al., 2012; Arabjamaloei et al., 2015; Li, 2020, Li et al., 2020; Li et al., 2021a; Li et al., 2021b), and so on.

Nuclear magnetic resonance (NMR) technology, as a nondestructive testing technique, has been widely used in the field of unconventional oil and gas in recent years, such as the fluid distribution characteristics (Mehana and El-Monier, 2016; Lawal et al., 2020; Liu et al., 2020), pore structure (Zhao et al., 2011; Li et al., 2018; Zhang J. et al., 2019; Zhang Q. et al., 2019; Liu et al., 2020; Ma et al., 2020; Wang et al., 2020), seepage characteristics (Sun et al., 2018a; Liu et al., 2020; Wang et al., 2020) and wettability (Sun et al., 2018b; Liu et al., 2020; Mao et al., 2020), etc. NMR technology has unique advantages in characterizing the micro-structural pore features and fluid mobility of reservoirs. Peng et al. (2018) classified the pores of clastic tuffs into micro-pore, small pore, medium pore, and large pore based on the boundary of 30 ms, 90 ms, and 200 ms. Wang et al. (2021) classified the pores in the core of tight reservoirs into completely immobile pores, partially mobile pores, and fully mobile pores based on the mobility of pore fluids. Dai et al. (2019) selected four characteristic points on the NMR T_2 spectrum and classified the pores into nano-pores, small pores, medium pores, and large pores. Li et al. (2022) classified the movable fluid pores in tight cores into four different pore types, P1, P2, P3 and P4 respectively with the fractal method of nuclear magnetic resonance. Based on the combination of multiple methods to form a "wide range, high accuracy, and large scale" pore structure system, which can provide an extremely enrichment pore structure information (Clarkson et al., 2012), such as Gao et al. (2019) used a combination of SEM, HMIP and C-MP to study the pore structure of the pores. In addition, the pore characteristics of tight cores are most widely analyzed by combined HMIP and NMR tests, which convert the NMR transverse relaxation time to pore radius, and this can better determine the quantitative relationship between the NMR transverse relaxation time (T_2) and pore throat radius (Gao and Li, 2015). Commonly, the short peak volume of T_2 distribution corresponds to small pores, and on the basis of pore radium conversion, the pores in tight reservoirs can further be classified into micro-sized large pores (>10 μm), micro-sized micro-pores (1–10 μm). submicro-pores (0.1–1 μm), and nano-pores (<0.1 μm), with submicron pores being the main contributor of movable fluids (Hu et al., 2020).

There have been numerous researches on the classification of pores in the tight-sandstone reservoirs, and the fluid mobility in the tight reservoirs. However, these studies mainly focus on the total fluid mobility in the tight reservoir, and the refined fluid mobility in various types of pores is not studied detailed. In this study, the tight-sandstone core samples of Middle Jurassic Xishanyao Formation in the Santanghu Basin, Norwest China were selected as the subject, and the fluid movable of cores under various centrifugal speeds of saturated simulated water were carried out, combined with the NMR fractal theory pore classification method provided by Li et al. (2022), the types of pores in the tight-sandstones were divided, and quantitatively characterizes the characteristics of fluid movability and the degree of movability in different types of pores were launched.

Experimental materials and experimental test procedures

Experimental materials

The core samples for this study were collected from the Middle Jurassic Xishayao Formation (J_2x) in Santanghu Basin, Northwest China. The tight reservoirs featured strong heterogeneity, and the tight core samples were collected from a nearby region in the full-diameter cores at the horizontal stratification direction. The core samples were polished to ensure that the planeness of the end face was less than 0.01 prior to the measurements. The porosity of the two tight-sandstone samples were extremely low, ranging from 2.72 to 3.97

TABLE 1 The basic information of core samples in this study.

Core no.	Formation	Depth/m	Length/mm	Diameter/mm	Permeability/10^{-3}μm^2	Porosity/%	Pore volume/cm^3
CTOS-7	J_2x	2619.58	25.12	24.62	0.0097	2.72	0.33
CTOS-19		2621.47	25.74	24.52	0.0239	3.97	0.48


项目类别：重点实验室项目

陕西省教育厅
重点科学研究计划项目
合　同　书

项目编号 20JS116
鄂尔多斯盆地东缘上古生界煤系
项目名称 气三节点法合采接替时机研究
项目负责人 李腾
项目起止时间 2020 年 01 月至 2021 年 12 月
陕西省油气田特种增产技术重点
依托平台 实验室
依托单位 西安石油大学

陕西省教育厅印制

FIGURE 1
The SEM photos of the CTOS-7 and CTOS-19 samples. (Yellow zone is the colloidal intergranular pore, green zone is the intergranular solution pores).

%, and the permeability ranging from 0.0097 × 10^{-3} μm^2 to 0.0238 × 10^{-3} μm^2, which are typical extra-low porosity and extra-low permeability reservoirs (Table 1). The test results based on argon ion polishing SEM show that due to the large burial depth, the tight-sandstone samples are compacted tightly and the pores are poorly developed, and the pore types are mainly mineral intergranular solution pores and colloidal intergranular pores, and the developed intergranular solution pores are mostly filled by calcite and clay minerals (Figure 1). The face porosity in CTOS-7 core sample is 3.86 %, while the porosity of intergranular pores in cement contributes almost 78.50 %. As a contrast, the face porosity in CTOS-19 is lower than that of CTOS-7, and the porosity of intergranular pores in cement contributes 67.40 %.

Methods

NMR techniques and fractal theory have unique advantages in characterizing fluid mobility and pore structure features in porous media. In this study, the Oxford Geospec 2/53 NMR high-temperature and high-pressure online displacement system was used to complete the measurements.

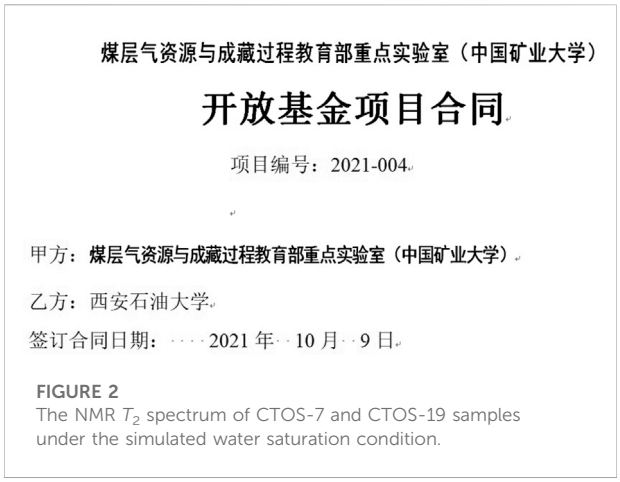
煤层气资源与成藏过程教育部重点实验室（中国矿业大学）

开放基金项目合同

项目编号：2021-004

甲方：煤层气资源与成藏过程教育部重点实验室（中国矿业大学）

乙方：西安石油大学

签订合同日期：2021 年 10 月 9 日

FIGURE 2
The NMR T_2 spectrum of CTOS-7 and CTOS-19 samples under the simulated water saturation condition.

The specific NMR testing procedures for fluid mobility of tight cores at different centrifugal speeds are as follows: 1) the oil-washed small-diameter cores were dried in a drying oven at 80°C for 48 h, and the porosity and permeability of the dried cores were tested; 2) the dried cores were saturated in a NM-V vacuum pressurized saturation device for 48 h to ensure that the cores were completely saturated with simulated water, and the saturated cores would be scanned by the NMR system; 3) the saturated cores would be put in a centrifuge and centrifuged at 1,300 r/min for 30 min, and then scanned the cores with NMR T_2 spectra; 4) repeat step 2 and complete centrifugation at 3,000 r/min, 4,200 r/min, 6,000 r/min and 8,500 r/min respectively.

The NMR relaxation time includes three parts, surface relaxation time, fluid relaxation time and molecular diffusion relaxation time. However, the latter two are usually ignored, and the surface relaxation time is often used to approximately characterize the transverse relaxation time of porous media (Kenyon et al., 1988; Howard et al., 1993; Guo and Kantzas, 2009). Combined with the fractal theory, the pore fractal characterization of porous media based on NMR can be realized,

$$\lg(S_v) = (3 - D)lgT_2 + (D - 3)lgT_{2max} \quad (1)$$

where S_v is the cumulative volume fraction of pores with aperture below r; D is the pore fractal dimension of pores with aperture below r; T_2 is the transverse relaxation time corresponding to pore radius r, ms; T_{2max} is the maximum transverse relaxation time, ms.

Based on the NMR fractal theory pore classification method provided by Li et al. (2022), the types of pores in the cores would firstly divided with a fractal dimension of 2, and then the pore fractal dimension correlation coefficient mutation point is used as the secondary pore classification point for the classified primary pore classification,

$$R^{2'} = \frac{R_{i+1}^2 - R_i^2}{R_i^2} \quad (2)$$

where R_i^2 is the correlation coefficient between lg (T_{2i}) and lg (S_{vi}) *at* T_{2i}; R_{i+1}^2 is the correlation coefficient between lg (T_{2i+1}) and lg (S_{vi+1}) *at* T_{2i+1}.

Based on this, the pore classification of porous media with the NMR fractal theory pore classification method is completed.

Results

Fluid distribution characteristics in the core under saturated water condition

The simulated water saturation experiments were carried out with two core samples using an ultra-vacuum saturation device. For the two samples, the simulated water showed a three-peak pattern distribution in the cores, and the left peak patters was higher than the middle peak, and significantly higher than the right one (Figure 2). Previous studies have shown that the distribution characteristics of fluids in NMR T_2 spectra of porous media are closely related to the distribution characteristics of pores at various scales, and the smaller lateral relaxation times tend to correspond to smaller-scale pores in porous media. Accordingly, it can be seen that the pores in CTOS-7 and CTOS-19 are dominated by smaller-scale pores and supplemented by larger-scale pores, in addition to the development of a certain number of micro-fractures in the cores. However, it is worth noticing that the smaller-scale pores in COTS-7 occupy the absolute dominant position, and the larger-scale pores in CTOS-7 are significantly less than those in CTOS-19. In addition, the rapid decrease of lateral duration in CTOS-7 at T_2 = 4 ms and T_2 = 100 ms also reflect the poor connectivity among its smaller-scale pores, larger-scale pores and micro-fractures. This also determines, to some extent, that the fluid mobility in CTOS-7 is worse than that in COTS-19.

Characteristics of movable fluid with different centrifugal speeds

Centrifugal tests were carried out at five different speeds of 1,300 r/min, 3,000 r/min, 4,200 r/min, 6,000 r/min and 8,500 r/min to understand the characteristics of movable fluids in the tight-sandstone samples at different speeds (Figure 3). This is mainly related to the low distribution in the larger-scale pores and micro-fractures in the samples. With the continuous increase of centrifugal speed, the percent movable fluid in CTOS-7 slowly increases to 7.81 %, while the percent movable fluid in CTOS-19 rapidly increases to 23.59 % (Figure 4). For CTOS-7, the fluid in the small amount of developed micro-fractures decreases rapidly,

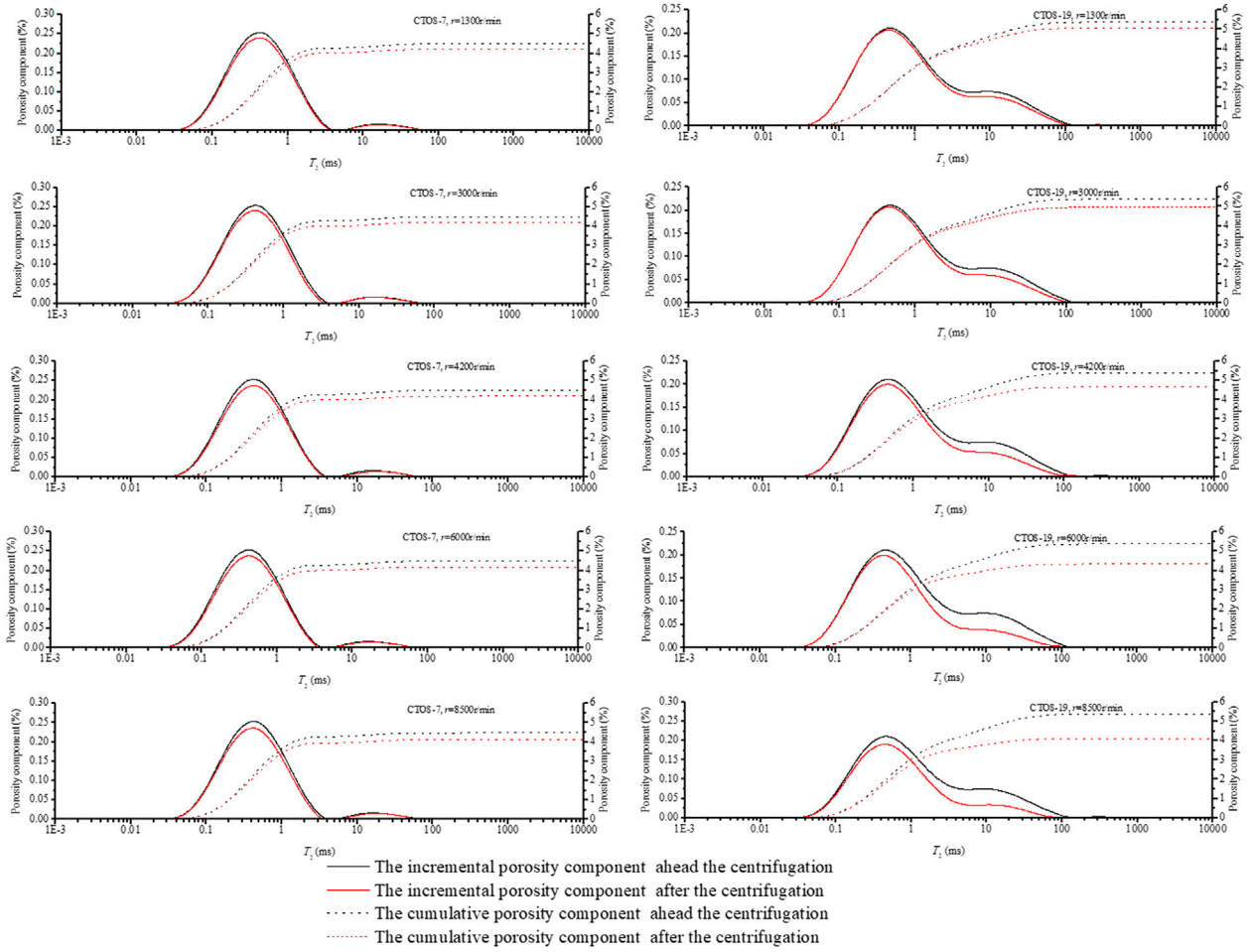

FIGURE 3
The NMR T_2 spectrum of CTOS-7 and CTOS-19 samples under various centrifugal speeds.

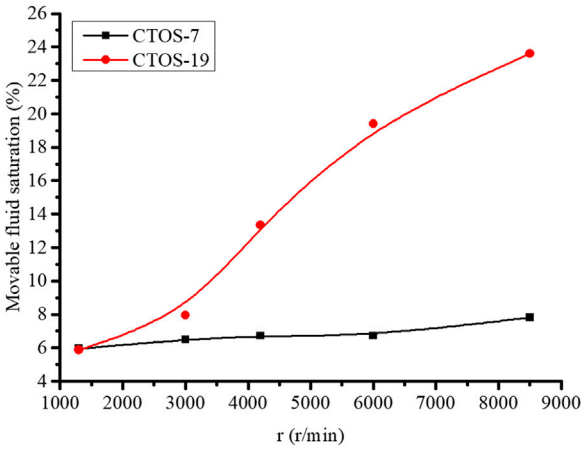

FIGURE 4
The movable fluid saturation of CTOS-7 and CTOS-19 samples under various centrifugal speeds.

and the fluid in the larger-scale pores hardly decreases due to the poor connectivity of pores, while the simulated water in the smaller pores also decreases a little. For CTOS-19 with more developed larger-scale pores, the simulated water in the micro-fractures and larger-scale pores decreased rapidly at small centrifugal speeds, and the simulated water in the smaller-scale pores begins to decrease continuously as the centrifugal speed continues to increase.

Discussion

Classification of pore types in tight-sandstone samples

The pore structure of porous media has typical fractal characteristics. With the NMR fractal theory pore classification method proposed by Li et al. (2022), the pores

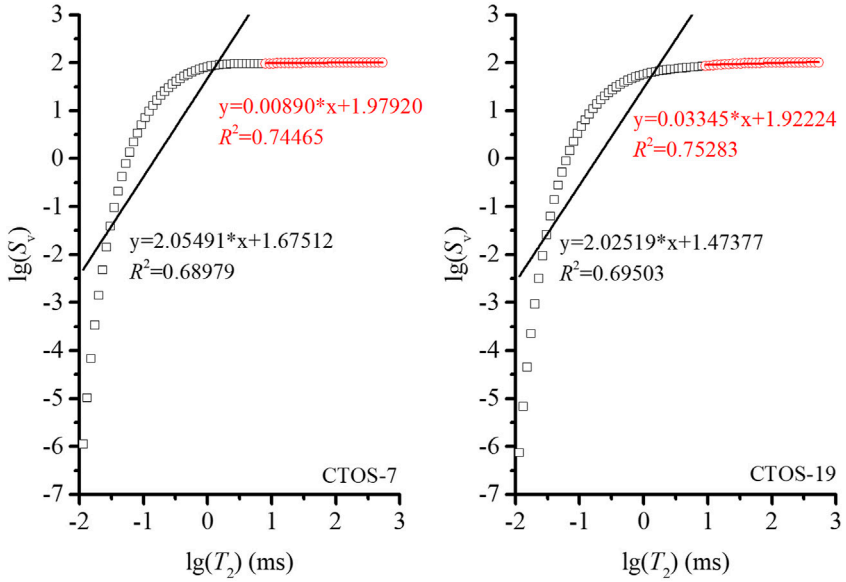

FIGURE 5
The primary pore classification of CTOS-7 and CTOS-19 samples.

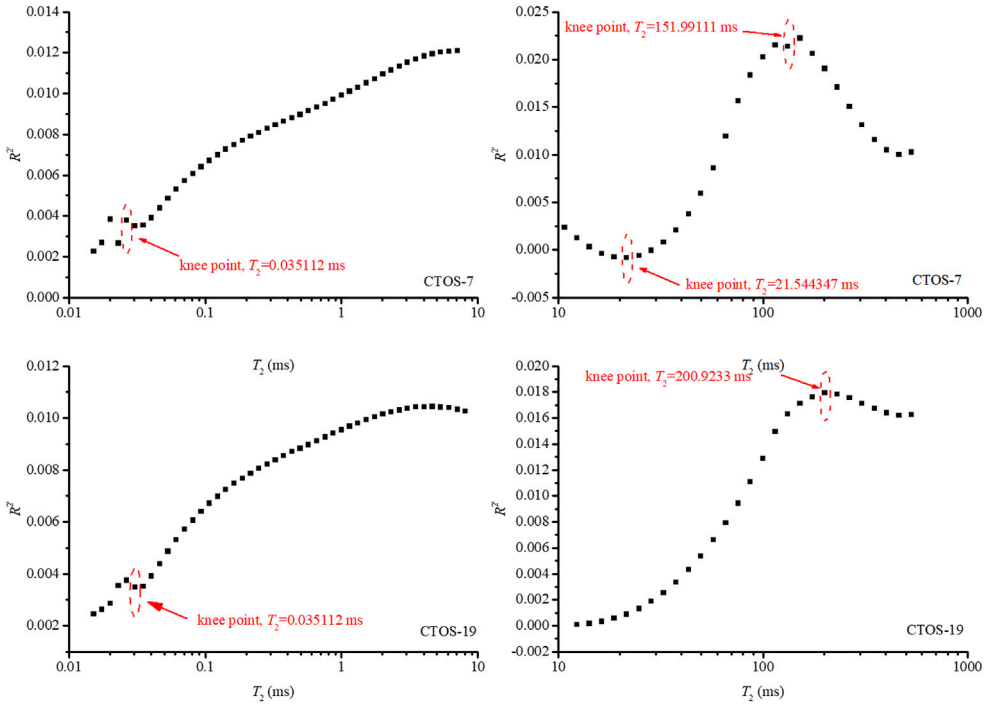

FIGURE 6
The secondary pore classification of CTOS-7 and CTOS-19 samples.

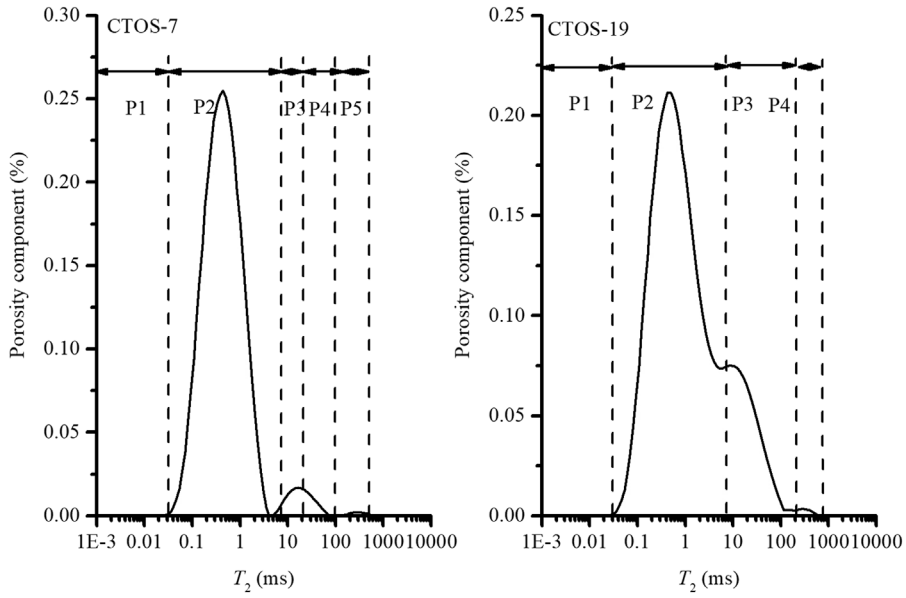

FIGURE 7
The various types of pores in CTOS-7 and CTOS-19 samples.

TABLE 2 The ratio of various types of pore in CTOS-7 and CTOS-19 samples.

Pore types	Ratio/%	
	CTOS-7	CTOS-19
P1	0.01	0.01
P2	39.91	53.13
P3	15.20	23.61
P4	27.27	23.25
P5	17.61	—

in CTOS-7 and CTOS-19 can be roughly divided into two segments with T_2 = 7.054802 ms and T_2 = 8.111,308 ms (Figure 5). On this basis, the T_2 value with the greatest variation in pore of the two previously divided sections was searched for on the principle of the greatest variation in adjacent variability. For CTOS-7, the pores distributed in the interval of T_2 < 7.054802 ms can be further divided into two different types of pores at T_2 = 0.035112 ms; while the pores distributed in the interval of $T_2 \geq 7.054802$ ms, bounded by T_2 = 21.544,347 ms and T_2 = 151.99111 ms, can be further divided into the part of pores can be further divided into three different types of pores (Figure 6). As for CTOS-19, the pores distributed in the interval of T_2 < 8.11308 ms can be further classified into two different types of pores at T_2 = 0.035112 ms; while the pores distributed in the interval of $T_2 \geq 8.11308$ ms can be further classified into two different types of pores with the boundary of T_2 = 200.9233 ms for this part of pores (Figure 6).

Based on the above pore classification principles, the pores in CTOS-7 are divided into five types, among which the type P2 pores are the main type, with a small number of P2 and P4 types pores, and a very small number of P5 type pores, while P1 type pores are almost undeveloped. The P2 type pore is also the main pore type in CTOS-19, followed by P3 type pore, a few P4 pores are developed, and P1 type pore is also not developed (Figure 7; Table 2).

Fractal characteristics of different types of pores

The pore fractal dimension of CTOS-7 shows a gradual increase in pore complexity as the pore radius increases, and the pore fractal dimension of the three different pore type P3, P4 and P5 are all higher, 2.97433, 2.99467 and 2.99727 respectively. The pore fractal characteristics for CTOS-19 are similar to CTOS-7. The pore fractal dimension of CTOS-7 and CTOS-19 with saturated water shows that the pore structure of larger pore is significantly more complex than that of smaller pore (Figure 8; Table 3).

The variability between different types of pore fractal dimension can also be reflected, to some extent, the connectivity between different scales of pores within a porous medium, which will further determine the connectivity of pores in a porous medium. In order to quantitatively characterize the

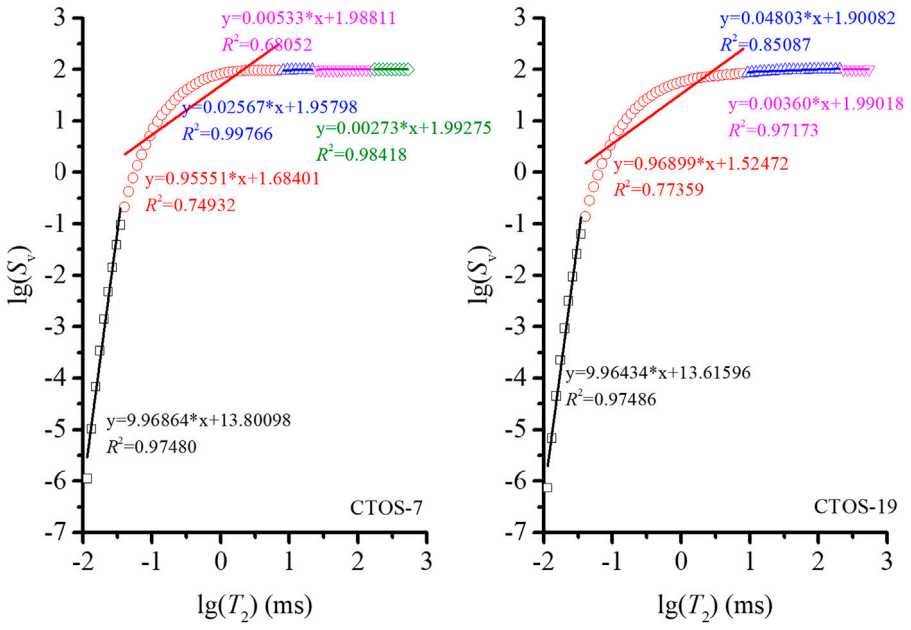

FIGURE 8
The pore fractal dimension of various pores in CTOS-7 and CTOS-19 samples.

TABLE 3 The fractal dimensions of various type of pore in CTOS-7 and CTOS-19 samples.

Pore types	Fractal dimension	
	CTOS-7	CTOS-19
P1	—	—
P2	2.04449	2.03101
P3	2.97433	2.95197
P4	2.99467	2.9964
P5	2.99727	—

variability of fractal dimension between different types of pores, d_p is introduced to characterize it.

$$dp = (Di + 1 - Di)/Di \quad (3)$$

where d_p is the difference index of adjacent pore types; D_i is the pore fractal dimension of the ith type of pore.

The d_p of COTS-7 is 0.4548 for P2 and P3 type pores, 0.0068 for P3 and P4 type pore, and 0.0026 for P4 and P5 type pore. It can be seen that as the pore size in tight-sandstone sample gradually increases, the connectivity between larger size pores is increasing, while the difference between smaller size pores and larger size pores is greater. The d_p of COTS-19 is 0.4534 for P2 and P3 type pores and 0.0151 for P3 and P4 type pore, and the variation pattern of pore difference index among different types of pores is consistent with that of CTOS-7. It is noteworthy that the pore variability index of P3 and P4 types in CTOS-19 is higher than that in CTOS-7, while the pore variability index of P2 and P3 types shows the opposite characteristics, and P2 and P3 types pores are the main pore types in both samples. Combining the fluid mobility characteristics of CTOS-7 and CTOS-19, it is clear that the fluid mobility characteristics of tight-sandstone samples are mainly controlled by both the number of major pore types and pore variability, especially the pore variability between major pore types, and the smaller the variability of major pore types, the better pore fluid mobility can be obtained.

The pore fractal dimension of different types of pores in the tight-sandstone sample will change dynamically as the centrifugal speed increases,. The fractal dimension of P3, P4 and P5 type pores hardly changed for CTOS-7, which also implies that the discharge of fluid from P2 type pore is the key to the increase of fluid mobility. The pore fractal dimension of P2 increases with the increase of centrifugal speed, while that for P3 pores is S-shaped in CTOS-19, and the pore (Figure 9). The continued discharge of fluids from simple pores in the P3 type pore leads to further strengthening of the remaining fluids by capillary action of more complex pore structures, which is the reason for the gradual increase of pore fractal dimension of P3 type pore. The decrease of the pore fractal dimension of the P2 type pore is mainly due to the discharge of fluids in pores more similar to the P3 type pore, and then the discharge of fluids bound by capillary forces leads to the increase of the pore fractal dimension.

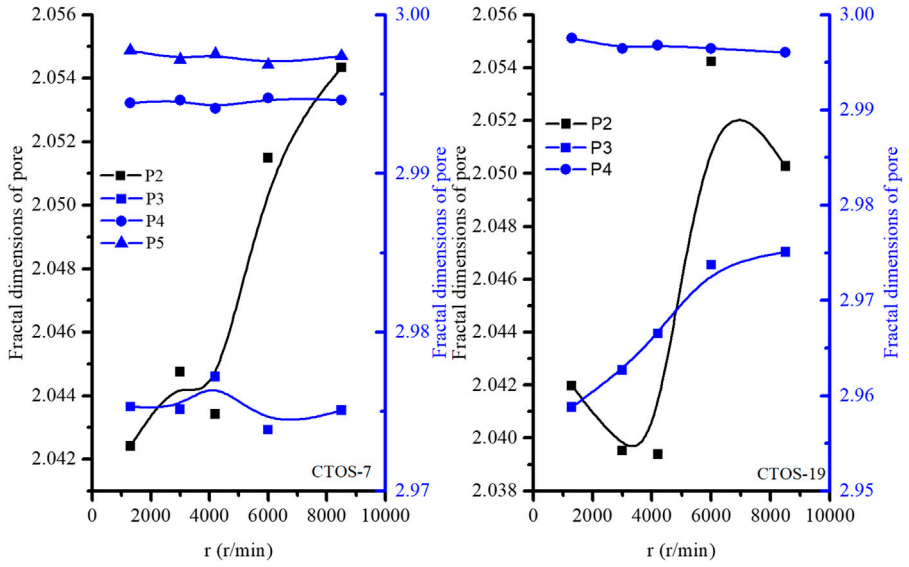

FIGURE 9
The difference change of pore fractal dimension for various pores in CTOS-7 and CTOS-19 samples.

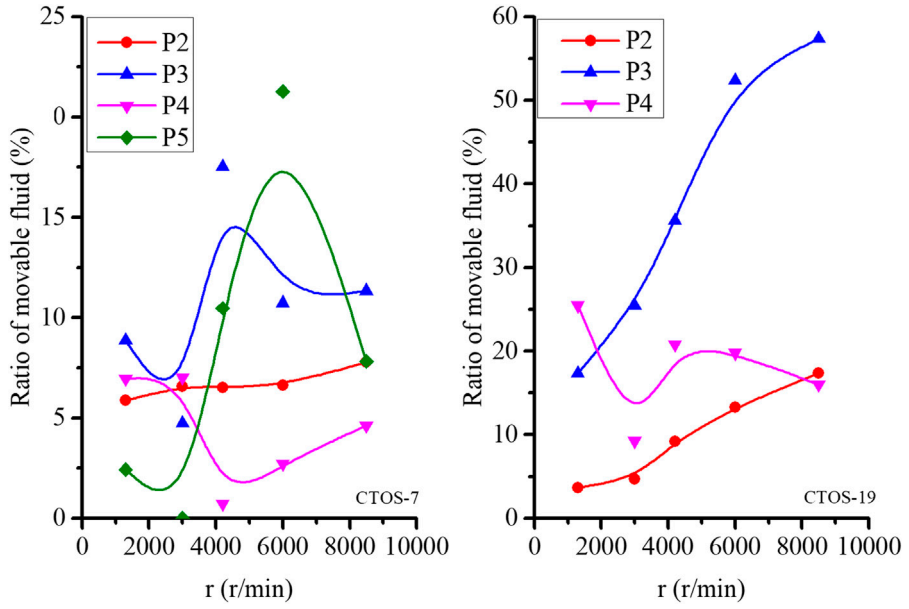

FIGURE 10
The difference mobility of fluids in various pores of CTOS-7 and CTOS-19 samples.

Characteristics of fluid mobility in different types of pores

It can be found that P2 type pore are dominant in COTS-7, and the pore structure complexity of P2 type pores is much smaller that other types of pores. However, due to the poor connectivity between P2 and P3 type pores, CTOS-7 can discharge less fluid through the centrifugation process. P2 and P3 type pores are the main pores in CTOS-19, the better pore connectivity of P2 and P3 pore types leads to the continuous linear discharge of fluids from those two types of pores. In addition, the larger pore size of P3 type pore also contributes to the rapid and large discharge of fluid from those types of pores (Figure 10).

Characteristics of pore fluid different mobility in different types of tight-sandstone samples

The two tight-sandstone samples used in this study are dominated by smaller size pore, but the typical pore development characteristics of the two samples determine significantly different fluid mobility characteristics. The predominance of small size pores and the poor pore connectivity between small size pores and larger size pores lead to a variety of pore types in the cores on the one hand, and poor connectivity between smaller size pores and larger size pores on the other hand, which ultimately leads to the inability of the fluid deposited in the smaller size pores to drain quickly. Further, fluid mobility is mainly controlled by the volume of the main pore types developed in the tight-sandstone and the connectivity between them.

Conclusion

1) The increase of centrifugal speed can effectively improve the fluid mobility in tight-sandstone sample. However, the pore structure connectivity within the tight-sandstone sample is the key to determine the fluid mobility, especially the connectivity between the main reservoir spaces of fluid deposits in the tight-sandstone.
2) The NMR fractal theory pore classification method can better reflect the complexity of pores in tight-sandstone. The more pore types, the stronger the pore complexity of the tight-sandstone, and the poorer the fluid mobility. In addition, the fluid discharge is extremely restricted in tight-sandstone with complex pore structure and poor pore connectivity.
3) In the process of gradual discharge of fluids, the pore fractal dimension of the main pore where fluids are endowed also shows a gradual increase, which is mainly the result of the capillary force of the remaining fluids by the complex pore structure.

Data availability statement

The data analyzed in this study is subject to the following licenses/restrictions: The data could be used when all of the authors agree that requests to access these datasets should be directed to liteng2052@163.com.

Author contributions

YG, ZZ, JY, and YZ completed the field data acquisition. TL completed the data analyses, and wrote the article. XL and HZ complete the measurements. All authors have read and agreed to the published version of the manuscript.

Funding

This work was supported by Scientific Research Program Funded by Shaanxi Provincial Education Department (Program No. 20JS116), and Key Laboratory of Coalbed Methane Resources and Reservoir Formation Process of Ministry of Education (China University of Mining and Technology) (Program No. 2021-004).

The authors declare that this study received funding from PetroChina. The funder was not involved in the study design, collection, analysis, interpretation of data, the writing of this article, or the decision to submit it for publication.

Acknowledgments

The writing and structure of manuscript was supported by Hai Huang.

Conflict of interest

ZZ, JY, YZ, XL, and HZ were employed by the Company PetroChina Changqing Oilfield Company.

The remaining authors declare that the research was conducted in the absence of any commercial or financial relationships that could be construed as a potential conflict of interest.

Publisher's note

All claims expressed in this article are solely those of the authors and do not necessarily represent those of their affiliated organizations, or those of the publisher, the editors and the reviewers. Any product that may be evaluated in this article, or claim that may be made by its manufacturer, is not guaranteed or endorsed by the publisher.

References

Arabjamaloei, R., Ruth, D. W., Mason, G., and Morrow, N. R. (2015). Solutions for countercurrent spontaneous imbibition as derived by means of a similarity approach. *J. Porous Media* 18 (2), 113–124. doi:10.1615/JPorMedia.v18.i2.30

Clarkson, C. R., Freeman, M., He, L., Agamalian, M., Melnichenko, Y. B., Mastalerz, M., et al. (2012). Characterization of tight gas reservoir pore structure using USANS/SANS and gas adsorption analysis. *Fuel* 95, 371–385. doi:10.1016/j.fuel.2011.12.010

Dai, C., Cheng, R., Sun, X., Liu, Y., Zhou, H., Wu, Y., et al. (2019). Oil migration in nanometer to micrometer sized pores of tight oil sandstone during dynamic surfactant imbibition with online NMR. *Fuel* 245, 544–553. doi:10.1016/j.fuel.2019.01.021

Gao, H., Cao, J., Wang, C., He, M., Dou, L., Huang, X., et al. (2019). Comprehensive characterization of pore and throat system for tight sandstone reservoirs and associated permeability determination method using SEM, rate-controlled mercury and high pressure mercury. *J. Pet. Sci. Eng.* 174, 514–524. doi:10.1016/j.petrol.2018.11.043

Gao, H., and Li, H. (2015). Determination of movable fluid percentage and movable fluid porosity in ultra-low permeability sandstone using nuclear magnetic resonance (NMR) technique. *J. Pet. Sci. Eng.* 133, 258–267. doi:10.1016/j.petrol.2015.06.017

Guo, R., and Kantzas, A. (2009). Assessing the water uptake of Alberta coal and the impact of CO_2 injection with low-field NMR. *J. Can. Pet. Technol.* 48 (7), 40–46. doi:10.2118/09-07-40

Howard, J. J., Kenyon, W. E., and Straley, C. (1993). Proton-magnetic resonance and pore-size variations in reservoir sandstones. *SPE Form. Eval.* 8 (3), 194–200. doi:10.2118/20600-PA

Hu, Y., Guo, Y., Shangguan, J., Zhang, J., and Song, Y. (2020). Fractal characteristics and model applicability for pores in tight gas sandstone reservoirs: A case study of the upper paleozoic in ordos basin. *Energy fuels.*. 34 (12), 16059–16072. doi:10.1021/acs.energyfuels.0c03073

Kenyon, W. E., Day, P. I., Straley, C., and Willemsen, J. F. (1988). A three part study of NMR longitudinal relaxation properties of water-saturated sandstones. *SPE Form. Eval.* 3 (3), 622–636. doi:10.2118/15643-PA

Lawal, L. O., Adebayo, A. R., Mahmoud, M., Dia, B. M., and Sultan, A. S. (2020). A novel NMR surface relaxivity measurements on rock cuttings for conventional and unconventional reservoirs. *Int. J. Coal Geol.* 231, 103605. doi:10.1016/j.coal.2020.103605

Li, T., Gao, H., Wang, C., Cheng, Z., Xue, J., Zhang, Z., et al. (2022). Oil utilization degree at various pore sizes via different displacement methods. *J. Pet. Explor. Prod. Technol.* 12 (8), 2271–2287. doi:10.1007/s13202-022-01464-7

Li, T. (2020). The dynamic change of pore structure for the low-rank coal with various pretreatment temperatures: A case study from southwestern ordos basin. *Geofluids* 2020, 1–13. doi:10.1155/2020/8879742

Li, T., Wu, C. F., and Wang, Z. W. (2021a). The dynamic change of pore structure for low-rank coal under refined upgrading pretreatment temperatures. *Pet. Sci.* 18, 430–443. doi:10.1007/s12182-020-00536-9

Li, T., Wu, C., and Wang, Z. (2020). Isothermal characteristics of methane adsorption and changes in the pore structure before and after methane adsorption with high-rank coal. *Energy Explor. Exploitation* 38 (5), 1409–1427. doi:10.1177/0144598720925979

Li, T., Wu, J. J., Wang, X. G., and Huang, H. (2021b). Particle size effect and temperature effect on the pore structure of low-rank coal. *Acs Omega* 6 (8), 5865–5877. doi:10.1021/acsomega.0c06280

Li, Z., Shen, X., Qi, Z., and Hu, R. (2018). Study on the pore structure and fractal characteristics of marine and continental shale based on mercury porosimetry, N_2 adsorption and NMR methods. *J. Nat. Gas. Sci. Eng.* 53, 12–21. doi:10.1016/j.jngse.2018.02.027

Liu, Z., Liu, D., Cai, Y., Yao, Y., Pan, Z., and Zhou, Y. (2020). Application of nuclear magnetic resonance (NMR) in coalbed methane and shale reservoirs: A review. *Int. J. Coal Geol.* 218, 103261. doi:10.1016/j.coal.2019.103261

Loucks, R. G., Reed, R. M., Ruppel, S. C., and Hammes, U. (2012). Spectrum of pore types and networks in mudrocks and a descriptive classification for matrix-related mudrock pores. *Am. Assoc. Pet. Geol. Bull.* 96 (6), 1071–1098. doi:10.1306/08171111061

Ma, X., Wang, H., Zhou, S., Feng, Z., Liu, H., and Guo, W. (2020). Insights into NMR response characteristics of shales and its application in shale gas reservoir evaluation. *J. Nat. Gas. Sci. Eng.* 84, 103674. doi:10.1016/j.jngse.2020.103674

Mao, Y., Xia, W., Peng, Y., and Xie, G. (2020). Wetting of coal pores characterized by LF-NMR and its relationship to flotation recovery. *Fuel* 272, 117737. doi:10.1016/j.fuel.2020.117737

Mehana, M., and El-monier, I. (2016). Shale characteristics impact on Nuclear Magnetic Resonance (NMR) fluid typing methods and correlations. *Petroleum* 2 (2), 138–147. doi:10.1016/j.petlm.2016.02.002

Melnichenko, Y. B., He, L., Sakurovs, R., Kholodenko, A. L., Blach, T., Mastalerz, M., et al. (2012). Accessibility of pores in coal to methane and carbon dioxide. *Fuel* 91, 200–208. doi:10.1016/j.fuel.2011.06.026

Peng, Y., Zhou, C., Fan, Y., Li, C., Yuan, C., and Cong, Y. (2018). A new permeability calculation method using nuclear magnetic resonance logging based on pore sizes: A case study on bioclastic limestone reservoirs in the A oilfield of the mid-ease. *Pet. explor. Dev.* 45 (1), 183–192. doi:10.1016/S1876-3804(18)30019-3

Slatt, E. M., and O'Neal, N. R. (2011). Pore types in the Barnett and Woodford gas shales: Contribution to understanding gas storage and migration pathways in fine-grained rocks. *Am. Assoc. Pet. Geol. Bull.* 95 (12), 2017–2030. doi:10.1306/03301110145

Sun, X., Yan, Y., Ripepi, N., and Liu, D. (2018a). A novel method for gas-water relative permeability measurement of coal using NMR relaxation. *Transp. Porous Med.* 124, 73–90. doi:10.1007/s11242-018-1053-y

Sun, X., Yao, Y., Liu, D., and Zhou, Y. (2018b). Investigations of CO_2-water wettability of coal: NMR relaxation method. *Int. J. Coal Geol.* 188, 38–50. doi:10.1016/j.coal.2018.01.015

Wang, F., Zeng, F., Wang, L., Hou, X., Cheng, H., and Gao, J. (2021). Fractal analysis of tight sandstone petrophysical properties in unconventional oil reservoirs with NMR and rate-controlled porosimetry. *Energy fuels.* 35 (5), 3753–3765. doi:10.1021/ACS.ENERGYFUELS.0C03394

Wang, G., Han, D., Qin, X., Liu, Z., and Liu, J. (2020). A comprehensive method for studying pore structure and seepage characteristics of coal mass based on 3D CT reconstruction and NMR. *Fuel (Lond).* 281, 118735. doi:10.1016/j.fuel.2020.118735

Yu, B. S. (2013). Classification and characterization of gas shale pore system. *Earth Sci. Front.* 20 (4), 211–220.

Zhang, J., Wei, C., Ju, W., Yan, G., Lu, G., Hou, X., et al. (2019a). Stress sensitivity characterization and heterogeneous variation of the pore-fracture system in middle-high rank coals reservoir based on NMR experiments. *Fuel* 238, 331–344. doi:10.1016/j.fuel.2018.10.127

Zhang, Q., Dong, Y., Liu, S., Elsworth, D., and Zhao, Y. (2019b). Shale pore characterization using NMR cryoporometry with octamethylcyclotetrasiloxane as the probe liquid. *Energy fuels.* 31 (7), 6951–6959. doi:10.1021/acs.energyfuels.7b00880

Zhao, Y., Sun, Y., Liu, S., Wang, K., and Jiang, Y. (2011). Pore structure characterization of coal by NMR cryoporometry. *Fuel* 190, 359–369. doi:10.1016/j.fuel.2016.10.121

frontiers | Frontiers in Earth Science

TYPE Opinion
PUBLISHED 09 January 2023
DOI 10.3389/feart.2022.1035771

OPEN ACCESS

EDITED BY
Zhilin Cheng,
Xi'an Shiyou University, China

REVIEWED BY
Dong Xiong,
China University of Petroleum, China
Qinglin Shan,
Shandong University of Science and Technology, China

*CORRESPONDENCE
Qiao Deng,
dengqiao2008@163.com

SPECIALTY SECTION
This article was submitted to Geochemistry, a section of the journal Frontiers in Earth Science

RECEIVED 03 September 2022
ACCEPTED 13 September 2022
PUBLISHED 09 January 2023

CITATION
Xia X, Deng Q, Sang P, Tan L, Yan L, Bao J and Li W (2023), Low-carbon oil exploitation: Carbon dioxide flooding technology.
Front. Earth Sci. 10:1035771.
doi: 10.3389/feart.2022.1035771

Low-carbon oil exploitation: Carbon dioxide flooding technology

Xueqin Xia[1,2], Qiao Deng[1,2,3]*, Pengfei Sang[4], Leichuan Tan[5], Liangzhu Yan[1,2,3], Jingwen Bao[1,2] and Wenlong Li[6]

[1]Cooperative Innovation Center of Unconventional Oil and Gas, Yangtze University (Ministry of Education and Hubei Province), Wuhan, Hubei, China, [2]Hubei Key Laboratory of Drilling and Production Engineering for Oil and Gas, Yangtze University, Wuhan, Hubei, China, [3]Carbon Hydrogen Epoch Technology Co. Ltd., Wuhan, Hubei, China, [4]Engineering Technology Research Institute of PetroChina Southwest Oil and Gas Field Company, Chengdu, Sichuan, China, [5]CNPC Chuanqing Drilling Engineering Co. Ltd., Chengdu, Sichuan, China, [6]Tianjin Branch of CNOOC Ltd., Tianjin, China

KEYWORDS

low carbon, CO_2 flooding, flooding mechanism, carbon capture utilization and storage, enhanced oil recovery

Introduction

It is well known that there are many technical methods for improving oil recovery, including gas miscible flooding, thermal oil recovery, chemical flooding, and microbial oil recovery. Among these, CO_2 flooding is one of the key technologies for improving oil recovery that achieves the goal of reducing carbon emissions (Jia et al., 2019). Given the increasing awareness regarding human environmental protection, the development of a low-carbon economy is an irresistible global trend. The concepts of "carbon peak" and "carbon neutrality" have gradually gained popularity. Carbon neutrality has also spawned the carbon capture, utilization, and storage (CCUS) industry (Zou et al., 2021). CO_2 flooding is one of the main carbon utilization technologies that makes full use of carbon resources to enhance oil recovery while promoting the development of a low-carbon economy. This paper reviews and summarizes the developments regarding CO_2 flooding in domestic and foreign scenarios, discusses the mechanism and process of CO_2 flooding, analyzes the technological challenges, and provides some corresponding solutions.

Research status

CO_2 flooding has been used globally to enhance oil recovery for more than 30 years and is becoming more popular. Therefore, an increasing number of researchers are engaged in research on CO_2 flooding (Chen et al., 2015). There are many reported CCUS-EOR projects from domestic and foreign investigators, as shown in Table 1. Research on CO_2 flooding began in the 1950s (Whorton et al., 1952), and some European countries had earlier used CO_2 flooding to enhance oil recovery. The former Soviet Union first began studying CO_2 injection enhanced oil recovery (EOR) technology in 1952. In 1968, CO_2 flooding tests were carried out in the Tuimajin Oilfield, which achieved a 15% increase in the final crude oil recovery (Qin et al., 2015). CO_2 flooding developed the

TABLE 1 International CCUS-EOR projects [modified according to Xiang et al. (2022)].

	Project name	Capture quantity million tons/year	Trapping mode	Utilization
International	Val Verde Natural Gas Plant	1.3	Natural gas processing	EOR
	LaBarge Gas Plant	7		
	Lost Cabin Gas Plant	0.8–1.0		
	Central Plant	8.4		
	Enid Fertilizer CO_2-EOR Project	0.7	Industrial separation	
	Great Plain Synfuel Plant and Weyburn-Midale Project	3	Precombustion capture	
	Air Products Steam Methane Reformer EOR Project	1	Hydrogen production from natural gas	
China	Research and Demonstration of CO_2-EOR in Jilin Oilfield	0.6	Chemical and physical absorption	
	Daqing Oilfield CO_2-EOR Demonstration Project			
	Shengli Oilfield CO_2-EOR Project	0.04	Chemical absorption	
	CO_2-EOR Project in Zhongyuan Oilfield	0.1		
	Karamay Dunhua Oil and Xinjiang Oilfield CO_2-EOR Project	0.1		
	CO_2-EOR Project in Changqing Oilfield	0.05	Low-temperature methanol wash	

fastest in the United States, which has the largest number of CO_2 flooding projects accounting for more than 90% of the global total. CO_2 flooding affords good economic benefits, with an annual oil production of about 1,500 × 104 t for five consecutive years and oil recovery increase of 7–15% (Hitesh et al., 2008; British Petroleum Company, 2017; British Petroleum Company, 2018). In the 21st century, greenhouse gas emission reductions have further promoted rapid development of CO_2 flooding technology (Shen and Liao, 2009; Koottungal, 2014).

Since the 1960s, China has started paying attention to CO_2 flooding technology and has successively carried out indoor research on CO_2 flooding. In 1963, the first study on CO_2 flooding was carried out in the Daqing Oilfield in China. From 1991 to 1993, immiscible displacement tests of CO_2 by alternating gas and water injection were carried out in the eastern Sanan Oilfield. In 1995, Jilin Oilfield carried out the CO_2 single-well huff and puff test and obtained 1420 t of increased crude oil through multiple tests. In 1998, Shengli Oilfield carried out the CO_2 single-well huff and puff test to obtain increased crude oil outputs by more than 200 t. Subsequently, China has continued to strengthen research on CO_2 flooding technology. At present, research on CO_2 flooding for EOR in the Jilin Oilfield is relatively mature (Chen et al., 2012).

Carbon dioxide flooding mechanisms, methods, and processes

CO_2 flooding has been increasingly used in recent times. Understanding and mastering the oil displacement mechanism can therefore promote technological progress.

Carbon dioxide flooding mechanisms

There are nine mechanisms of CO_2 flooding:

1) Viscosity reduction: Carbon dioxide and crude oil have good mutual solubilities. Temperature and pressure also affect the solubility of CO_2 in crude oil, and extremely high temperatures are not conducive to viscosity reduction (Li et al., 2008).
2) Improve oil–water mobility ratio: CO_2 increases the viscosity of water and decreases the viscosity of crude oil. These two viscosities tend towards each other, thus improving the mobility ratio of crude oil to water and expanding the swept volume (Luo et al., 2012).
3) Expansion effect: The dissolution of CO_2 in crude oil greatly expands the volume of the oil. The greater the degree of expansion, the stronger is the ability to flow and easier it is to replace (Gu et al., 2007).
4) Extraction and gasification of light hydrocarbons in crude oil: CO_2 can be used to extract and gasify light components in crude oil, thereby reducing the relative density of crude oil and enhancing recovery (Roper et al., 1992).
5) Miscible effect: When the pressure reaches the miscible pressure, CO_2 mixes with the light hydrocarbons in crude oil to form an oil zone, which greatly improves oil recovery during the oil displacement process (Grigg and Siagian, 1998).
6) Molecular diffusion: The water phase hinders diffusion of carbon dioxide molecules into the oil phase, completely inhibiting the release of the light hydrocarbons from the oil phase to carbon dioxide. Therefore, sufficient time is required for the carbon dioxide molecules to fully diffuse into the oil phase.

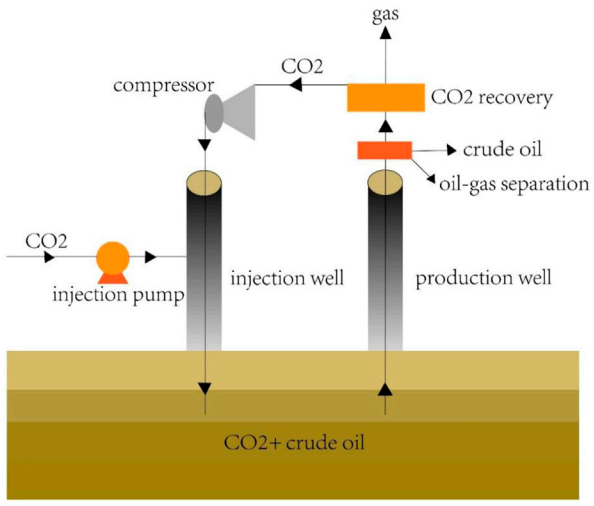

FIGURE 1
CO_2 enhanced oil recovery (EOR) process flowchart.

7) Reduce interfacial tension: In the process of CO_2 flooding, mixing CO_2 and the light components in crude oil (C2–C6) effectively reduces the oil–water two-phase interfacial tension, reduces the resistance of CO_2 in the displacement process, and enhances oil recovery (Desch et al., 1984).
8) Dissolved gas flooding: CO_2 injected into the oil layer increases its pressure, but in the displacement process, the pressure reduction causes CO_2 to escape from the crude oil and occupy the pore spaces, thereby allowing dissolved gas flooding that is conducive to flooding (Gu et al., 2007).
9) Acidizing plugging improves permeability: CO_2 dissolved in water generates carbonic acid and renders the aqueous solution acidic. To a certain extent, massive injection of CO_2 can flush out blockages, dredge oil circulation, and restore the production capacity of a single well (Rao et al., 2004).

Carbon dioxide flooding methods

CO_2 flooding can be divided into two types: CO_2 immiscible and CO_2 miscible flooding. Expansion viscosity reduction is the main mode of CO_2 immiscible flooding. For reservoirs with low pressures, high temperatures, and heavier components, the surface tension between CO_2 and crude oil is large. CO_2 can be used to extract some light components of crude oil, thereby expanding the crude oil, reducing its viscosity, and improving recovery. The essence of CO_2 huff and puff is immiscible flooding, and the mechanism involves expanding the volume of crude oil continuously so that the tension and viscosity of the crude oil interface can be reduced. This method allows injection of carbon dioxide into the bottom of the production well. After shutting down, the carbon dioxide penetrates the reservoir, which is ultimately conducive to continued production from the well. When the formation pressure is greater than the CO_2 miscible pressure and less than the formation fracture pressure, CO_2 miscible flooding occurs. The injection methods may be continuous or simple, among others. Studies have shown that miscible flooding enables greater recovery than immiscible flooding.

Carbon dioxide flooding processes

The flooding processes include primary, secondary, and tertiary flooding. Primary flooding is the method of extracting crude oil using only natural energy. Secondary flooding is the method of increasing the reservoir pressure by injecting gas or water. EOR technology involves the use of high pressures to inject supercritical/dense-phase CO_2 into the reservoir, which allows the CO_2 to drive the flow of crude oil to the production well, thereby increasing oil recovery. The CO_2-EOR process flow chart is as shown in Figure 1. After the CO_2 is compressed, it is injected into the injection well. Then, the production well produces the oil–gas mixture, which further helps separation of the crude oil.

Prospects

In recent years, with increasing awareness regarding environmental protection, CO_2-EOR technology has developed gradually. This not only eases the pressure on environmental pollution but also enhances oil recovery. However, there are still some problems and challenges: 1) it is necessary to strengthen measures to tackle the problem of low CO_2 oil recovery; 2) the economic issues with regard to use of CO_2, such as the fact that CO_2 is corrosive to the pipeline during gathering and transportation, accelerate the costs from pipeline damage; 3) gas source of CO_2 flooding: owing to the increased distance between the oilfield and the city, the costs of gathering and transportation are high, which limit the development of CO_2 flooding technologies.

This paper therefore suggests two areas of improvement: 1) China should continue to strengthen technical research on improving oil recovery; 2) China needs to develop breakthrough carbon dioxide capture technologies and provide inexpensive natural gas sources.

Author contributions

All authors conceived and designed the study. Write the first draft, XX and QD; Writing review and editing, PS and LT; Format modification, LY, JB, and WL.

Funding

This work was supported by the Open Foundation of Cooperative Innovation Center of Unconventional Oil and Gas, Yangtze University (Ministry of Education and Hubei Province, No. UOG 2022-03), Open Fund of Hubei Key Laboratory of Drilling and Production Engineering for Oil and Gas (Yangtze University, No. YQZC202206), and Hubei Provincial Natural Science Foundation Youth Project of 2022 (No. ZRMS2022000846).

Conflict of interest

PS was employed by the company Engineering Technology Research Institute of PetroChina Southwest Oil and Gas Field Company, LT was employed by the company Chuanxi Drilling Company, CNPC Chuanqing Drilling Engineering Co. Ltd.; QD and LY were employed by the company Carbon Hydrogen Epoch Technology Co. Ltd. WL was employed by the company CNOOC Ltd.

The remaining authors declare that the research was conducted in the absence of any commercial or financial relationships that could be construed as a potential conflict of interest.

Publisher's note

All claims expressed in this article are solely those of the authors and do not necessarily represent those of their affiliated organizations, or those of the publisher, the editors and the reviewers. Any product that may be evaluated in this article, or claim that may be made by its manufacturer, is not guaranteed or endorsed by the publisher.

References

British Petroleum Company (2017). *BP statistical review of world energy*. London: BP Company.

British Petroleum Company (2018). *BP statistical review of world energy[R]*. London: BP Company.

Chen, Huanqing, Hu, yongle, and Tian, Changbing (2012). Research progress of CO2 flooding and storage [J]. *Oilfield Chem.* 29 (01), 116–121+127.

Chen, Huanqing, Hu, Yongle, and Tian, Changbing (2015). Researches on CO2 flooding and sequestration and its significance in low carbon economy [J]. *J. Southwest Petroleum Univ. Soc. Sci. Ed.* 17 (5), 7. doi:10.11885/j.issn.1674-5094.2015.01.29.01

Desch, J. B., Larsen, W. K., Lindsay, R. F., and Nettle, R. L. (1984). Enhanced oil recovery by CO2 miscible displacement in the little knife field, billings county, North Dakota. *J. Pet. Technol.* 36 (09), 1592–1602. doi:10.2118/10696-PA

Grigg, R. B., and Siagian, U. W. R. (1998). *Understanding and exploiting four-phase flow in low temperature CO2 floods*. Midland, Texas: SPE Permian Basin Oil and Gas Recovery.

Gu, Libing, Li, Zhiping, and Jin, Ou (2007). The existing state of enhanced oil recovery by utilizing carbon dioxide[J]. *China Min.* 16 (10), 66–68. doi:10.3969/j.issn.1004-4051.2007.10.020

Hitesh, M., Marshall, C., and Khosrow, B. (2008). *The potential for additional carbon dioxide flooding projects in the United States[R]*. Tulsa, Oklahoma, USA: SPE Symposium on Improved Oil Recovery.

Jia, Kaifeng, Ji, Dongchao, and Gao, Jindong (2019). The existing state of enhanced oil recovery by CO2 flooding in low permeability reservoirs [J]. *Unconv. oil gas* 6 (1), 9.

Koottungal, Leena (2014). 2014 world EOR survey[J]. *Oil Gas J.* 112 (4), 79–91.

Li, Yongtai, Liu, Yifei, and Tang, Changjiu (2008). *Principle and method of enhanced oil recovery [M]*. Beijing: Petroleum Industry Press, 180–188.

Luo, Zhongwei, Fang, Mengxiang, and Li, Mingyuan (2012). *Carbon dioxide capture, storage and utilization technology [M]*. Beijing: China Electric Power Press, 208–231.

Qin, Jishun, Han, Haishui, and Liu, Xiaolei (2015). Application and enlightenment of carbon dioxide flooding in the United States of America [J]. *Petroleum Explor. Dev.* 42 (02), 209–216. doi:10.11698/PED.2015.02.10

Rao, D. N., Ayirala, S. C., Kulkarni, M. M., and Sharma, A. P. (2004). *Development of gas assisted gravity drainage (GAGD) process for improved light oil recovery*. USA: SPE/DOE Symposium on Improved Oil Recovery.

Roper, M. K., Pope, G. A., and Sepehrnoori, Kamy (1992). *Analysis of tertiary injectivity of carbon dioxide*. Midland, Texas: Permian Basin Oil and Gas Recovery.

Shen, Pingping, and Liao, Xinwei (2009). *Carbon dioxide geological storage and enhanced oil recovery technology [M]*. Beijing: Petroleum Industry Press.

Whorton, L. P., Brownscombe, E. R., and Dyes, A. B. (1952). *Method for producing oil by means of carbon dioxide*. USA: U. S. Patent.

Xiang, Yong, Hou, Li, Du, Meng, Jia, Ninghong, and Lv, Weifeng (2022). Research progress and development prospect of CCUS-EOR technologies in China [J]. *Oil gas Geol. recovery* 5, 1–17. doi:10.13673/j.cnki.cn37-1359/te.202112048

Zou, Caineng, Xue, Huaqing, and Xiong, Bo (2021). Connotation, innovation and vision of "carbon neutral. *J. Nat. Gas. ind.* 41 (8), 12. doi:10.3787/j.issn.1000-0976.2021.08.005

frontiers | Frontiers in Earth Science

TYPE Opinion
PUBLISHED 16 January 2023
DOI 10.3389/feart.2022.1053307

OPEN ACCESS

EDITED BY
Zhilin Cheng,
Xi'an Shiyou University, China

REVIEWED BY
Yang Yang,
Chengdu University of Technology, China
Kun Xie,
Northeast Petroleum University, China

*CORRESPONDENCE
Qi Gao,
xuxingguang123@126.com

SPECIALTY SECTION
This article was submitted to Geochemistry, a section of the journal Frontiers in Earth Science

RECEIVED 25 September 2022
ACCEPTED 20 October 2022
PUBLISHED 16 January 2023

CITATION
Zhu Z, Song Y, Gao Q and Wang C (2023), The application of CO_2-responsive materials on enhanced oil recovery for fractured tight oil reservoirs.
Front. Earth Sci. 10:1053307.
doi: 10.3389/feart.2022.1053307

The application of CO_2-responsive materials on enhanced oil recovery for fractured tight oil reservoirs

Zhuoyan Zhu[1], Yingzhi Song[2], Qi Gao[3]* and Chao Wang[1]

[1]Research Institute of Petroleum Exploration and Development, Beijing, China, [2]PetroChina Ji Dong Oilfield Company, Tangshan, China, [3]Key Laboratory of Theory and Technology of Petroleum Exploration and Development in Hubei Province, China University of Geosciences, Wuhan, China

KEYWORDS

CO_2-responsive, foam, worm-like micelle, gel, enhanced oil and gas recovery (EOR and EGR), fractured oil reservoir

Introduction

According to the statistics, about 38% of oil and gas fields in the world and 46% in China are contributed by low-permeability reservoirs. The effective development of low permeability oil and gas fields has important strategic significance to ensure the sustainable development and exploitation of oil and gas resources in China. Due to lack of natural energy in the formation and the difficulty of water injection, the oil recovery rate and factor of these reservoirs are fairly low (WANG, et al. 2007; LI, 2020).

CO_2 flooding is often used as a EOR technology to improve oil recovery in low permeability reservoirs due to its good solubility and strong extraction ability. It is mainly used to facilitate oil displacement by reducing the viscosity of crude oil, improving the mobility ratio, expanding the volume of crude oil, and reducing the interfacial tension (ZHAO, et al. 2017). However, due to the strong heterogeneity and the existence of natural and induced fractures, as well as the influence of injection-production well parameters and fluid properties, CO_2 is prone to channeling along the high seepage zone (LI, 2018; WANG, 2019). Avoiding gas channeling during the process of gas flooding has become a major issue. It is vital to increase the sweep volume and improve the performance of CO_2 flooding to reduce the heterogeneity of reservoir and plug the breakthrough channels such as fractures, throats and pores (LIU, et al. 2022).

Water-alternate-gas (WAG) injection, gas thickening, foam plugging and polymer gel plugging are common methods to address gas channeling (PENG, 2013; YUN, 2013; WEN, 2019; ZHAO, et al. 2020). However, these measures are generally one-time plugging, which limits the effectiveness on gas channeling. In this work, a variety of CO_2 responsive plugging systems are summarized and analyzed, including CO_2 responsive foams, surfactant solutions and gels. The main mechanism of these systems is that in saturated CO_2 solution, amine-containing compounds spontaneously or combine with surfactant molecules to form worm-like micelles (WLMs) after deprotonation, so as to improve the viscosity of the solution and achieve precise and efficient blocking of gas channeling.

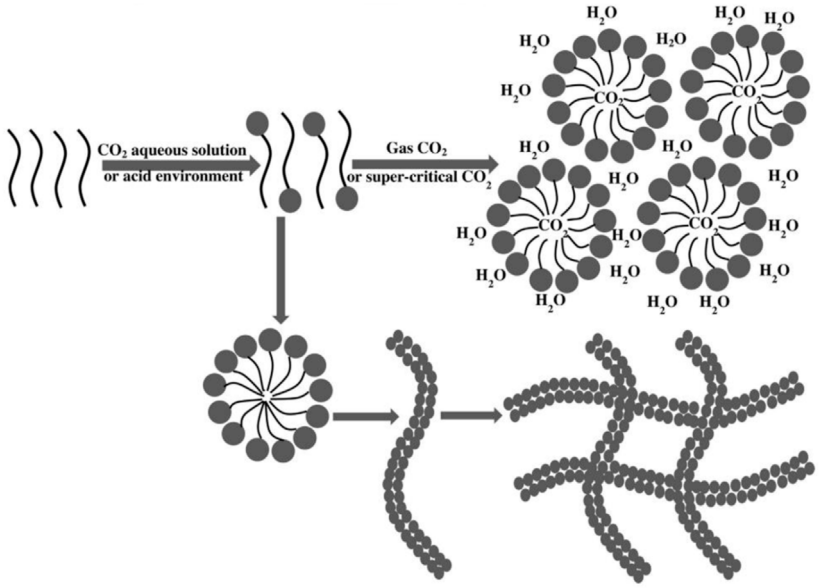

FIGURE 1
Schematic diagram of structure change of surfactant—amine system stimulated by CO_2 (LI, et al., 2015).

Types of plugging agent

CO_2-responsive foam

A formula of CO_2 responsive foam system was proposed previously by (LV, et at. 2021). The system had obvious shear-thinning characteristics and was more viscoelastic than the conventional foam system. The FCI value of the foam system could be more than 11 times than that of the conventional foam system, which could effectively inhibit gas channeling in strongly heterogeneous reservoir, and improve the CO_2 flooding development efficiency. Li et al. screened the surfactant with the best performance from five surfactants (ODPTA, AC-1810, AC-1815, SDS, OTAC) and constructed a CO_2 sensitive and self-enhanced foam system for mobility control (LI, et al. 2017). ODPTA had a carbon chain consisting of an amine group and 18 carbon atoms, which could not be ionized in water. However, in the acidic environment caused by CO_2, the amine group was protonated and ion pairs ($C_{18}H_{37}$-NH-$(CH_2)_3$-NH_2^+-$(CH_2)_3$-NH_3^+ and $C_{18}H_{37}$-NH-$(CH_2)_3$-NH-$(CH_2)_3$-NH_2-CO_2^-) are formed. The results showed that the CO_2 foam prepared by ODPTA is sensitive to CO_2 and had good plugging and mobility control performance at low concentration. Even under the harsh conditions of 7.8 MPa and 160°C, the resistance factor could still reach 274.

CO_2-responsive surfactant

Some studies showed that the use of CO_2 as an external stimulus to transform surfactant micelles was currently a simple and environmentally friendly way to prepare micelles. (SU, et al. 2013; ZHENG, et al. 2015; ZHANG, et al. 2016). Su et al. prepared an anionic worm-like micellar system with CO_2 response using sodium octadecyl sulfate ($C_{18}H_{37}SO_4Na$) and N, n-dimethylethanolamine (DMAE) at 60°C. DMAE was positively charged by protonation under CO_2 stimulation and then self-assembles with the anionic surfactant $C_{18}H_{37}SO_4Na$ under electrostatic attraction to form worm-like micelles. When N_2 was injected, the high viscosity system returned to the initial viscosity state. And this process could be repeated more than three times, and the maximum viscosity formed without a big deviation (SU, et al. 2013). Shen et al. screened ten compounds containing tertiary amine groups, and finally determined N, N-Dimethyl Erucamide tertiary amine (DMETA) as the research object. The results showed that the DMETA solution forms WLMs in saturated CO_2 solution, and the viscoelastic fluid could effectively reduce gas flow during CO_2 gas flooding in low-permeability fractured cores, and had a strong ability to withstand high temperature. WLMs had the ability of self-repair and had high residual resistance even after gas channeling (SHEN, et al. 2021).

CO_2-responsive gel

The mechanism of gel-blocking gas channeling was discussed in detail, and the future development direction of CO_2 trapping and interpenetrating gel system was prospected. CO_2 responsive intelligent gel can solve the problem of poor acid resistance of HPAM. The cross-linking formed a three-dimensional network structure after CO_2 treatment, with increased viscosity and volume, and remained stable for a long time under acidic CO_2 conditions (LIU, et al. 2022). A CO_2 responsive gel system mainly using small molecule amine (DMTA) and a modified long chain alkyl anionic surfactant (NADS) was prepared (DAI, et al. 2020). The experimental results showed that the DMTA-NADS system exhibited viscoelastic properties and shear thinning properties at high shear rates. The environment scanning electron microscope (ESEM) visually showed that the connection mode of its internal structure changed from lamellar to three-dimensional network structure. It was confirmed by NMR that amine molecules can bridge two anionic surfactant molecules by non-covalent electrostatic attraction after protonation. The core physical simulation experiment proved that the system could effectively block the CO_2 channeling channel, and the blocking efficiency was more than 90%, which increased the sweep volume of the subsequent CO_2 gas flooding and improved the recovery efficiency. It provided effective guidance for solving the practical problem of gas channeling and plugging in low permeability CO_2 gas flooding development reservoir.

Comparative analysis of different materials

The mainly mechanism of CO_2 responsive materials involved in this paper is shown in Figure 1.

It is shown that CRMs are effective measures to prevent gas channeling during gas flooding. When the CRMs encounters CO_2, its structure changes and the viscosity of the solution increases, which can be observed in both bulk and porous media. The three CRMs mentioned in this paper have essentially the same mechanism, but different plugging systems can be obtained by changing the type and concentration of surfactants, amines, and volume and rate of CO_2 injection according to different purposes of using.

Compared with other plugging agents, CRMs has a better application prospect in tight fractured reservoirs. Before CRMs gelling, the solution viscosity is low (1–2 mPa s), resulting in easy injecting. It can quickly form high viscosity gel after CO_2 injection and has strong blocking ability. Using suitable surfactants and amines, CRMs can maintain high stability under high temperature and high salt conditions.

Conclusion

1) The mechanism of CO_2 responsive plugging system is that the molecular structure in aqueous solution changes upon CO_2 stimulation, forming worm-like micelles. The macroscopic behavior is that the viscosity of the system changes, which is reversible and controllable.
2) By using different materials to interact with amine compounds, CRMs are low viscosity solutions before injection and can be formed as CO_2 responsive blocking systems after reaction with CO_2 in porous media such as CO_2 responsive foam, CO_2 responsive surfactant solution and CO_2 responsive gel. With good injection ability, CRMs can effectively block the gas channeling, force the gas to turn to the unswept zone, and improve the degree of reservoir production. At present, it is necessary to develop a low cost and high tolerance CO_2 responsive plugging system for the development of fractured tight oil reservoirs, so as to improve the production capacity and benefit of oil fields. (LIU AND LIU, 2022), (LV et al., 2021).

Author contributions

ZZ: investigation and research, writing manuscript draft; YS: resources and conceptualization; QG: modify analysis; CW: typesetting and supervision.

Funding

This work is supported by PetroChina “Fourteenth Five Year” Significant Programs (No. 2021DJ3203).

Conflict of interest

Author YS was employed by the company PetroChina Ji Dong Oilfield Company.

The remaining authors declare that the research was conducted in the absence of any commercial or financial relationships that could be construed as a potential conflict of interest.

Publisher’s note

References

Dai, M. L., Wei, F. L., Lu, Y. J., Xiong, C. M., Shao, L. M., and Song, Y. Z. (2020). A new type of CO2 responsive gel based channeling blocking system. *OIL Drill. Prod. Technol.* 45 (6), 772–778.

Li, D. X., Ren, B., Zhang, L., Ezekiel, J., Ren, S. R., and Feng, Y. J. (2015). CO2-sensitive foams for mobility control and channeling blocking in enhanced WAG process. *Chem. Eng. Res. Des.* 102, 234–243. doi:10.1016/j.cherd.2015.06.026

Li, D. X., Ren, S. R., Zhang, P. F., Zhang, L., Feng, Y. J., and Jing, Y. B. (2017). CO2 -sensitive and self-enhanced foams for mobility control during CO 2 injection for improved oil recovery and geo-storage. *Chem. Eng. Res. Des.* 120, 113–120. doi:10.1016/j.cherd.2017.02.010

Li, C. L. (2018). Gas channeling influencing factors and patterns of CO, -flooding in UItra-low permeability oil reservoir. *Special Oil Gas Reservoirs* 25 (3), 82–86. (In Chinese).

Li, Y., Xiao, K., Huang, C., Wang, J., Gao, M., and Hu, A., (2020). Enhanced potassium-ion storage of the 3D carbon superstructure by manipulating the nitrogen-doped species and morphology. *Nanomicro. Lett.* 27 (1), 1–10. (In Chinese). doi:10.1007/s40820-020-00525-y

Liu, Y. J., and Liu, Q. (2022). A review of channeling blocking gel systems for CO2 flooding. *Petroleum Geol. Recovery Effic.* 29 (3), 1–13.

Liu, F., Yue, P., Wang, Q., Yu, G., Zhou, J., and Wang, X., (2022). Experimental study of oil displacement and gas channeling during CO2 flooding in ultra—low permeability oil reservoir. *Energies* 15 (14), 5119. doi:10.3390/en15145119

Lv, W., Liu, X. C., Bai, H. L., and Peng, M. L. (2021). Laboratory test study of CO2 responsive enhanced foam system. *Pet. Drill. Tech.* 49 (5), 88–93. (In Chinese).

Peng, S. S. (2013). Gas channeling rules of CO2 flooding in extra-low permeability reservoirs in zhenglizhuang oilfield. *J. Oil Gas Technol. (J. JPI)* 35 (3), 147–150. (In Chinese).

Shen, H., Yang, Z., Li, X., Peng, Y., Lin, M., Zhang, J., et al. (2021). CO2-responsive agent for restraining gas channeling during CO2 flooding in low permeability reservoirs. *Fuel* 292, 120306. doi:10.1016/j.fuel.2021.120306

Su, X., Cunningham, M. F., and Jessop, P. G. (2013). Switchable viscosity triggered by CO2 using smart worm-like micelles. *Chem. Commun.* 49 (26), 2655–2657. doi:10.1039/c3cc37816k

Wang, G. F., Liao, R. F., Li, J. L., Yuan, X. C., Zhan, C. G., Jiang, Y. J., et al. (2007). The development situation and future of low permeability oil reservoirs of SINOPEC. *PEIROLEUM GEOIOGY RECOVERY EFFC ENCY* 14 (3), 84–89. (In Chinese).

Wang, Y. X. (2019). *Mechanism research of CO2 enhanced oil recovery for tight sand oil reservoir ——take yanchang formation 4+5 reservoir in A oil area of northern shaanxi as an example*. Kirkland,USA: Northwest University. (In Chinese).

Wen, F. G. (2019). *CO2 flooding experiment research of low permeability oil reservoir in the Ordos Basin -A case study of the Chang6 of M area of A oilfield*. Kirkland,USA: Northwest University. (In Chinese).

Yun, B. B. (2013). Field test of carbon dioxide gas channeling foam plugging. *Appl. Mech. Mater.* 2369, 316–317.

Zhang, Y., Wang, C., Liu, X., Fang, Y., and Feng, Y. (2016). CO2-Responsive microemulsion: Reversible switching from an apparent single phase to near-complete phase separation. *Green Chem.* 18 (2), 392–396. doi:10.1039/c5gc01411e

Zhao, X. S., Shi, L. H., Wang, W. B., Bai, Y., and Tian, F. (2017). CO2 channeling sealing in UItra-low-permeability reservoirs. *J. Southwest Petroleum Univ. Technol. Ed.* 39 (6), 131–139. (In Chinese).

Zhao, F., Wang, P., Huang, S., Hao, H., Zhang, M., and Lu, G. (2020). Performance and applicable limits of multi-stage gas channeling control system for CO2 flooding in ultra-low permeability reservoirs. *J. Petroleum Sci. Eng.* 192 (C), 107336. doi:10.1016/j.petrol.2020.107336

Zheng, Z. B., Liu, C. Y., and Qiao, W. H. (2015). pH-Responsive and CO2-responsive vesicles can be formed by N-decylimidazole. *Eur. J. Lipid Sci. Technol.* 117 (10), 1673–1678. doi:10.1002/ejlt.201400429

frontiers | Frontiers in Earth Science

TYPE Mini Review
PUBLISHED 17 January 2023
DOI 10.3389/feart.2022.1063042

OPEN ACCESS

EDITED BY
Zhilin Cheng,
Xi'an Shiyou University, China

REVIEWED BY
Fengtao Qu,
China University of Petroleum, China
Ming Zhong,
China University of Geosciences, China

*CORRESPONDENCE
Jiajia Hu,
hujiajia_yangtze@163.com
Qiao Deng,
dengqiao2008@163.com

SPECIALTY SECTION
This article was submitted to Geochemistry, a section of the journal Frontiers in Earth Science

RECEIVED 06 October 2022
ACCEPTED 01 November 2022
PUBLISHED 17 January 2023

CITATION
Yan L, Hu J, Fang Q, Xia X, Lei B and Deng Q (2023), Eco-development of oil and gas industry: CCUS-EOR technology.
Front. Earth Sci. 10:1063042.
doi: 10.3389/feart.2022.1063042

Eco-development of oil and gas industry: CCUS-EOR technology

Liangzhu Yan[1,2,3,4], Jiajia Hu[5]*, Qiongyao Fang[1,3,4], Xueqing Xia[1,3,4], Banyu Lei[1,3,4] and Qiao Deng[1,2,3,4]*

[1]Cooperative Innovation Center of Unconventional Oil and Gas, Yangtze University (Ministry of Education & Hubei Province), Wuhan, China, [2]Carbon Hydrogen Epoch Technology Co., Ltd., Wuhan, China, [3]Key Laboratory of Drilling and Production Engineering for Oil and Gas, Wuhan, China, [4]School of Petroleum Engineering, Yangtze University:National Engineering Research Center for Oil & Gas Drilling and Completion Technology, Wuhan, China, [5]School of Geoscience, Yangtze University, Wuhan, Hubei, China

The current status and development prospects of CCUS-EOR technology development are sorted out from the perspective of ecological development. A good foundation is laid to promote the world low-carbon development pattern and the development of CCUS-EOR technology in oil-rich, low-permeability reservoirs. By analyzing the differences between China and the United States regarding the technology level, application scale, and production effect, the development gaps between different countries in terms of CO_2 burial for enhanced oil and gas recovery are derived. In response to these gaps, recommendations for responsive technology research and supporting infrastructure construction are proposed, which are of reference significance for advancing the development of large-scale CCUS technology for all of humanity.

KEYWORDS

oil and gas industry, ecological development, CO_2 flooding, EOR, CCUS

1 Introduction

Global climate change is gradually affecting normal human activities, and reducing greenhouse gas emissions has become an international consensus to address climate change (ROCCO et al., 2018; PARTANI et al., 2022). The shares of coal, oil, and natural gas in China's energy consumption in 2019 are 57.7%, 18.9%, and 8.1%, respectively (LIAO and MING, 2019). In September 2020, the Chinese government pledged that China's CO_2 emissions will strive to peak by 2030 and achieve carbon neutrality by 2060. CCUS will be the only technology option to achieve near-zero emissions from this part of fossil energy (LIU et al., 2021).

According to IEA estimates, CCUS can contribute 15%–20% of the net zero emissions of CO_2 (OU et al., 2021). According to the China Petroleum Institute of Economic and Technological Research forecast, more than 85% of coal and gas power will be equipped with CCUS by 2050 (GUPTA et al., 2021). Cai Bofeng et al. (Cai et al., 2021) calculated that, under the current technology development, the amount of CO_2 emission reduction needed to achieve the goal of carbon neutrality by 2050 and 2060 through CCUS technology is 6×10^8 to 14×10^8t and 10×10^8 to 18×10^8 t, respectively (LIU et al., 2022). The conditions required for hydrocarbon and CO_2 accumulation are very close,

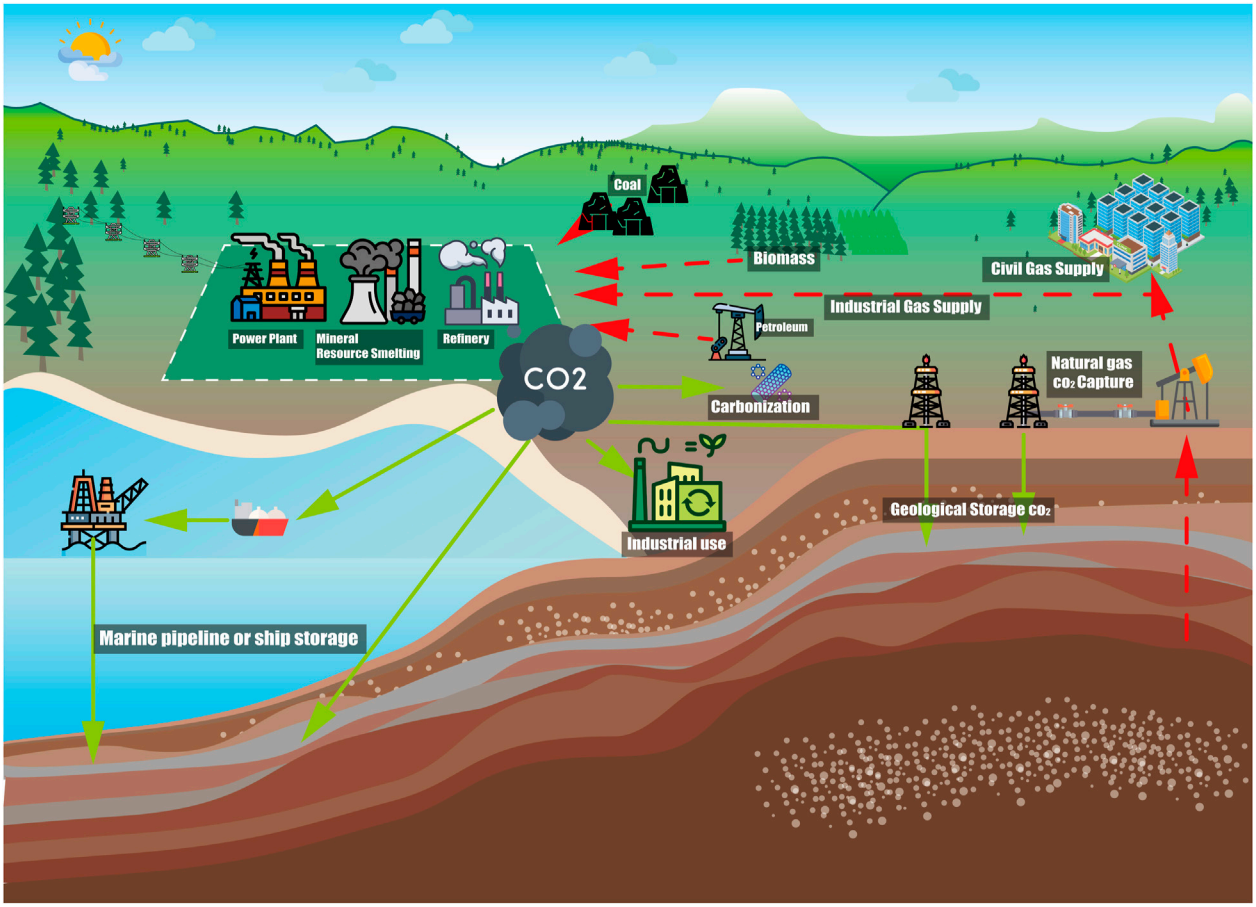

FIGURE 1
CCUS-EOR technology roadmap.

and the technology can not only improve oil recovery to achieve ecological development of the oil and gas industry but also achieve CO_2 emission reduction.

2 Ecological CCUS-EOR

Ecological development stems from a reflection on the environmental and ecological damage caused by modern technologies. In engineering design, it is essential to consider the ecological, social, and site-specific impacts of the technologies used, to put ecological factors at the forefront from the point of view of the whole life cycle of materials, and to carry out all work with the Earth at the center (LI et al., 2022). The ecological development of the oil and gas industry means that we can significantly reduce the total CO_2 emissions from the oil and gas industry through ecological development. At this stage, we cannot achieve the ecological effect of the oil and gas industry without the CCUS-EOR technology (Figure 1).

Compared to conventional EOR technology, CCUS-EOR technology not only provides an effective way to store and utilize CO2 but also offers a more attractive increase in recovery rate compared to EOR technology. When the ecological costs are included in the calculation, CCUS-EOR technology will be less expensive than EOR technology and more widely welcomed.

The CCUS-EOR technology, as a CCUS utilization for the ecological development aspect of the oil and gas industry, promotes the flow of carbon materials in the oil and gas industrial process. By establishing a multifaceted and continuous resource cycle process through recycling, the carbon-containing waste from the previous production process is used as a production material in the next stage to serve the next phase of production activities (WANG et al., 2019). That is, by capturing CO_2 and injecting it into the reservoir. CO_2 enters the reservoir and reduces the viscosity of crude oil, improves the flow ratio of crude oil to water, expands the volume of crude oil, and extracts and vaporizes light hydrocarbons in crude oil. The oil is

driven by mechanisms such as the mixing effect, molecular diffusion, reduction of interfacial tension, dissolved gas drive, and increased permeability to improve recovery. Alleviate environmental pollution at the same time, while it can make a large amount of CO_2 buried underground, potentially changing the relationship between the oil and gas industry and the natural environment and promoting the impact of the oil and gas industry on the ecology from degradation to regeneration.

3 Current status of CCUS-EOR technology development

Foreign CCUS-EOR projects are mainly carried out in the United States, Canada and other countries. Especially, the United States has a mature CCUS-EOR industrial system. The U.S. CCUS-EOR project started in the 1950s, carried out fundamental technology research in the 1960s and 1970s, expanded the scale of industrial trials in the 1970s and 1990s, matured the technology package, and entered the commercialization and promotion stage after the 1980s. Since the 1980s, the scale of industrial application of CCUS-EOR technology in the United States has expanded rapidly. The project has achieved excellent application results, taking the CCUS-EOR project in the Kelly-Snyder field SACROC block in the Permian Basin of the United States as an example: the reservoir permeability of the block is 1×10^{-3}–30×10^{-3} μm (ROCCO et al., 2018), geological reserves of about 4.1×10^8 t, and in 1998 The oil production declined to 40×10^4 t in 1998, the CO_2 mixed-phase drive project was implemented in 2002, and the oil production exceeded 150×10^4 t in 2005, and the production has been stable for 16 years until 2020, with a cumulative oil increase of $2{,}456 \times 10^4$ t and a cumulative injection of CO_2 3.9×10^8 t, which is expected to improve the recovery rate by more than 26 percentage points (LIN and TAN, 2021).

China's CCUS-EOR research started early, and oil companies and related institutions started to explore CO_2 oil drive technology as early as the 1960s. Still, industrialization lagged due to gas source, mechanism understanding, equipment, and other problems. Since the 21st century, the state and oil companies have set up CCUS-EOR primary scientific and technological research and demonstration projects, which have extensively promoted the breakthrough of critical technologies and the success of minefield tests (ADU et al., 2019). China Petroleum & Chemical Corporation Limited has conducted several field trials in Jiangsu, Shengli, and East China oilfields; CO_2 oil drive projects have been implemented to cover geological reserves of $2{,}512 \times 10^4$ t, with a cumulative oil increase of 25.58×10^4 t. Among them, the CO_2 near-mixed phase drive pilot test in High 89-1 block of Shengli oilfield, with a cumulative CO_2 injection of 31×10^4 t and a cumulative oil increase of 8.6×10^4 t as of August 2021. It is predicted to improve the recovery rate by 17.2 percentage points. Yanchang Oilfield is also actively exploring CCUS-EOR technology and has made positive progress in integrated technology research and development and entire process low-cost commercialization engineering demonstration, and has built an annual processing capacity of 15×10^4 t in Jingbian and Wuqi pilot areas. A CCUS demonstration project with an annual processing capacity of 15×10^4 t has been built in Jingbian and Wuqi pilot areas, injecting 21.6×10^4 t of CO_2.

4 CCUS-EOR ecological future

Although there is a contradiction between oil production and low-carbon development, it can be achieved by constructing an ecological development concept with technological progress and scientific innovation. In terms of social benefits, annual buried CO_2 of $3{,}000 \times 10^4$ t can absorb the carbon emissions of more than ten extensive refining and chemical enterprises (Zhao et al., 2021). Based on the goal of achieving carbon neutrality by 2060, the current high carbon emission infrastructure has a useful life of fewer than 40 years. By addressing a portion of CO_2 emissions from coal power, cement and steel industries through the CCUS-EOR industry, we can avoid the early shutdown of newly invested infrastructure and wasted investment and enhance the cost-effectiveness of the carbon neutrality process.

In terms of economic benefits, CO_2 drive is one of the main technologies to replenish reservoir formation energy and improve crude oil recovery effectively. According to the 2020 evaluation results of the China Petroleum Exploration and Development Research Institute, the geological reserves of low-permeability reservoirs suitable for CO_2 drive to improve recovery in some oil fields of China are 67.3×10^8 t, which are expected to improve recovery by 16.5 percentage points on average and add 11.1×10^8 t of recoverable reserves, and can effectively bury CO_2 29.5×10^8 t in the drive phase (TANG et al., 2016).

According to the preliminary evaluation of the CO_2 geological storage potential of the main oil and gas reservoirs in the major oil and gas basins in China, the CO_2 storage potential of reservoirs exceeds 140×10^8 t. Among them, the CO_2 burial potential in the main oil areas of Songliao, Ordos, Bohai Bay and Junggar basins is high, and they are the key areas for implementing CCUS-EOR. The theoretical CO_2 burial potential in the deep saline layer of major basins in China is even larger, reaching more than 6×10^{12} t. In addition, promoting the development of new CCUS-EOR industries on a large scale can also provide many employment opportunities for society.

5 Prospects and challenges of CCUS-EOR technology development

Compared with foreign countries, the main problem facing CO_2 capture in China is the high capture cost and challenges of

TABLE 1 Comparison of Chinese and US CO_2 oil drive technologies (Xiang et al).

Projects	The U.S.	China
Geological conditions	Main marine sedimentary reservoirs; relative homogeneous physical properties	Onshore sedimentary reservoirs with strong inhomogeneity and thin reservoirs
Mixed phase	Low mixed-phase pressure, 90% of mixed-phase drive can be achieved	High mixed-phase pressure, the small difference between formation pressure and mixed-phase pressure
Seepage mechanism	more mature conventional seepage mechanism theory and experimental methods; much studied multi-phase cross-scale seepage theory; less experiments	Breakthroughs in the study of CO_2 drive phase state, and the core replacement experimental method is relatively complete; less research on multiphase seepage theory and simulation in porous media
Reservoir Description	Large oil layer thickness; good continuity, no attention to small layer subdivision contrast and dominant channel portrayal	Thin oil layer; small scale of sand spreading; the formation is based on single sand level reservoir fine description technology, the boundary and delineation of CO_2 drive dominant channel is to be clarified
Annual production	$1,550 \times 10^4$ t	20×10^4 t
Cost	15–30 USD/t	47–55 USD/t

the large-scale capture of low-concentration CO_2 (PARK et al., 2021). Low-concentration chemical amine capture CO_2 technology has been commercialized in foreign countries for more than 5 years at the megaton level. However, China is still in the demonstration operation stage, and steam consumption is more than 40% more than abroad (Qin et al., 2020). In terms of large-scale integrated process optimization, foreign countries have already realized commercialized process packages for million-ton carbon capture. In contrast, China still has no commercialized standard process package to offer. Foreign governments have integrated heat recovery of composite amine liquid purification technology, while China only has partial process technology integration. Foreign countries have a complete adaptation of the device transformation optimization and solutions. China is still in the initial stage of research (Zou et al., 2021).

At this stage, China and North America CCUS-EOR need to be further improved in terms of technology level, application scale and production effect (Table 1). The current CO_2 oil recovery enhancement range is 10%–25%, and the CO_2 burial rate is about 60%–70%. Under the current technical conditions, more than 50% of the geological reserves of crude oil remain in the subsurface at the end of the oil drive life cycle. Therefore, we need more in-depth research on the mechanism of multiphase seepage in CO_2-driven porous media, characterization techniques of gas drive dominant channels in strongly inhomogeneous reservoirs, rational good networks and development laws, and expansion of wave volume (ZHANG et al., 2013). The CO_2 burial mechanism and main control factors of different injection methods and different geological bodies have been clarified, and the contribution degree and characterization methods of CO_2 burial mechanisms such as "volume replacement, dissolution retention and mineralization reaction" of reservoir geological bodies have been determined, the evaluation methods of CO_2 safe burial potential of natural gas reservoirs, saline water reservoirs and coal-bed methane reservoirs have been established, and the technique of CO_2 concentration, soil concentration, and mineralization reaction have been developed. CO_2 concentration, soil carbon flux, stable isotopes, and other integrated methods to monitor the CO_2 leakage burial safety monitoring technology system (ZHANG et al., 2015).

6 Conclusion

CCUS-EOR technology is one of the effective means to reduce carbon emissions and one of the fundamental ways to utilize CO_2. From the perspective of ecological development, China and the United States, as essential components in driving the world toward carbon neutrality, both countries have good potential in CCUS-EOR technology, and the combination of CO_2 drive and buried reservoirs is also a significant trend for future development. By sorting out the current status and development prospects of CCUS-EOR technology development. To establish a new direction for the development of dual carbon in the world and also for the large reservoirs of low permeability in China, where the traditional water drive is inadequate, the oil and gas production enhancement scheme based on CCUS-EOR technology is proposed. The international development pattern regarding large-scale oil-driven burial and intelligent monitoring technologies is also dissected. In this way, we present the research of responsive technologies and the construction of supporting infrastructure, which to some extent, promote the large-scale use of CCUS technology for all humankind (ABUOV et al., 2022).

Author contributions

All authors conceived and designed the study. Write the first draft, LY, and QD; Writing review and editing, JH, and QF; Format modification, BL, XX.

Funding

Supported by the Open Foundation of Cooperative Innovation Center of Unconventional Oil and Gas, Yangtze University (Ministry of Education & Hubei Province), No. UOG2022-03; Supported by Open Fund of Hubei Key Laboratory of Drilling and Production Engineering for Oil and Gas (Yangtze University), No. YQZC202206; Supported by the Key Program of Hubei Provincial Department of Education, No. D20221303; Supported by the Natural Science Foundation of Hubei Province, No. ZRMS2022000846.

Conflict of interest

Author QD and LY were employed by Carbon Hydrogen Epoch Technology Co. Ltd.

The remaining authors declare that the research was conducted in the absence of any commercial or financial relationships that could be construed as a potential conflict of interest.

Publisher's note

Reference

Abuov, Y., Serik, G., and Lee, W. (2022). Techno-economic assessment and life cycle assessment of CO_2-EOR [J]. *Environ. Sci. Technol.* 56 (12), 8571–8580. doi:10.1021/acs.est.1c06834

Adu, E., Zhang, Y., and Liu, D. (2019). Current situation of carbon dioxide capture, storage, and enhanced oil recovery in the oil and gas industry. *Can. J. Chem. Eng.* 97 (5), 1048–1076. doi:10.1002/cjce.23393

Cai, B., Cao, L., Lei, Y., Wang, C., Zhang, L., Zhu, J., et al. (2021). Carbon dioxide emission pathways under China's carbon neutrality target %J China's Population. *Resour. Environ. [J]* 31 (01), 7–14. doi:10.12062/cpre.20210101

Gupta, A., Davis, M., and Kumar, A. (2021). An integrated assessment framework for the decarbonization of the electricity generation sector. *Appl. Energy* 288, 116634. doi:10.1016/j.apenergy.2021.116634

Li, T., Shi, Z., and Han, D. (2022). Research on the impact of energy technology innovation on total factor ecological efficiency. *Environ. Sci. Pollut. Res.* 29 (24), 37096–37114. doi:10.1007/s11356-021-18204-9

Liao, X., and Ming, J. (2019). Pressures imposed by energy production on compliance with China's 'Three Red Lines' water policy in water-scarce provinces. *Water Policy* 21 (1), 38–48. doi:10.2166/wp.2018.211

Lin, B., and Tan, Z. (2021). How much impact will low oil price and carbon trading mechanism have on the value of carbon capture utilization and storage (CCUS) project? Analysis based on real option method [J]. *J. Clean. Prod.* 298, 126768. doi:10.1016/j.jclepro.2021.126768

Liu, G., Cai, B., Li, Q., Zhang, X., and Ouyang, T. (2022). China's pathways of CO_2 capture, utilization and storage under carbon neutrality vision 2060 [J]. *Carbon Manag.* 13 (1), 435–449. doi:10.1080/17583004.2022.2117648

Liu, W., Fan, W., Hong, Y., and Chen, C. (2021). A study on the comprehensive evaluation and analysis of China's renewable energy development and regional energy development. *Front. Energy Res.* 9. doi:10.3389/fenrg.2021.635570

Ou, Y., Roney, C., Alsalam, J., Calvin, K., Creason, J., Edmonds, J., et al. (2021). Deep mitigation of CO_2 and non-CO_2 greenhouse gases toward 1.5 degrees C and 2 degrees C futures [J]. *Nat. Commun.* 12 (1), 6245. doi:10.1038/s41467-021-26509-z

Park, C., Jeong, S., Park, H., Woo, J. H., Sim, S., Kim, J., et al. (2021). Challenges in monitoring atmospheric CO_2 concentrations in seoul using low-cost sensors [J]. *Asia. Pac. J. Atmos. Sci.* 57 (3), 547–553. doi:10.1007/s13143-020-00213-2

Partani, S., Qiu, A., Sattiraju, R., Tayade, S., and Schotten, H. D. (2022). Quantitative assessment of CCAM applications on greenhouse gas emissions. proceedings of the 2022 IEEE 95th Vehicular Technology Conference: (VTC2022-Spring), F]. 19-22 June 2022. Helsinki, Finland. IEEE.

Qin, J., Li, Y., Wu, D., Weng, H., and Wang, G. (2020). CCUS global progress and Chinese countermeasures and suggestions. *J Oil Gas Geol. Recovery [J]* 27 (01), 20–28. doi:10.13673/j.cnki.cn37-1359/te.2020.01.003

Rocco, M. V., Ferrer, R. J. F., and Colombo, E. (2018). Understanding the energy metabolism of World economies through the joint use of Production- and Consumption-based energy accountings. *Appl. Energy* 211, 590–603. doi:10.1016/j.apenergy.2017.10.090

Tang, J., Ji, S., and Jiang, L. (2016). The design of a sustainable location-routing-inventory model considering consumer environmental behavior. *Sustainability* 8 (3), 211. doi:10.3390/su8030211

Wang, M., Liu, P., Gu, Z., Cheng, H., and Li, X. (2019). A scientometric review of resource recycling industry. *Int. J. Environ. Res. Public Health* 16 (23), 4654. doi:10.3390/ijerph16234654

Xiang, Y., Hou, L., Du, M., Jia, N. H., and Lv, W. F. Research progress and development prospect of CCUS-EOR technology in China. *Oil Gas Geol. Recovery [J]*, 1–17.

Zhang, L., Ren, B., Huang, H., Li, Y., Ren, S., Chen, G., et al. (2015). CO_2 EOR and storage in Jilin oilfield China: Monitoring program and preliminary results [J]. *J. Petroleum Sci. Eng.* 125, 1–12. doi:10.1016/j.petrol.2014.11.005

Zhang, X., Fan, J-L., and Wei, Y-M. (2013). Technology roadmap study on carbon capture, utilization and storage in China. *Energy Policy* 59, 536–550. doi:10.1016/j.enpol.2013.04.005

Zhao, Z. Q, Zhang, H., Jiao, C., Wang, Q., and Lin, X. (2021). Analysis of global CCUS technology and application status. *J. Mod. Chem. Ind. J.* 41 (04), 5–10.

Zou, Caicai, Xue, Huaqing, Xiong, Bo, Zhang, G., Pan, S., Jia, C., et al. (2021). Connotation, innovation and vision of "carbon neutrality". *Nat. Gas. Ind. B* 8, 523–537. doi:10.1016/j.ngib.2021.08.009

frontiers | Frontiers in Earth Science

TYPE Opinion
PUBLISHED 18 January 2023
DOI 10.3389/feart.2022.1060213

OPEN ACCESS

EDITED BY
Zhilin Cheng,
Xi'an Shiyou University, China

REVIEWED BY
Yang Wang,
Xi'an Shiyou University, China
Yongpeng Sun,
China University of Petroleum, Huadong, China

*CORRESPONDENCE
Athumani Omari Mmbuji,
593451044@qq.com

SPECIALTY SECTION
This article was submitted to Geochemistry, a section of the journal Frontiers in Earth Science

RECEIVED 03 October 2022
ACCEPTED 31 October 2022
PUBLISHED 18 January 2023

CITATION
Wang C, Zhao L, He B, Zhang X and Mmbuji AO (2023), Comparative analysis of matrix-retarded acidizing methods for tight carbonate reservoirs: Gelled acid, micro-emulsified acid, and foamed acid.
Front. Earth Sci. 10:1060213.
doi: 10.3389/feart.2022.1060213

Comparative analysis of matrix-retarded acidizing methods for tight carbonate reservoirs: Gelled acid, micro-emulsified acid, and foamed acid

Chao Wang[1], Limin Zhao[1], Bing He[2], Xiwen Zhang[1] and Athumani Omari Mmbuji[3,4]*

[1]Research Institute of Petroleum Exploration and Development, Beijing, China, [2]Zhenhua Oil Co. Ltd., Beijing, China, [3]Department of Petroleum Engineering, China University of Geosciences, Wuhan, China, [4]Arusha Technical College, Arusha, Tanzania

KEYWORDS

tight carbonate reservoirs, matrix acidizing, gelled acids, foamed acidizing fluid, micro-emulsified acid

Introduction

The matrix acidizing method has been widely employed in the petroleum industry to increase the output of oil and gas from reservoirs that have low permeability and are experiencing formation degradation as a result of drilling, stimulation, and completion activity (Mohsin et al., 2019). It is a method of dissolving carbonate reservoirs (calcite or dolomite) by injection of HCl, which reacts with minerals in the rock formation to increase permeability and production close to the wellbore (Buijse and Domelen, 1998). The new 'wormhole' channels are created by the introduction of the treatment fluid at a downhole injection pressure just below the fracturing pressure to bypass the damaged zone near the wellbore (Amro, 2002; Kiani et al., 2021). The wormholes are formed from the reaction of HCl with the $CaCO_3$ and $CaMg(CO_3)_2$ minerals in the matrix, which avoids the possibility of formation damage (Chang et al., 2007).

Importance of matrix acidizing for tight carbonate reservoirs

In carbonate formations, the purpose of matrix acidizing is primarily to restore and enhance the formation's productivity; but, it also reduces near-wellbore damage and establishes novel hydrocarbon flow channels (wormholes) (Ibrahim et al., 2020). By obstructing the path that the acid normally takes, these agents redirect it to the less permeable, untreated zones as shown in Figure 1 (Ghommem et al., 2015). The use of HCl alone for acidization, especially in higher temperature reservoirs, has suffered some signal failures. A large volume of acid is required because the rapid reaction of the acid

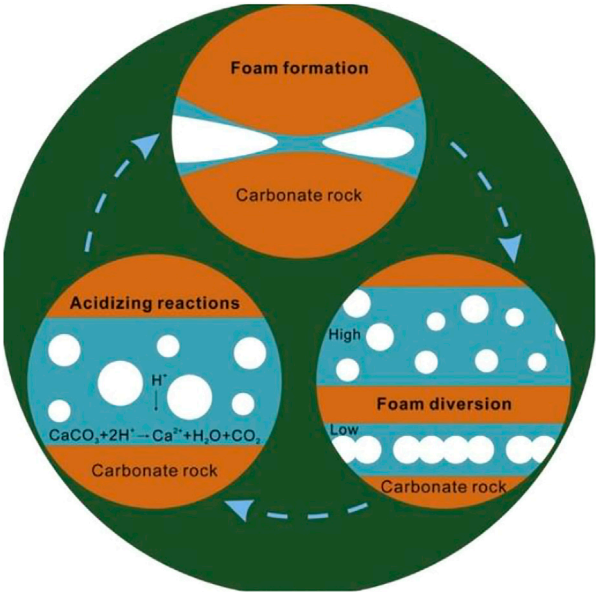

FIGURE 1
Induced acid diversion by foam-based acid (Yan et al., 2019).

with the carbonate minerals of the formation consumes acid at a far faster rate (Chavez, 2007). Due to the shorter residence time of the acid in the formation, especially at high temperatures, the wormholes created are less efficient hydrocarbon channels (Chacon and Pournik, 2022). Therefore, gelled acid, foamed acid, micro-emulsified acids, and other chemical agents have been formulated in an effort to circumvent the drawbacks of the fast acid-rock reaction by lowering H^+ ion dissociation, reducing H+ ion mass transfer, and changing the wettability of the rock surface (Zhu et al., 2022).

Comprehensive review

Gelled acid

The gelled acid fluid is comprised of water, a water-dispersible polymer, an acid, and a gelling agent (Chang et al., 2007; Ismail and Kweh, 2012). Two types of polymer-based acid have been used in the field for matrix acidization: gelled acid for acid retardation and *in situ* gelled acids for acid diversion. The *in situ* formulation includes polymers or VES, crosslinkers, and pH-controlled breakers to achieve dissolution by preventing the acid from passing through highly permeable zones and diverting it to less-permeable zones (Ratnakar et al., 2012; Gomaa and Nasr-El-Din, 2015). In matrix acidization, the gelled acid relies on the viscosity difference of the fluid to reduce the mass transfer of H^+ ions and consequently the acid reaction rate. The use of polymers as viscosifiers poses a challenge, however, because of the buildup of residual chemicals in the formation, which can damage it (Chang et al., 2007).

Micro-emulsified acid

The formulation of a micro-emulsion acid requires that the hydrochloric acid is the internal phase and that the hydrocarbons (crude oil and diesel) act as the external phase (Zakaria et al., 2015). The hydrocarbons reduce the diffusion rate of the HCl droplets and lower the dissolution rate of the rock surface, thus generating highly permeable wormholes (Carvalho et al., 2019). The use of micro-emulsified acid has an advantage over other matrix acidizing methods in that it creates more conductive channels and reduces the mobility or effective diffusivity of HCl without jeopardizing the formation productivity (Fredd et al., 2016). A transient skin factor is created in the high permeability zones, thus diverting the acid to the lower permeability zones (Liu et al., 2013). The reduction in contact time and area between the acid and the casing and tubing minimizes corrosion (Liu et al., 2013; Derendyaev et al., 2022).

Foamed acid

Foamed acid is formed by mixing acid and surfactants and injecting gas (N_2/CO_2). Compared to traditional acidizing processes, foaming has the advantages of diversion, moderate speed, low water sensitivity, increased energy to assist discharge, and less damage to the formation; thus, foam diversion acidizing technology has attracted much attention in recent years (Motta et al., 2021; Yuan et al., 2021). Foamed acid may be used to uniformly treat the entire formation by temporarily limiting acid access to the higher permeability zones and channeling it to the less permeable zones (Letichevskiy et al., 2017; Yan et al., 2019). In comparison to typical acid treatments, foamed-VES formulations have shown excellent acid diversion performance and also pose little threat of formation damage because they contain no polymers (Chang et al., 2007; Yan et al., 2019). They also contain no solids that could impair permeability, and the gas expansion in the foam allows easy flow back during well cleaning (Chang et al., 2007). The retarding action of foaming slows down the speed with which the acid reacts with the rock, resulting in deep matrix acidification (Stringfellow et al., 2017; Zhang et al., 2021).

Conclusion

Due to the fact that carbonate reservoirs are heterogeneous with varied permeability zones and a high temperature

environment, the selection criteria for choosing one of the three proposed matrix acidizing methods must be careful observed. Various researchers have reported that foam-based acids were superior to traditional acidizing methods. They provided effective diversion, reduced the acid reaction rate and water sensitivity, increased energy for discharge of acid into the formation, and caused less harm to the formation. Foaming lowered the effective acid diffusion coefficients into the formation, thus regulating convection and diffusion rate. Foamed acid remains in contact longer with the less permeable zones of the formation, and the process prevents the carbonate-acid reaction from happening too rapidly in the highly permeable zones. At low injection rates, the poor diffusivity of micro-emulsified acid produces narrow but deeper effective wormholes.

The gelled acid relies on viscosity differences in the fluid to reduce the mass transfer of H^+ and the acid reaction rate. Despite its good volumetric efficiency and acid diversion tendency, the field application of gelled acid is limited by the buildup of residuals that impair the flow of oil back through the wormholes to the wellbore. The polymers used as viscosifiers can remain as residual chemicals in the formation and lead to damage; therefore, VES formulations are preferred.

Author contributions

CW: investigation and research, writing manuscript draft; LZ: resources and conceptualization; BH: modify analysis; XZ: typesetting; AM: supervision.

Conflict of interest

Author BH was employed by Zhenhua Oil Co. Ltd.

The authors declare that this study received funding from PetroChina "Fourteenth Five Year" Significant Programs (No. 2021DJ3203). The funder had the following involvement in the study: design, collection, analysis, interpretation of data, and the writing of this article.

Publisher's note

References

Amro, M. M. (2002). Laboratory study and field matching of matrix acidizing of petroleum reservoir rocks. *J. King Saud Univ. Eng. Sci.* 14 (1), 119–135. doi:10.1016/S1018-3639(18)30748-7

Buijse, M. A., and Domelen, M. S. (1998). "SPE 39583 novel application of emulsified acids to matrix stimulation of heterogeneous formations," in *SPE formation damage control conference* (Lafayette, Louisiana: Society of Petroleum Engineers).

Carvalho, R. T. R., Oliveira, P. F., Palermo, L. C. M., Ferreira, A. A. G., and Mansur, C. R. E. (2019). Prospective acid microemulsions development for matrix acidizing petroleum reservoirs. *Fuel* 238, 75–85. doi:10.1016/j.fuel.2018.10.003

Chacon, O. G., and Pournik, M. (2022). Matrix acidizing in carbonate formations. *Processes* 10 (1), 174. doi:10.3390/pr10010174

Chang, F. F., Qiu, X., and Nasr-El-Din, H. A. (2007). "Chemical diversion techniques used for carbonate matrix acidizing: An overview and case histories," in *Proceedings - SPE international symposium on oilfield chemistry* (Houston, Texas, U.S.A: Society of Petroleum Engineers), 574–579. doi:10.2118/106444-ms

Chavez, M. R. (2007). Evaluation and optimisation of combinatorial optimization heuristic algorithms. arXiv.

Derendyaev, R. A., Novikov, V. A., Martyushev, D. A., Liu, Z., and Yang, Y. (2022). Acid treatment of carbonate reservoir with a new dual action microemulsion: Selection of optimal application conditions. *J. Petroleum Sci. Eng.* 216, 110809. doi:10.1016/j.petrol.2022.110809

Fredd, C. N., Hoefner, M. L., Fredd, C. N., Hoefner, M. L., Fogler, H. S., and Fogler, H. S. (2016). *Microemulsion applications applications in microemulsion in carbonate carbonate reservoir reservoir stimulation stimulation*. London: IntechOpen. doi:10.5772/65973

Ghommem, M., Zhao, W., Dyer, S., Qiu, X., and Brady, D. (2015). Carbonate acidizing: Modeling, analysis, and characterization of wormhole formation and propagation. *J. Petroleum Sci. Eng.* 131, 18–33. doi:10.1016/j.petrol.2015.04.021

Gomaa, A. M., and Nasr-El-Din, H. A. (2015). Effect of elastic properties on the propagation of gelled and *in-situ* gelled acids in carbonate cores. *J. Petroleum Sci. Eng.* 127, 101–108. doi:10.1016/j.petrol.2015.01.031

Ibrahim, A. F., Nasr-El-Din, H., and Jiang, L. (2020). "HP/HT matrix acidizing treatments of carbonate rocks using a new retarded HCl acid system," in *International petroleum technology conference 2020 IPTC* (Dhahran, Kingdom of Saudi Arabia: Society of Petroleum Engineers), 1–14. doi:10.2523/iptc-19646-ms

Ismail, I., and Kweh, W. L. (2012). Matrix acidizing with gelled acid. *J. Teknol.* 38, 13–24. doi:10.11113/jt.v38.505

Kiani, S., Jafari, S., Apourvari, S. N., and Mehrjoo, H. (2021). Simulation study of wormhole formation and propagation during matrix acidizing of carbonate reservoirs using a novel *in-situ* generated hydrochloric acid. *Adv. Geo-Energy Res.* 5 (1), 64–74. doi:10.46690/ager.2021.01.07

Letichevskiy, A., Nikitin, A., Parfenov, A., Makarenko, V., Lavrov, I., and Samaraneftegaz, J. S. C. (2017). "SPE-187844-MS foam acid treatment - the key to stimulation of carbonate reservoirs in depleted oil fields of the samara region," in *SPE Russian petroleum technology conference* (Moscow, Russia: Society of Petroleum Engineers).

Liu, M., Zhang, S., Mou, J., Zhou, F., and Shi, Y. (2013). Diverting mechanism of viscoelastic surfactant-based self-diverting acid and its simulation. *J. Petroleum Sci. Eng.* 105, 91–99. doi:10.1016/j.petrol.2013.03.001

Mohsin, M., Mysara, Y., Mohyaldinn, E., Muhammad, E., Abdalla, M., Amir, A., et al. (2019). Synthesis and evaluation of Jatropha oil-based emulsified acids for

matrix acidizing of carbonate rocks. *J. Pet. Explor. Prod. Technol.* 9 (2), 1119–1133. doi:10.1007/s13202-018-0530-8

Motta, A. B. G., Thompson, R. L., Favero, J. L., Dias, R. A. C., Silva, L. F. L. R., Costa, F. G., et al. (2021). Rheological effects on the acidizing process in carbonate reservoirs. *J. Petroleum Sci. Eng.* 207, 109122. doi:10.1016/j.petrol.2021.109122

Ratnakar, R. R., Kalia, N., and Balakotaiah, V. (2012). Carbonate matrix acidizing with gelled acids: An experiment-based modeling study. *SPE Prod. Operations Symposium, Proc.* 1, 207–222. doi:10.2118/154936-ms

Stringfellow, W. T., Camarillo, M. K., Domen, J. K., Sandelin, W. L., Varadharajan, C., Jordan, P. D., et al. (2017). Identifying chemicals of concern in hydraulic fracturing fluids used for oil production. *Environ. Pollut.* 220, 413–420. doi:10.1016/j.envpol.2016.09.082

Yan, Y. li, Xi, Q., Unachibuike, C. B. W., Dou, L., and Wu, C. s. (2019). A novel acidizing technology in carbonate reservoir: *In-situ* formation of CO2 foamed acid and its self-diversion. *Colloids Surfaces A Physicochem. Eng. Aspects* 580, 123787. doi:10.1016/j.colsurfa.2019.123787

Yuan, H., Chen, X., Li, N., Zhou, H., Gong, Y., and Wang, Y. (2021). Numerical simulation of foam diversion acidizing in heterogeneous reservoirs. *Petroleum*. doi:10.1016/j.petlm.2021.01.006

Zakaria, A. S., Nasr-El-Din, H. A., and Ziauddin, M. (2015). Flow of emulsified acid in carbonate rocks. *Ind. Eng. Chem. Res.* 54 (16), 4190–4202. doi:10.1021/ie504167y

Zhang, L., He, J., Wang, H., Li, Z., Zhou, F., and Mou, J. (2021). Experimental investigation on wormhole propagation during foamed-VES acidizing. *J. Petroleum Sci. Eng.* 198, 108139. doi:10.1016/j.petrol.2020.108139

Zhu, D., Hill, D., Ugursal, A., Shuchart, C., Purdy, C., Weissenberger, M., et al. (2022). A modified acid system to enhance carbonate matrix acid stimulation: An experimental study. *Can. J. Chem. Eng.* 100 (6), 1187–1201. doi:10.1002/cjce.24251

Frontiers in Earth Science

Investigates the processes operating within the major spheres of our planet

Advances our understanding across the earth sciences, providing a theoretical background for better use of our planet's resources and equipping us to face major environmental challenges.

Discover the latest Research Topics

See more →

Frontiers

Avenue du Tribunal-Fédéral 34
1005 Lausanne, Switzerland
frontiersin.org

Contact us

+41 (0)21 510 17 00
frontiersin.org/about/contact